QUANTUM COHERENCE AND COLLECTIVE PHENOMENA: FROM SPECTROSCOPY TO ACCELERATING DETECTORS

A Dissertation

by

TUGULDUR BEGZJAV

Submitted to the Office of Graduate and Professional Studies of
Texas A&M University
in partial fulfillment of the requirements for the degree of

DOCTOR OF PHILOSOPHY

Chair of Committee,	Marlan O. Scully
Committee Members,	Girish S. Agarwal
	Olga Kocharovskaya
	Robert D. Nevels
	Suhail M. Zubairy
Head of Department,	Grigory Rogachev

August 2020

Major Subject: Physics

ABSTRACT

During the last half-century, quantum coherence has been of great interest due to its own right and also due to its broad range of applications in many areas of physics. The reason for that is the technological progress made last century, especially, the invention of coherent light sources and their commercialization. Indeed, coherent laser sources allow us to coherently excite atoms and molecules, as a consequence, to study a variety of coherent and collective phenomena in atomic physics, for instance, coherent optical spectroscopy, superradiance, superfluorescence, lasing without inversion and so forth. Interestingly, recent studies in biological systems also seem to exhibit coherent processes, in particular, photosynthetic transport and avian compass.

In this study, we present some of the theory and applications of the quantum coherence. This study considers (i) application of quantum coherence to enhance output signals of coherent anti-Stokes Raman spectroscopy of optically active media (chiral molecules), (ii) a way to find general formulas of single- and double-excited subradiant Dicke states using symmetry group theory, (iii) an impact of Fano-Agarwal coupling and other virtual processes arising from non-rotating wave approximation on the decay of super and subradiant timed Dicke states, and finally (iv) quantum coherence and collective phenomena of relativistically and uniformly accelerating atoms.

Applications of the results presented in this work may be a new method for resolving chirality of molecules using coherent anti-Stokes Raman spectroscopy - Raman optical activity, and a sidewise excitation method for single- and double-excited subradiant states. The obtained results also advance our theoretical understanding of quantum coherence specially theory of super and subradiance.

DEDICATION

To my mother Damtsagdulam Chimed and my father Begzjav Tsedee

ACKNOWLEDGMENTS

I sincerely thank my adviser Prof. Marlan O. Scully, director of the Institute for Quantum Science and Engineering (IQSE) who has been supportive of my academic and research lives. Without his never-ceasing encouragement, valuable advice and financial support, this work would not have been possible. During these years, I had the privilege to work with this pioneer of quantum optics where I benefited from his research guidance and constant encouragement, and learned a lot from him. I am also deeply indebted to Girish Agarwal, who gave a great deal of assistance and support over these years. It was such an honor to collaborate with these great experts on quantum optics. Moreover, I would like to recognize the assistance that I received from my other committee members: Olga Kocharovskaya, Robert D. Nevels and Suhail M. Zubairy.

I would also like to extend my deepest gratitude to my colleagues: Dr. Reed Nessler (Texas A&M University), Dr. Jonathan Ben-Benjamin (Texas A&M University), Dr. Zhenhuan Yi (Texas A&M University), Dr. Hui Dong (Graduate School of China Academy of Engineering Physics), Dr. Luojia Wang (Tongji University), Dr. Arash Azizi (Texas A&M University), Dr. Hichem Eleuch (Abu Dhabi University), Dr. Imran Mirza (Miami University), Dr. Yuri Rostovtsev (University of North Texas), Dr. Gavriil Shchedrin (Colorado School of Mines), Dr. Anatoly Svidzinsky (Texas A&M University) and Dr. Moochan Kim (Texas A&M University) for their research collaboration. Especially, I am extremely grateful to Dr. Alexei Sokolov, Dr. Gombojav Ariunbold and Dr. Narangerel Altangerel, for their stimulating discussion and valuable advice; Kim Chapin, Mariya Khmelenko, Teng Ma, Yasa Rathnayaka and all other IQSE members for their kind help and great assistance. I also thank the Herman F. Heep and Minnie Belle Heep Foundation and the Robert A. Welch Foundation (Grant No. A-1261) for financial support.

Nobody has been more important to me than my family in the pursuit of this work. I would like to thank my lovely wife Pagamdulam Naidansuren, my wonderful children Ninjinlkham Tuguldur and Ninjinsaikhan Tuguldur for their unending inspiration, support, and patience during these

years.

CONTRIBUTORS AND FUNDING SOURCES

Contributors

This work was supported by a dissertation committee consisting of Professors Marlan O. Scully [advisor], Girish S. Agarwal, Olga Kocharovskaya and Suhail M. Zubairy of the Department of Physics and Astronomy and Robert D. Nevels of the Department of Electrical and Computer Engineering.

All other work conducted for the dissertation was completed by the student independently.

Funding Sources

Graduate study was supported by the Herman F. Heep and Minnie Belle Heep Texas A&M University Endowed Fund held/administered by the Texas A&M Foundation and Robert A. Welch Foundation (Grant No. A-1261).

NOMENCLATURE

ROA	Raman optical activity
CARS	Coherent AntiStokes Raman spectroscopy
CARS-ROA	Coherent AntiStokes Raman spectroscopy - Raman optical activity
Lin-Cir CARS-ROA	Linear-Circular CARS-ROA
Cir-Lin CARS-ROA	Circular-Linear CARS-ROA
SU(4)	Special unitary group of degree 4
S_N	Symmetric group of degree N
$\mathbb{C}S_N$	Group algebra of symmetric group of degree N
BS	Beam splitter
M	Mirror
TD	“timed" Dicke
OD	Ordinary Dicke
FA	Fano-Agarwal
RWA	Rotating wave approximation
NRWA	Non-rotating wave approximation

TABLE OF CONTENTS

Page

LIST OF FIGURES

FIGURE Page

LIST OF TABLES

TABLE Page

1. INTRODUCTION

1.1 Research objectives

Quantum collective effects being quantum interference, super and subradiance and other quantum phenomena due to quantum coherence are the most intriguing phenomena in quantum physics and studies of this field have been taken a tremendous amount of effort in the last half-century.

The goal of my Ph.D research is to study various kinds of coherent and collective phenomena in physics. Specifically, it is to develop a new way of enhancing chiral spectroscopic signals using quantum coherence; to improve mathematical understanding of single- and double-excited subradiant states applying Young operator method; to investigate Fano-Agarwal couplings between timed Dicke superradiant and subradiant states; to study collective dynamics of accelerating detectors employing quantum optical methods.

1.2 Contemporary state of research

Since the advent of quantum mechanics in 1920s quantum coherence has been fruitful and broad research area in physics. Quantum coherence is a direct theoretical consequence of wave-particle duality — the fundamental concept of quantum theory. As long as quantum coherence is a pure theoretical notion, it leads to a variety of intriguing and fascinating quantum phenomena. For example, one of the most well-known phenomena based on quantum coherence is superradiance first predicted by Robert Dicke in 1954 [3]. As a matter of fact, quantum coherence has an effect on spontaneous emission of the atoms confined in small volume whose linear size is much shorter than atomic transition wavelength and specifically, quantum coherence introduces enhanced or suppressed spontaneous emission rates of the atoms depending on the symmetry of an atomic state. The enhanced (suppressed) spontaneous emission is called superradiance (subradiance). Theoretical and experimental investigations of super and subradiance have a long-standing history that lasts over half-century. The recent studies primarily focus on experimental investigations of subradiant states since subradiant states are substantially stable against spontaneous emission due

to vacuum fluctuation and in turn, these states are thought as great resources in quantum state-storage and quantum computing [4, 5, 6, 7, 8, 9, 10, 11]. Another recent interest on super and subradiance is an application of group theory to improve our understanding of coherent phenomena of many identical atoms. Indeed, group theory allows us to speed up numerical calculation of complex system otherwise impossible [12, 13, 14, 15, 16, 17, 18]. Moreover, group theory also can be exploited to generate subradiant states in superconducting qubit systems [19].

Another experimentally well-studied phenomenon based on quantum coherence is molecular coherent excitation and emission. Actually, it has very wide applications in optical spectroscopy and this interdisciplinary subject of research is called coherent optical spectroscopy. In particular, coherent excitation of molecules establishes well-defined phase relationships between molecular wavefunctions. As a consequence it results in well-defined phase relations between probability amplitudes of the photons emitted from individual molecules that establish strong directional coherent emission due to constructive interference. This is how coherent emission forms. Broad range of coherent spectroscopic tools have been developed so far and prominent examples could be stimulated Raman spectroscopy and coherent anti-Stokes Raman spectroscopy. Recently, much effort has been made to apply coherent anti-Stokes Raman spectroscopy to resolve biological chiral molecules [20, 21, 22, 23, 24]. Furthermore, it is shown that molecular coherence can enhance spectroscopic emission from chiral molecules [25].

The most recent study of quantum coherence is not restricted by non-relativistic physics. Surprisingly, recent studies show that non-inertial or accelerating atoms exhibit an interesting physics due to quantum coherence [26, 27, 28, 29]. Indeed, for the accelerating atoms, collective dynamics, resonance interaction and Casimir-Polder forces have different features in comparison with inertial atoms. Besides, the most recent studies focus on the interplay between Dicke superradiance and acceleration radiation [30].

List of phenomena based on quantum coherence is endless for instance, we can continue it by lasing without inversion [31, 32], electromagnetically induced transparency [33], superflourescence [34, 35], avian compass [36, 37], coherence in photosynthetic transport [38] and so forth.

1.3 Quantum coherence

One feature that distinguishes quantum physics from classical physics is quantum superposition state. Many fascinating concepts including quantum coherence are actually traced to the quantum superposition state. To be clear, we start with a classical mixed state whose density operator is given as follows

$$\rho_{\text{cl}} = \sum_j c_j c_j^* |\psi_j\rangle\langle\psi_j|, \tag{1.1}$$

where c_j is probability amplitude associated with quantum state $|\psi_j\rangle$. The state ρ_{cl} is mixed and there are no off-diagonal terms. On the other hand, Schrödinger equation allows us to claim that any superposition of two or more solutions is also a solution of the Schrödinger equation. Thus, the superposition state is

$$|\Psi\rangle = \sum_j c_j |\psi_j\rangle \tag{1.2}$$

and corresponding density operator has the following form

$$\rho = \sum_j c_j c_j^* |\psi_j\rangle\langle\psi_j| + \sum_{i\neq j} c_i c_j^* |\psi_i\rangle\langle\psi_j|. \tag{1.3}$$

The first term in Eq. (1.3) is just a classical term as in Eq. (1.1) however, the last term which is off-diagonal term represents quantum coherence. Indeed, in the density matrix representation, off-diagonal terms ρ_{ij}, $i \neq j$ is a measure of quantum coherence. Thus, whenever we discuss quantum coherence we refer to the off-diagonal terms of the density matrix. Furthermore, there is a possibility of confusion that we should make clear. Quantum coherence is not concerned as a statistical feature of many quantum systems. As shown by Eq. (1.3) however, it is concerned as a feature of a single quantum system.

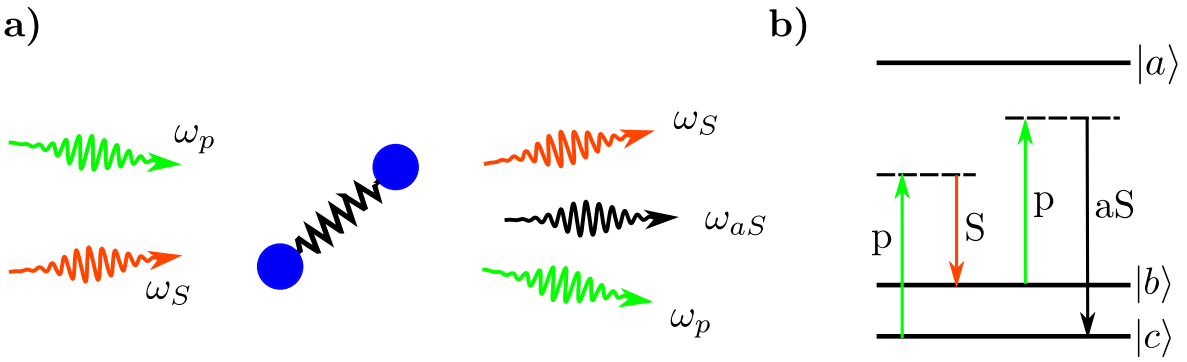

Figure 1.1: a) The CARS system where pump ω_p and Stokes ω_S fields are incident on molecules and it results in blue-shifted anti-Stokes signal ω_{aS}. b) Molecular level scheme and CARS transition pathway.

1.4 Coherent anti-Stokes Raman spectroscopy (CARS)

In CARS, two fields: pump and Stokes with frequency ω_p and ω_S, respectively, are incident on a sample and in the output anti-Stokes field with frequency ω_{aS} is produced provided that the difference frequency $\omega_p - \omega_S$ is resonant with molecular vibrational frequency ω_v (see Figure 1.1(a)). It is worth mentioning that the laser fields are all in the optical range and neither electronic nor vibrational transitions are on one-photon resonance. In contrast with spontaneous Raman scattering, CARS signal is coherent and highly directional. In the microscopic level, a combination of the pump and Stokes photons coherently excite the molecules in the sample to the excited vibrational level $|b\rangle$ (see Figure 1.1(b)). Immediately after that (typical CARS) or after a certain amount of delay time (time-resolved CARS), another pump photon de-excites the molecules and as a result directional coherent anti-Stokes photon at the frequency ω_{aS} is produced.

The CARS spectroscopy has several advantages over conventional spontaneous Raman spectroscopy. One of them is that the CARS intensity scales squared number of molecules N^2 whereas for spontaneous Raman, intensity scales number of molecules N. Physical interpretation for the N^2 dependence of the anti-Stokes signal is nicely explained in paper by Petrov et al. [39]. Using effective Raman Hamiltonian formalism and the Heisenberg equation of motion they found an

average number of anti-Stokes photons $\langle n_{aS} \rangle$ as follows

$$\langle n_{aS} \rangle = \langle n_p \rangle \frac{(G/\hbar)^2}{|\Delta\omega|^2} \left[\sum_i \rho^i_{bb} + \sum_{i \neq j} \mathrm{e}^{-i(\mathbf{k}_{aS} - 2\mathbf{k}_p + \mathbf{k}_S)\cdot(\mathbf{r}_j - \mathbf{r}_i)} \rho^i_{cb} \rho^j_{bc} \right], \tag{1.4}$$

where $\langle n_p \rangle$ is average number of pump field, G is molecular field coupling constant, $\Delta\omega = \omega_{aS} - \omega_p - \omega_b + \omega_c + i\gamma_{bc}$, ρ^j is the jth molecular density matrix and $\mathbf{r}_j$ is position of the jth molecule. The sum must be taken over all molecules in the sample. In Eq. (1.4), some of notations are changed and bit modified into conventional CARS from the original equation in the papers [39, 40] which are for time-resolved CARS.

Equation (1.4) is a sum of two terms which depends on density matrix elements. The first term indicates that more population in the level $|b\rangle$ generates more anti-Stokes signal, however, its dependence on the number of molecules is linear because of the single sum over i. Fortunately, we have the second term whose dependence on the number of molecules is quadratic in terms of N provided phase-matching condition is satisfied. Remarkably, N^2 dependence comes from coherence term ρ_{bc} whereas N dependence originates from population ρ_{bb}. That is why the CARS signal is coherent and stronger than spontaneous Raman signal.

Furthermore, Petrov et al. [39] found the ratio of the photon numbers generated by the CARS and the spontaneous Raman. It is given by

$$\frac{\langle n_{aS} \rangle_{CARS}}{\langle n_S \rangle_{Spon}} \cong \lambda^2 \frac{N}{V} \frac{|\rho_{bc}|^2}{\rho_{cc}} R, \tag{1.5}$$

where R is the radius of the sample, V is volume of the sample, and λ is pump field wavelength. For maximum coherence condition $\rho_{bc} = 1/2$, Eq. (1.5) tells us that the ratio is proportional to the number of molecules per λ^2 area which again confirms the advantage of the CARS over the spontaneous Raman.

Another clear explanation of the N^2 dependence is given in the paper by Scully et al. [1]. They claim that, in the case of CARS, the electric fields emitted from the individual molecules have the same phase, so that, when those add up, the net electric field is proportional to N. However, the net

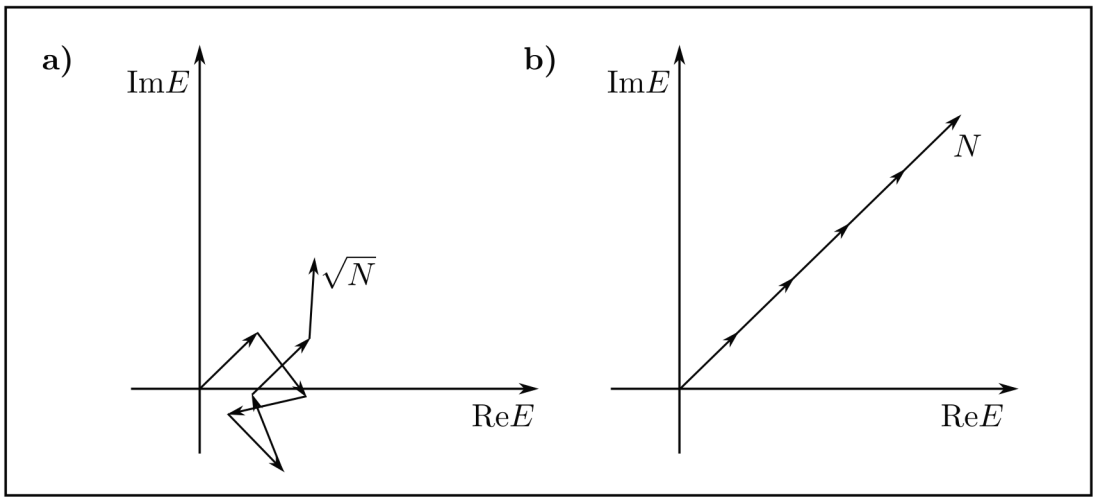

Figure 1.2: a) In the case of spontaneous Raman, electric fields emitted from individual molecules oscillate incoherently. These electric fields are added up with a random phase, so that, net electric field scales $\sqrt{N}$. b) The same plot for coherent CARS electric field. In contrast with the previous situation, electric fields are added up with the same relative phase and as a result net electric field scales N.

electric field is proportional to $\sqrt{N}$ in the case of incoherent spontaneous Raman (see Figure 1.2).

1.5 Dicke superradiance

In 1954, Robert Dicke predicted that quantum coherence has a substantial effect on spontaneous emission of the collection of atoms [3]. Indeed, he introduced the concept of superradiance — cooperative spontaneous emission of bulk atoms due to quantum coherence. Incoherently excited atoms do not have any phase relationships between their wavefunctions and as a consequence these atoms emit radiation in an incoherent manner. In this case, the net electric field of radiated emission is zero $\langle E \rangle = 0$ because it is described as a vector sum of random electric field vectors. But, the intensity of radiated emission is linearly proportional to the number of atoms $\langle E^2 \rangle \propto N$. The physical picture is completely different when atoms are coherently excited. Then, atoms emit photons with constant relative phase and electric fields of photons emitted from different atoms are just summed up. Subsequently, the net electric field goes like N and therefore, the intensity of

radiated emission is proportional to N^2. This emission called superradiance is more intense and faster than typical incoherent emission.

Quantitative interpretation of Dicke superradiance can be shown quickly in the case of two two-level atoms. Eigenstates of Hamiltonian of the system is given by the states: $|a,a\rangle$ – both atoms in the excited state a, $|b,b\rangle$ – both atoms in the ground state b, $|+\rangle$ – symmetric state and $|-\rangle$ – antisymmetric state. Here, $|+\rangle$ and $|-\rangle$ states are single-excited states. Now we calculate total transition dipole moments between $|+\rangle$ and $|b,b\rangle$, and also $|-\rangle$ and $|b,b\rangle$ as follows

$$\begin{aligned} \langle +|\hat{d}_1 + \hat{d}_2|b,b\rangle &= \sqrt{2}d \\ \langle -|\hat{d}_1 + \hat{d}_2|b,b\rangle &= 0, \end{aligned} \tag{1.6}$$

where $\hat{d}_1$ and $\hat{d}_2$ are corresponding dipole moment operators and d is the expectation value of the dipole moment operators. According to Eq. (1.6) spontaneous emission rate is 2γ for the transition $|+\rangle \rightarrow |b,b\rangle$ and 0 for the transition $|-\rangle \rightarrow |b,b\rangle$. Here, γ is spontaneous emission rate of a single atom. This simple calculation clearly shows that atoms in the symmetric state emit twice faster than a single atom whereas atoms in the antisymmetric state do not emit. Latter is called subradiance. Therefore, symmetric state is called superradiant state whereas antisymmetric state is called subradiant state. Furthermore, the super and subradiance can be explained by introducing interference between emissions of individual atoms. In particular, constructive and destructive interferences lead to superradiance and subradiance, respectively.

As shown above, the symmetry of states is involved in super and subradiance. Therefore, group theory helps to understand superradiance. Indeed, superradiant states are a set of symmetric states in the sense that these states do not change under any permutation of N atoms. The superradiant states form the basis of an irreducible subspace of symmetric group S_N of degree N. All other states belong to the set of subradiant states and they have suppressed spontaneous emission rate for the transition to the symmetric states. The subradiant states are also not accessible from symmetric state. These symmetric and antisymmetric states are also called ordinary Dicke (OD) states. Group

theoretical explanation of super and subradiance is explained in chapter 4 in detail.

However, things are much interesting when a large cloud of atoms excited by a single photon is concerned. Interestingly, it has been shown that the large cloud of atoms really emits coherent emission whose direction is determined by the direction of the exciting photon. For the large sample, the atoms are excited not at the same time because atoms in front of the sample get excited first and others later. Therefore, the spatial dimension of the sample matters and symmetric and subradiant states should have spatial dependent phase factor as following [41]

$$|+\rangle_{\mathbf{k}_0} = \frac{1}{\sqrt{N}} \sum_{j=1}^{N} \mathrm{e}^{i\mathbf{k}_0 \cdot \mathbf{r}_j} |b_1 b_2 \ldots a_j \ldots b_N\rangle, \tag{1.7}$$

where $\mathbf{k}_0$ is wave vector of the exciting photon and $\mathbf{r}_j$ is the position of the jth atom. These states are called timed Dicke (TD) single photon states. Spatial distribution and excitation time becomes important for the case of large samples and these are the primary reason why the spontaneous emission of extended large samples is directional.

1.6 Accelerating detector

In this section, we consider a single accelerating detector for the purpose of giving a basic understanding of the Unruh effect [42]. Details of quantum coherence of many co-accelerating atoms will be discussed in chapter 6.

In the late 1970s S. Fulling, P. Davies and W. Unruh discovered that uniformly accelerating observer in Minkowski vacuum sees particles with thermal spectrum [43, 44, 42]. This effect is called the Unruh effect. To explain the Unruh effect we consider the problem where a single accelerating two-level atom interacting with a massless scalar field in $1+1$ dimension. The initial state is a ground state $|b\rangle$ for an atom and zero-photon state $|0\rangle$ (vacuum) for the field. Then, because of the acceleration and counter-rotating terms in interaction Hamiltonian, excitation of two-level atom followed by emission of single photon of the field is made possible. Here, we will calculate the probability of this event. It is worth mentioning that what follows is a qualitative calculation rather than rigorous calculation.

In the interaction picture, Hamiltonian of the system composed of a two-level atom with transition frequency ω and a single mode massless scalar field of frequency ν is given by [45]

$$\hat{V}(\tau) = \mu(\hat{a}\mathrm{e}^{ikz(\tau)-i\nu t(\tau)} + \hat{a}^{\dagger}\mathrm{e}^{-ikz(\tau)+i\nu t(\tau)})(\hat{\sigma}_{+}\mathrm{e}^{i\omega\tau} + \hat{\sigma}_{-}\mathrm{e}^{-i\omega\tau}), \tag{1.8}$$

which is in the atomic rest frame. In Eq. (1.8), τ is atomic proper time, μ is a coupling constant. Atomic rising and lowering operators are denoted by $\hat{\sigma}_{+}$ and $\hat{\sigma}_{-}$, respectively and field annihilation and creation operators are denoted by $\hat{a}$ and $\hat{a}^{\dagger}$, respectively. The functions $z(\tau)$ and $t(\tau)$ are Minkowski coordinate z and time t. Explicit forms of these functions are given by hyperbolic functions as follows

$$z(\tau) = \frac{1}{a}\cosh(a\tau), \quad t(\tau) = \frac{1}{a}\sinh(a\tau), \tag{1.9}$$

where a is a constant acceleration. Probability of excitation of the atom due to counter-rotating term $\hat{a}^{\dagger}\hat{\sigma}_{+}$ is calculated with the use of first-order perturbation theory as follows

$$P_{exc} = \left| \int_{0}^{\infty} d\tau \langle a, 1_k | \hat{V}(\tau) | b, 0 \rangle \right|^2, \tag{1.10}$$

where $|a\rangle$ is excited state of the atom and 1_k is single photon state in mode k. After simple algebra, the integral in Eq. (1.10) has a form

$$\mu \int_{0}^{\infty} d\tau \mathrm{e}^{-ikz(\tau)+i\nu t(\tau)+i\omega\tau} \tag{1.11}$$

and plugging the explicit form of $z(\tau)$ and $t(\tau)$ from Eq. (1.9) into Eq. (1.11) we obtain the excitation probability as follows

$$P_{exc} = \left| \frac{i\mu}{\nu} \left(\frac{a}{i\nu} \right)^{-\frac{i\omega}{a}-1} \Gamma\left(-\frac{i\omega}{a} \right) \right|^2. \tag{1.12}$$

Here, $\Gamma(-i\omega/a)$ is a gamma function. With the help of useful expression

$$|\Gamma(ib)|^2 = \frac{\pi}{b\sinh(\pi b)}, \tag{1.13}$$

where b is real number, we obtain

$$P_{exc} = \frac{2\pi\mu^2/\omega a}{\mathrm{e}^{2\pi\omega/a} - 1}. \tag{1.14}$$

Thus, the above simple calculation shows that uniformly accelerating atom in its ground state through Minkowski vacuum has non-zero excitation probability due to counter-rotating term $\hat{a}^\dagger\hat{\sigma}_+$ and the excitation probability P_{exc} goes as Planck factor associated with Unruh temperature $a/2\pi$. One remark that must be mentioned here is that the Planck factor does not indicate the thermal spectrum of Rindler photons. The reason for that is not clear and it could be a single mode of the field. More rigorous calculation taking all possible modes of massless scalar field into account is presented in chapter 6. Nevertheless, the result given by Eq. (1.14) is a straightforward implication of the Unruh effect.

More accurate calculation without introducing accelerating atom can be done by Bogolyubov transformation [46] which results in mean photon number of Rindler photons as follows

$$\overline{n}_\Omega = \frac{1}{\mathrm{e}^{2\pi\Omega/a} - 1}, \tag{1.15}$$

where Ω is photon frequency. Therefore, an accelerating observer in Minkowski vacuum sees Rindler photons with thermal distribution given by Eq. (1.15).

A physical interpretation of the Unruh effect is as follows. An accelerating atom interacts with the Minkowski vacuum that is a small fluctuations of a field and this interaction results in the excited atom due to counter-rotating term in the interaction Hamiltonian. However, vacuum fluctuation does not provide any energy to excite an atom. Rather, part of work done by the force to accelerate the atom contributes to the energy spent on excitation of the atom [46, 47]. Therefore,

the excitation energy comes from external accelerating force which is not concerned here as a part of the system.

Until now, we consider only how an accelerating observer in Minkowski vacuum gets excited. However, on the other hand, a more intriguing question, here, is what happens in terms of Minkowski observer when accelerating observer gets excited. The problem has been concerned by several authors in the last four decades and unfortunately, still there is no commonly accepted solution to this problem. In one hand, Unruh and Wald [48], and Ginzburg and Frolov [49] show that an accelerating observer in Minkowski vacuum radiates Minkowski particles of a field at infinity and they call it acceleration radiation. On the other hand, some other authors disagree on the acceleration radiation [50, 51, 52]. Hence, one needs to experimentally demonstrate the Unruh effect and acceleration radiation as well. Recently, much effort has been made on the direct and indirect experimental demonstration of the Unruh effect and its intriguing outcome – acceleration radiation [53, 54, 55, 56, 57, 58]. Unfortunately, no one has demonstrated the Unruh effect so far. Actually, the experimental demonstration is challenging because, in order to see Rindler particles of Unruh temperature 1 K, one needs to achieve huge acceleration more than 10^{20} m/s^2.

1.7 Organization of the Dissertation

The dissertation consists of seven chapters and is organized as follows.

Theoretical concepts of quantum coherence and their relations to the considered phenomena in this dissertation are given in Chapter 1. Some of the recent interests of quantum coherence is also summarized in Chapter 1.

In chapter 2, we concentrate on a new way to enhance CARS spectroscopic signals scattered from chiral molecules using molecular (quantum) coherence. In our simplified theoretical model, pump and Stokes pulses that coherently excite molecules are properly excluded from the calculation and accordingly density matrix calculation is much simplified. Two experimental configurations namely Lin-Cir and Cir-Lin CARS-ROA are discussed. Enhancement factors of spectroscopic chiral signals are estimated for the concerned configurations of the experiment. Chapter 2 also considers the enhancement of heterodyne chiral signals.

The mathematical method for the rotational average of odd-rank tensors is concerned in chapter 3. This is a completely mathematical problem and the result is potentially important to the theory of optical spectroscopy. The chapter presents the core concepts of the method in the example of low odd-rank tensors and the developed method is successfully applied to high odd-rank tensors namely 9th and 11th rank tensors.

Chapter 4 is devoted to the problem "how to utilize the theory of permutation to reveal the symmetry of subradiant states and also to design sidewise excitation method to create Dicke subradiant states". The chapter provides complete basic mathematical concepts of permutation symmetry, Young tableau as well as Young operator. Moreover, simple interpretation of the irreducible representation of the symmetric group is given in the corresponding Appendix E.

In chapter 5, we concentrate on Fano-Agarwal couplings between TD super and subradiant states excluding and including Lamb shift. The chapter illustrates the effect of Fano-Agarwal coupling on collective spontaneous decay rates of TD states.

Chapter 6 is devoted to quantum coherence of relativistically accelerated detectors and their enhanced acceleration radiation. Probability amplitude and master equation methods are applied to the problem.

Finally in chapter 7, we summarize our research results presented in the dissertation.

The dissertation is based on the research projects performed by the author during his Ph.D study (2015-2019). The other project performed by the author not included in the main text of the dissertation is presented in Appendix G.

2. ENHANCED CHIRAL SIGNALS FROM CHIRAL MOLECULES VIA MOLECULAR COHERENCE*

2.1 Introduction

Raman scattering from chiral molecules results in different scattered intensities for right- and left-circularly polarized incident light. This is the fundamental concept of the chiroptical spectroscopic tool called Raman optical activity (ROA) [59, 60, 61, 62, 63, 64, 65]. Since the pioneering works by L. D. Barron et al. in the early 1970s, ROA has been of great interest due to its potential applications in the study of biomolecules. Applications of ROA are widespread since it allows us to retrieve molecular structural and conformational information through spectral analysis of vibrational modes of chiral biomolecules that is sometimes unobtainable by other methods. Nowadays, the ROA method is advanced enough and commercialized [61]. However, the intensity of the chiral signal provided by ROA is not strong enough due to weak magnetic dipole and electric quadrupole interactions. In spite of extensive studies on chirality via ROA, enhancing the chiral signal is still a challenge. Thus one is constantly examining newer methods for the study of chiral signals [66, 67, 68, 69].

Coherent anti-Stokes Raman scattering (CARS) is known to be extremely useful in studying molecular vibrations and has several advantages over spontaneous Raman spectroscopy [70]. Thus, it has been argued that it is better to study chirality by using CARS [20, 21] and we might refer to this as CARS-ROA. The first experimental realization of infrared- as well as visible-excited CARS-ROA was reported in [22, 23, 24]. It was found that the contrast of the visible-excited CARS-ROA spectrum of $(-)$-β-pinene compared with spontaneous ROA measurement can be higher by two orders of magnitude [22].

Molecules with high molecular coherence oscillate in phase i.e. molecular vibrational dipole moments share the same phase. Therefore, any interference built up between these oscillating

*Reprinted with permission from "Enhanced signals from chiral molecules via molecular coherence" by Tuguldur Kh. Begzjav, Zhedong Zhang, Marlan O. Scully and Girish S. Agarwal, 2019. Optics express 27, 13965-77, Copyright [2019] Optical Society of America under the terms of the OSA Open Access Publishing Agreement.

molecules are only constructive. As a result, the typical CARS signal is coherent and its magnitude is several times stronger than spontaneous Raman signal due to molecular coherence[39, 71, 72, 73]. Consequently, it seems to be that enhancement due to molecular coherence is also valid for chiral nonlinear signals. This question is still unanswered. Thus, unlike early theoretical works [20, 21] on CARS-ROA which consider complete electrodynamical treatment of the problem, we focus on molecular coherence and its role on enhancement of CARS-ROA signals [†]. Particularly, we develop theoretical model for CARS-ROA and show how molecular coherence allow us to obtain stronger CARS-ROA signal (see Figure 2.1). In our model, CARS-ROA process is separated into two parts in sequential time; one with preparing the molecular system with well-defined coherence and another with using a laser field to scatter from molecular coherence to produce a chiral anti-Stokes signal. It is estimated that the CARS-ROA signal is more than four orders of magnitude bigger than that produced by spontaneous Raman techniques. We also discuss many advantages of heterodyning the CARS-ROA signal with a local oscillator at the anti-Stokes frequency and of pre- and post-choosing the polarizations. Heterodyning gives the most direct measurement of the chirality coefficient, especially the one arising from a nonvanishing magnetic dipole contribution.

2.2 Theoretical model of CARS-ROA

In this section we present our model for the enhancement of CARS-ROA signals. The generation of the spontaneous ROA signal is depicted in Figure 2.2(a). The system is excited by a pump beam of frequency ω_l and the scattered beam (or the spontaneously generated radiation) carries the information about the chirality of the molecule. The chiral contributions arising from the magnetic dipole and the quadrupole contributions have been extensively evaluated [59]. On the other hand, K. Hiramatsu et al. [22, 23, 24] reported the observation of ROA signals via coherent anti-Stokes Raman scattering (see Figure 2.2(b–d)). The generated signal at $2\omega_l - \omega_s$ is coherent and carries signatures of the Raman optical activity.

Guided by the advantages of molecular coherence [74] we consider that the molecular system

[†]At this point, it is worth mentioning that the enhancement here is for actual detectable signals rather than circular intensity difference since the latter is mostly 10^{-3} for any type of spectroscopic tools.

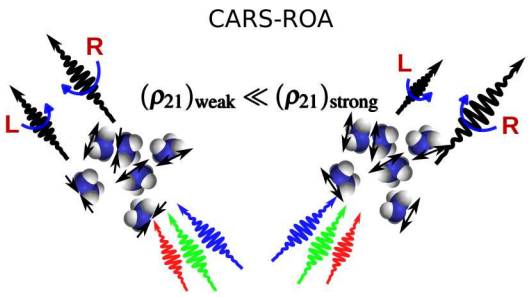

Figure 2.1: Sketch for CARS-ROA. Left: Weak incident laser fields are scattered from a molecular system with low coherence $(\rho_{21})_{\text{weak}}$ into L (left circularly polarized) or R (right circularly polarized) scattering field. Black arrows attached to the molecules indicate stretching ($\leftarrow\rightarrow$) or compressing ($\rightarrow\leftarrow$) vibration. Difference in the intensity of L and R fields indicated by the length difference between black wiggly arrows L and R is so small as the molecules vibrate nearly out of phase. Right: Scattering of strong incident lasers from a molecular system results in L or R field. Unlike weak incident fields, the generated molecular coherence $(\rho_{21})_{\text{strong}}$ is relatively high as the molecules vibrate in phase therefore, the difference in the intensity of L and R fields is much larger than that for the left one. Reprinted with permission from [25].

has been prepared in a coherent superposition of the levels $|1\rangle$ and $|2\rangle$. This can be done by using ultrashort pulses (much shorter than the transverse relaxation time T_2 for the molecule). This initial preparation has the advantage of preparing all the molecules vibrating in unison. Thus, the situation we consider is shown in Figure 2.2(b–d) where we assume the molecular system with moderate amount of molecular coherence. Note that the maximum allowed value of coherence is $1/2$. The molecular coherence has a frequency close to the vibrational frequency ω_v, and it will decay as $\exp\{(-t/T_2)\}$. We next scatter the laser field of frequency ω_l for molecular coherence to produce a coherent scattered signal at the anti-Stokes frequency $\omega_{as} = \omega_l + \omega_v$. Advantages of using molecular coherence in CARS-ROA measurement are discussed after we present expressions for the signals. For the model of Figure 2.2(b–d) we need to calculate the induced polarization and magnetization to first order in the field E_l. It is necessary to include both dipole and quadrupole contributions. The signal at frequency ω_{as} can then be obtained using the Maxwell equations.

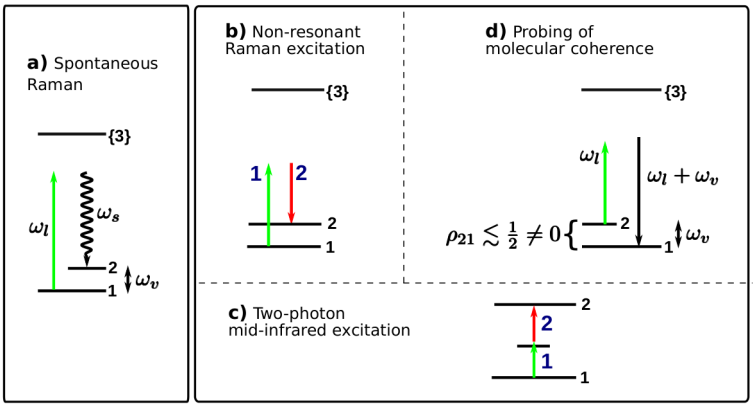

Figure 2.2: Simple scheme for spontaneous ROA is illustrated in (a) where field of frequency ω_l is scattered from a molecule into frequency ω_s. Since scattered field mode ω_s is initially empty, each molecule emits spontaneously and independently from others (wiggly black arrow). Thus, molecular coherence is negligibly small $\rho_{21} = 0$. We also show two ways to create molecular coherence, namely non-resonant Raman excitation (b) and two-photon mid-infrared excitation (c). These two methods are principally analogous except the difference in wavelength of incident lasers. Attainable magnitude of molecular coherence ρ_{21} is of order 10^{-5} to 10^{-3} depending on intensity of the incident lasers [1, 2]. Probing of molecular coherence is depicted in (d). Incident laser field of frequency ω_l scatters from molecules with initially prepared molecular coherence ρ_{21}. As a result, enhanced signal at frequency $\omega_l + \omega_v$ comes out. Reprinted with permission from [25].

The semiclassical Hamiltonian of the molecule–field system is written as

$$\hat{H} = \hat{H}_0 + \hat{H}_{\text{int}}, \tag{2.1}$$

where

$$\begin{aligned} \hat{H}_0 &= \sum_r \hbar\omega_r |r\rangle\langle r|, \\ \hat{H}_{\text{int}} &= -\hat{\boldsymbol{\mu}} \cdot \mathbf{E}_l(t, \mathbf{r}) - \hat{\mathbf{m}} \cdot \mathbf{B}_l(t, \mathbf{r}) - \frac{1}{3} \sum_{\alpha,\beta} \hat{q}_{\alpha\beta} \nabla_\alpha E_{l,\beta}(t, \mathbf{r}). \end{aligned} \tag{2.2}$$

The free Hamiltonian of a molecule with transition frequency ω_r is denoted by $\hat{H}_0$ and $\{|r\rangle\}$ are molecular electronic and vibrational states. The interaction Hamiltonian $\hat{H}_{\text{int}}$ consists of three terms, namely electric dipole $\hat{\boldsymbol{\mu}}$, magnetic dipole $\hat{\mathbf{m}}$ and electric quadrupole moment $\hat{q}_{\alpha\beta}$. The

electric and magnetic fields of the incident laser pulse at time t are denoted by $\mathbf{E}_l(t)$ and $\mathbf{B}_l(t)$, respectively. Without loss of generality, we choose the z-axis as propagation direction of the incident laser pulse throughout this chapter. First, let us assume the incident laser pulse to be x-polarized and denote it by $E_{l,x}(t)$. We choose this electric field of incident laser pulse to have center frequency $\omega_l^{(0)}$ and delay time τ as $E_{l,x}(t) = \mathcal{E}_{l,x}(t-\tau)\mathrm{e}^{-i\omega_l^{(0)}t}$ in the time domain and $E_{l,x}(\omega_l) = \mathcal{E}_{l,x}(\omega_l - \omega_l^{(0)})\mathrm{e}^{i(\omega_l-\omega_l^{(0)})\tau}$ in the frequency domain.

Using first-order perturbation theory, the βth components of induced dipole and quadrupole moments are found to be

$$
\begin{aligned}
\mu_\beta^{(e)}(\omega_{as}) &= \frac{1}{\pi}\int_{-\infty}^{\infty} \mathrm{d}\omega_l\, \tilde{\alpha}_{\beta\alpha}(\omega_{as}-\omega_v)\frac{\mathcal{E}_{l,\alpha}(\omega_l-\omega_l^{(0)})\mathrm{e}^{i(\omega_l-\omega_l^{(0)})\tau}}{\Gamma^2+(\omega_{as}-\omega_v-\omega_l)^2}\Gamma\rho_{21}(0),\\
\mu_\beta^{(m)}(\omega_{as}) &= \frac{1}{\pi}\int_{-\infty}^{\infty} \mathrm{d}\omega_l\, \tilde{G}_{\beta\alpha}(\omega_{as}-\omega_v)\frac{\mathcal{B}_{l,\alpha}(\omega_l-\omega_l^{(0)})\mathrm{e}^{i(\omega_l-\omega_l^{(0)})\tau}}{\Gamma^2+(\omega_{as}-\omega_v-\omega_l)^2}\Gamma\rho_{21}(0),\\
m_\beta(\omega_{as}) &= \frac{1}{\pi}\int_{-\infty}^{\infty} \mathrm{d}\omega_l\, \tilde{\mathscr{G}}_{\beta\alpha}(\omega_{as}-\omega_v)\frac{\mathcal{E}_{l,\alpha}(\omega_l-\omega_l^{(0)})\mathrm{e}^{i(\omega_l-\omega_l^{(0)})\tau}}{\Gamma^2+(\omega_{as}-\omega_v-\omega_l)^2}\Gamma\rho_{21}(0),\\
\mu_\beta^{(q)}(\omega_{as}) &= \frac{ik_\gamma}{3\pi}\int_{-\infty}^{\infty} \mathrm{d}\omega_l\, \tilde{A}_{\beta,\gamma\alpha}(\omega_{as}-\omega_v)\frac{\mathcal{E}_{l,\alpha}(\omega_l-\omega_l^{(0)})\mathrm{e}^{i(\omega_l-\omega_l^{(0)})\tau}}{\Gamma^2+(\omega_{as}-\omega_v-\omega_l)^2}\Gamma\rho_{21}(0),\\
q_{\gamma\beta}(\omega_{as}) &= \frac{1}{\pi}\int_{-\infty}^{\infty} \mathrm{d}\omega_l\, \tilde{\mathscr{A}}_{\alpha,\gamma\beta}(\omega_{as}-\omega_v)\frac{\mathcal{E}_{l,\alpha}(\omega_l-\omega_l^{(0)})\mathrm{e}^{i(\omega_l-\omega_l^{(0)})\tau}}{\Gamma^2+(\omega_{as}-\omega_v-\omega_l)^2}\Gamma\rho_{21}(0),
\end{aligned}
\tag{2.3}
$$

where $\rho_{21}(0)$ is the off-diagonal term of the molecular density matrix at initial time 0 and k_γ is the γth component of the wavevector of the incident laser pulse. Explicit forms of the electric dipole polarizability tensor $\tilde{\boldsymbol{\alpha}}$, electric dipole–magnetic dipole optical activity tensors $\{\tilde{\boldsymbol{G}}, \tilde{\boldsymbol{\mathscr{G}}}\}$ and electric dipole–electric quadrupole optical activity tensors $\{\tilde{\boldsymbol{A}}, \tilde{\boldsymbol{\mathscr{A}}}\}$ are given in Appendix B. The tilde in these expressions indicates that the tensors are complex valued. The superscripts e, m and q in Eq. (2.3) represent the perturbation due to electric dipole, magnetic dipole and electric quadrupole interactions, respectively. Here, we focus on the contribution coming from the molecular coherence ρ_{21} as the contributions from ρ_{22} and ρ_{11} will be small. This is justified as the populations ρ_{22} and ρ_{11} are subject to incoherent emission whose dependence on the number of molecules N is linear. On the contrary, molecular coherence ρ_{21} contributes to coherent emission whose dependence is

quadratic i.e. N^2. It should be noted that the conventional calculation of the ROA involves the ground state population ρ_{11} and hence the tensors arising from the use of the molecular coherence are somewhat different due to the use of the initial conditions.

Unlike traditional ROA signals which are due to spontaneous Raman processes, we concentrate here on the CARS-ROA signals. This is possible as the system in prepared with significant molecular coherence and all the molecules contribute coherently to the signal. Thus the CARS-ROA signal is proportional to N^2, where N is the number of molecules in the laser beam:

$$I(\text{CARS-ROA}) = N^2 |E(\omega_{as})|^2, \tag{2.4}$$

where $E(\omega_{as})$ is electric field of scattered anti-Stokes light at frequency ω_{as}. The signal Eq. (2.4) is to be compared with the incoherent ROA signal

$$\frac{I(\text{CARS-ROA})}{I(\text{ROA})} \cong N \frac{|\rho_{21}|^2}{\rho_{11}}, \tag{2.5}$$

and clearly CARS-ROA can be many orders larger than $I(ROA)$. Here, we have assumed that the laser pulse is applied immediately after molecular coherence has been created. A more flexible scenario would be to apply the laser pulse after a delay τ. Then one needs to take into account the decay of the molecular coherence $\rho_{21}(t) \rightarrow \rho_{21}(0) \exp(-i\omega_v t - \Gamma t)$, where $\Gamma = 1/T_2$ is the molecular dephasing constant. For this scenario, it is more convenient to work in the frequency domain where the molecular coherence has the form $\left(1/\sqrt{2\pi}\right) \int_{-\infty}^{\infty} dt \theta(t) \rho_{21}(t) \mathrm{e}^{i\omega t}$. Therefore, the anti-Stokes signal at ω_{as} will be produced from the laser pulse at frequency $\omega_{as} - \omega_v$ and the molecular coherence at ω_v.

Scattered anti-Stokes field only at forward direction z is under consideration. In this case, right- and left-circularly polarized components $E^x_{R/L} = \mathbf{e}_{L/R} \cdot \mathbf{E}^x$ of scattered anti-Stokes field $\mathbf{E}^x$ are found to be proportional to the molecular coherence ρ_{21} between ground $|1\rangle$ and excited $|2\rangle$ states when we omit frequency dependence of polarizability and optical activity tensors. Clearly, the net

signal will be given by

$$E^{x}_{R/L}(\omega_{as},\tau) \propto \frac{N}{\sqrt{2}}\Bigg(\alpha_{xx} \pm i\alpha_{yx} + \frac{ik_l}{3}A_{x,zx} - \frac{ik_{as}}{3}A_{x,zx} \\ \pm \frac{1}{c}G'_{yy} \mp \frac{k_l}{3}A_{y,zx} \pm \frac{1}{c}G'_{xx} \pm \frac{k_{as}}{3}A_{x,yz}\Bigg) F(\omega_{as},\tau), \tag{2.6}$$

where

$$F(\omega_{as},\tau) = \frac{1}{\pi}\int_{-\infty}^{\infty} \mathrm{d}\omega_l \, \frac{\mathcal{E}_{l,\alpha}(\omega_l - \omega_l^{(0)})\mathrm{e}^{i(\omega_l-\omega_l^{(0)})\tau}}{\Gamma^2 + (\omega_{as} - \omega_v - \omega_l)^2}\Gamma\rho_{21}(0). \tag{2.7}$$

Here, the sign at the top (bottom) refers to right- (left-) circularly polarized component of the scattered field. The tensors $\boldsymbol{\alpha}$, $\boldsymbol{G'}$ and $\boldsymbol{A}$ are now real-valued (see Appendix B for details) and their values are replaced by the values at the central value $\omega_l^{(0)}$ of the incident laser pulse.

For simplicity, finite duration of pump and Stokes fields is disregarded in Eq. (2.7). Its inclusion will modify $\rho_{21}(0)$ to

$$\rho_{21}(0) \simeq \sum_{\{|3\rangle\}} \frac{i\langle 2|\hat{\mu}_\beta|3\rangle\langle 3|\hat{\mu}_\alpha|1\rangle}{2\hbar^2}\int_{-\infty}^{\infty}\mathrm{d}\omega_p \, \frac{\mathcal{E}_{s,\beta}(\omega_v - \omega_p + \omega_s^{(0)})\mathcal{E}_{p,\alpha}(\omega_p - \omega_p^{(0)})}{\omega_{31} - \omega_p - i\Gamma_3} \tag{2.8}$$

where $\mathcal{E}_{p,\alpha}$ and $\mathcal{E}_{s,\beta}$ are the electric fields of pump and Stokes, respectively and Γ_3 is decay constant of the levels $\{|3\rangle\}$. The result Eq. (2.8) also holds for two-photon mid-infrared excitation shown in Figure 2.2(c). Detailed derivation of this expression is given in Appendix A.

We have already discussed two methods for producing molecular coherence in the beginning of this section (Figure 2.2). It has been shown that two-photon excitation of the system is preferable over direct one photon IR excitation [75] as in the latter case the molecular coherence averages out due to orientation averaging. Another method for producing molecular coherence is chirped-pulse adiabatic control where molecular coherence is efficiently controlled by linearly chirped pump and Stokes pulses or constant chirp in the pump and sign flipped chirp in the Stokes pulses [76]. This is a robust and efficient control on molecular coherence.

In the next sections we discuss various special cases of CARS-ROA by pre- and post-selecting

polarizations.

2.3 Lin-Cir and Cir-Lin CARS-ROA

When the laser pulse is linearly polarized along the x-axis, the circular components of the scattered emission can be measured for studying chiral molecules. We name this configuration of measurement Lin-Cir CARS-ROA. In this case, using expression Eq. (2.6) for the anti-Stokes electric field, the difference spectrum $I_R^x - I_L^x$ and circular intensity sum $I_R^x + I_L^x$ are found to be

$$I_R^x - I_L^x \propto \left(\frac{180aG' + 4\gamma^2(G')}{45c} - \frac{6\gamma^2(A) - 2(\omega_{as}/\omega_l)\gamma^2(A)}{45c} \right) N^2 |F|^2 \tag{2.9}$$

and

$$I_R^x + I_L^x \propto \frac{45a^2 + 7\gamma^2(\alpha)}{45} N^2 |F|^2. \tag{2.10}$$

The real-valued tensor invariants a, G', $\gamma^2(\alpha)$, $\gamma^2(G')$ and $\gamma^2(A)$ are defined by [77, 63]

$$\begin{aligned}
a^2 &= \frac{1}{9}\alpha_{\lambda_1\lambda_1}\alpha_{\lambda_2\lambda_2}, \\
\gamma^2(\alpha) &= \frac{1}{2}(3\alpha_{\lambda_1\lambda_2}\alpha_{\lambda_1\lambda_2} - \alpha_{\lambda_1\lambda_1}\alpha_{\lambda_2\lambda_2}), \\
aG' &= \frac{1}{9}\alpha_{\lambda_1\lambda_1}G'_{\lambda_2\lambda_2}, \\
\gamma^2(G') &= \frac{1}{2}(3\alpha_{\lambda_1\lambda_2}G'_{\lambda_1\lambda_2} - \alpha_{\lambda_1\lambda_1}G'_{\lambda_2\lambda_2}), \\
\gamma^2(A) &= \frac{\omega_l}{2}\epsilon_{\lambda_2\lambda_3\lambda_4}\alpha_{\lambda_1\lambda_2}A_{\lambda_3,\lambda_4\lambda_1},
\end{aligned} \tag{2.11}$$

where we use Einstein summation convention for repeated indices, for example $\alpha_{\lambda_1\lambda_1} = \alpha_{xx} + \alpha_{yy} + \alpha_{zz}$. Eqs. (2.9) and (2.10) are very similar to the signal terms found by L. D. Barron [59]. The small difference disappears upon making the nonphysical assumption $\omega_l = \omega_{as}$. However, these equations now have more deep physical meaning since these signals depend on molecular coherence ρ_{21} and most importantly on N^2. In addition, note that the difference spectrum Eq. (2.9) and circular intensity sum Eq. (2.10) are τ-dependent.

As discussed in Figure 2.2, the generated molecular coherence can be of the order 10^{-5} to 10^{-3} depending on the intensities of the pump and Stokes fields (Figure 2.2(b)) or the intensity of the mid-infrared field (Figure 2.2(c)) (see for example [1, 2]). Thus, we can have additional gain of a factor like 10^4 in the signal $I_R^x \mp I_L^x$ for Lin-Cir CARS-ROA if stronger excitation is used to produce molecular coherence. Here, we should note that not only the difference spectrum is enhanced but also the circular intensity sum. Therefore, the circular intensity difference $\Delta = (I_R^x - I_L^x)/(I_R^x + I_L^x)$ does not change. However, the enhancement in absolute magnitude of difference spectrum allows us to significantly increase the signal-to-noise ratio for the chiral signal.

For circularly polarized laser and linearly polarized scattered light, we call this configuration Cir-Lin CARS-ROA. The difference spectrum can be found as

$$I_x^R - I_x^L \propto \left(\frac{180aG' + 4\gamma^2(G')}{45c} - \frac{6(\omega_{as}/\omega_l)\gamma^2(A) - 2\gamma^2(A)}{45c} \right) N^2 |F|^2, \tag{2.12}$$

and the circular intensity sum $I_x^R + I_x^L$ is the same as that of Lin-Cir CARS-ROA (see Appendix C and D for details). Since the dependence on molecular coherence remains in Eq. (2.12), the enhancement factors are the same for Lin-Cir and Cir-Lin CARS-ROA.

2.4 Heterodyne measurements with a local oscillator

In the case of heterodyne measurement with a local oscillator $\mathbf{E}_{LO}$ of frequency ω_{as}, the heterodyne signal is defined as

$$I_{R/L}^x \propto |E_{R/L}^x + E_{LO}|^2, \tag{2.13}$$

where $E_{LO} = E_{LO,R/L} = \mathbf{e}_{L/R} \cdot \mathbf{E}_{LO}$, that is, we assume right- and left-circularly polarized components of the local oscillator are equal to each other. The local oscillator can be obtained from the laser pulse used to create CARS-ROA by modulating it. Then, the difference spectrum

and circular intensity sum are found to be

$$I_R^x - I_L^x \propto \left(\frac{180aG' + 4\gamma^2(G')}{45c} - \frac{6\gamma^2(A) - 2(\omega_{as}/\omega_l)\gamma^2(A)}{45c} \right) N^2|F|^2 + \frac{8}{\sqrt{2}c} G' N \,\mathrm{Re}(F E_{LO}^*) \tag{2.14}$$

and

$$I_R^x + I_L^x \propto \frac{45a^2 + 7\gamma^2(\alpha)}{45} N^2|F|^2 + \frac{4}{\sqrt{2}} aN \,\mathrm{Re}(F E_{LO}^*). \tag{2.15}$$

The first terms in Eqs. (2.14) and (2.15) are Lin-Cir CARS-ROA signals whereas the second terms are heterodyne signals. In order to recover the heterodyne signal we need to remove the first terms in Eqs. (2.14) and (2.15). The way to do so is to measure signal Eqs. (2.14) and (2.15) with two different phases of E_{LO}, namely ϕ and $\phi + \pi$ phases, and to subtract the two heterodyne difference spectra (similar method for CARS was reported in [78]). This enables us to measure only the heterodyne chiral parameter G' and achiral parameter a, that are,

$$\begin{aligned} (I_R^x - I_L^x)_\phi - (I_R^x - I_L^x)_{\phi+\pi} &\propto \frac{16}{\sqrt{2}c} G' N \,\mathrm{Re}(F|E_{LO}| \exp(i\phi)), \\ (I_R^x + I_L^x)_\phi - (I_R^x + I_L^x)_{\phi+\pi} &\propto \frac{8}{\sqrt{2}} aN \,\mathrm{Re}(F|E_{LO}| \exp(i\phi)). \end{aligned} \tag{2.16}$$

Note the striking aspect of Eq. (2.16): it directly determines the ratio of tensor invariants G' and a. This would be the first direct measurement of this ratio. Furthermore, the expressions in Eq. (2.16) still depend on the molecular coherence ρ_{21} via F. Hence, the heterodyne chiral signal (2.16) can be enhanced by factor of 10^2 at most. An estimate of the magnetic and quadrupole contributions is given in the experiments of D. Che and L. A. Nafie [79], where it is reported that such contributions to ROA signals are about 1000 times smaller than the electric dipole one.

2.5 Conclusions

We predict that, depending on the type of measurement configuration, a chiral signal $10^2 - 10^4$ times stronger in magnitude can be obtained by creating strong molecular coherence. This is for Lin-Cir and Cir-Lin CARS-ROA. As shown above, molecular coherence enhances not only the difference spectrum but also the intensity sum too. This is one of the key points of the present chapter.

Furthermore, we present a new heterodyne measurement scheme that allows us to experimentally determine the ratio of tensor invariants G' and a. A general expression for the CARS-ROA signal consists of not only the actual heterodyne signal but also the signal coming from interference between chiral and achiral terms which includes the product of aG' and other anisotropic tensor invariants $\gamma^2(G')$ and $\gamma^2(A)$. This interference term makes the heterodyne measurement less accurate. To overcome this difficulty one may measure the heterodyne difference spectrum and circular intensity sum with two different phases of local oscillator and eliminate the interference term coming from chiral and achiral terms by subtracting the measured signals. As a result, the measured signal only depends on G' and a, which enables us to obtain the ratio between G' and a.

For materials that are not heat resistant, such as biological molecules, we suggest either the two-photon mid-infrared excitation method or resonant Raman excitation method for inducing molecular coherence. Both methods use low power of excitation, and consequently, they are expected to be safe for most samples.

In summary, we demonstrated that the chiral signal could be enhanced via molecular coherence in comparison with ROA signals where molecular coherence essentially plays no role. In the case of non-resonant Raman excitation, the enhancement factor is estimated up to 10^4. Such benefit of the molecular coherence provides a new alternative technique for investigating chiral molecules in stereochemistry and biochemistry. Although we have restricted to the lowest-order optically active processes, we expect molecular coherence to play an equally important role in higher-order optically active processes.

3. ROTATIONAL AVERAGE OF ODD-RANK TENSORS*

3.1 Introduction

In most nonlinear optical problems, we work in a lab-fixed frame of reference, but the molecules comprising the system are oriented randomly with respect to that frame [80]. In this situation, averaging molecular quantities over the random orientation of the molecules is usually of great interest. Moreover, the three-dimensional rotational average of high-rank isotropic tensors often appears in the theory of nonlinear spectroscopy — specifically, linear dichroism [81], Raman [77, 82, 83, 84], Raman optical activity [59, 62], third harmonic scattering [85, 86, 87, 88], coherent anti-Stokes Raman scattering [21, 20] — and has been extensively examined in the physical and mathematical context in the last half century [89, 90, 91, 83, 92, 93, 94, 95, 96, 97]. For example, coherent anti-Stokes Raman scattering in optically active medium [20, 21] is a four-photon process that requires ninth-rank tensor averaging [98]. Recently, this problem is receiving renewed interest as the demand for developing nonlinear spectroscopic tools in optically active medium increases [66, 68, 24, 25]. Our method for $n = 5, 7$ recovers the results in literature whereas for rank $n = 9, 11$, explicit results are obtained for the first time [99].

Let $T_{\lambda_1\lambda_2\cdots\lambda_n}$ be a tensor of rank n, where the indices $\lambda_1, \lambda_2, \ldots, \lambda_n$ refer to coordinates in the molecule-fixed frame. Then the tensor T in the lab-fixed frame turns out to be

$$T_{i_1 i_2 \cdots i_n} = l_{i_1\lambda_1} l_{i_2\lambda_2} \cdots l_{i_n\lambda_n} T_{\lambda_1\lambda_2\cdots\lambda_n} \tag{3.1}$$

where $i_1, i_2, \ldots, i_n$ are coordinates in the lab-fixed frame. Here $l_{i_1\lambda_1}, l_{i_2\lambda_2}, \ldots, l_{i_n\lambda_n}$ denote direction cosines that can be expressed in terms of Euler angles in the z-x-z convention† [100] as

*Reprinted with permission from "On three-dimensional rotational averages of odd-rank tensors" by Tuguldur Kh. Begzjav and Reed Nessler, 2019. Physica Scripta 94, 105504, Copyright [2019] IOP Publishing.

†According to the convention z-x-z, Euler angles are defined by subsequent counterclockwise rotations of angle ϕ, θ and ψ about the axes z, x, and z, respectively. Note that the first z here is in the initial coordinate system whereas the second and third letters x and z refer to the x-axis in the intermediate set of coordinates after the first rotation and the z-axis in the intermediate set of coordinates after the second rotation.

follows,

$$l = \begin{pmatrix} C_\psi C_\phi - C_\theta S_\phi S_\psi & C_\psi S_\phi + C_\theta C_\phi S_\psi & S_\psi S_\theta \\ -S_\psi C_\phi - C_\theta S_\phi C_\psi & -S_\psi S_\phi + C_\theta C_\phi C_\psi & C_\psi S_\theta \\ S_\theta S_\phi & -S_\theta C_\phi & C_\theta \end{pmatrix}, \tag{3.2}$$

where $C_\psi = \cos\psi$, $S_\psi = \sin\psi$ and so forth. Then a straightforward method for computing the rotational average of the tensor T is an integral over Euler angles:

$$\langle T_{i_1 i_2 \cdots i_n} \rangle = \left(\frac{1}{8\pi^2} \int_0^{2\pi} \mathrm{d}\psi \int_0^{2\pi} \mathrm{d}\phi \int_0^{\pi} \sin\theta \, \mathrm{d}\theta \, l_{i_1\lambda_1} l_{i_2\lambda_2} \cdots l_{i_n\lambda_n} \right) T_{\lambda_1\lambda_2\cdots\lambda_n}. \tag{3.3}$$

The expression in parentheses in Eq. 3.3 is a rotational average of direction cosines and denoted by $I^{(n)}_{i_1 i_2 \cdots i_n;\lambda_1\lambda_2\cdots\lambda_n}$ i.e.

$$I^{(n)}_{i_1 i_2 \cdots i_n;\lambda_1\lambda_2\cdots\lambda_n} = \frac{1}{8\pi^2} \int_0^{2\pi} \mathrm{d}\psi \int_0^{2\pi} \mathrm{d}\phi \int_0^{\pi} \sin\theta \, \mathrm{d}\theta \, l_{i_1\lambda_1} l_{i_2\lambda_2} \cdots l_{i_n\lambda_n}. \tag{3.4}$$

This integral can be evaluated easily in the case of low-rank tensors but for higher-rank tensors ($n > 4$) its evaluation requires prohibitively much labor or computer time, in general.

If $f^{(n)}_r$ and $g^{(n)}_\alpha$ are the rth and αth linearly independent isotropic tensors of rank n in lab- and molecule-fixed frames, respectively then, according to Weyl's theorem [101], the rotational average of direction cosines $I^{(n)}_{i_1\cdots i_n;\lambda_1\cdots\lambda_n}$ can be uniquely expressed as a linear combination of products of the tensors $f^{(n)}_r$ and $g^{(n)}_\alpha$. Explicitly,

$$I^{(n)}_{i_1\cdots i_n;\lambda_1\cdots\lambda_n} = \sum_{r,\alpha} M^{(n)}_{r\alpha} f^{(n)}_r g^{(n)}_\alpha \tag{3.5}$$

where coefficients are denoted by $M^{(n)}_{r\alpha}$. Therefore, first of all, it is essential to establish complete bases $f^{(n)}_r$ and $g^{(n)}_\alpha$, and second, to find the matrix $\mathbf{M}^{(n)}$ of coefficients $M^{(n)}_{r\alpha}$.

Now we state some properties of isotropic tensors of rank n. For even rank n, any product of $n/2$ Kronecker deltas is isotropic, whereas for odd rank n, any product of one Levi-Civita epsilon tensor and $(n-3)/2$ Kronecker deltas is isotropic. For example, $\delta_{i_1 i_8}\delta_{i_2 i_7}\delta_{i_3 i_6}\delta_{i_4 i_5}$ and

$\epsilon_{i_1 i_3 i_5}\delta_{i_2 i_6}\delta_{i_4 i_8}\delta_{i_7 i_9}$ are isotropic tensors of rank 8 and 9. By simply permuting all indices in products one can find a full (i.e. spanning) set of isotropic tensors of a given rank n whose number is given by

$$N_n = \begin{cases} \frac{n!}{2^{n/2}(n/2)!} & \text{for even } n, \\ \frac{n!}{3\cdot 2^{(n-1)/2}((n-3)/2)!} & \text{for odd } n. \end{cases} \tag{3.6}$$

These isotropic tensors are not linearly independent in general. A method to find a linearly independent subset of the full set of N_n isotropic tensors was developed by G. F. Smith [89] using standard Young tableaux in 1968. Using this linearly independent set of isotropic tensors one can easily find the rotational average $I^{(n)}$ (i.e. $\mathbf{M}^{(n)}$).

However, the full set of N_n isotropic tensors is more convenient for expressing the rotational average of direction cosines, especially for odd-rank tensors. Therefore, we develop a new method that allows us to find the rotational average $I^{(n)}$ for odd-rank tensors in the linearly dependent set of isotropic tensors. We use a prime sign in the matrix, $\mathbf{M}'^{(n)}$, to indicate that it is with respect to the linearly dependent set or overcomplete basis.

3.2 Method

The classic late-1970s work by D. L. Andrews et al. presented a well-known method for finding the matrix $\mathbf{M}'^{(n)}$ for high-rank tensors. Primarily, this method is based on an independent set of isotropic tensors and exhibits the very simple formula

$$\mathbf{M}^{(n)} = (\mathbf{S}^{(n)})^{-1}, \tag{3.7}$$

where the contraction matrix $\mathbf{S}^{(n)}$ is given by a contracted product of two isotropic tensors as $S_{uv}^{(n)} = f_u^{(n)} f_v^{(n)} = g_u^{(n)} g_v^{(n)}$. To exploit the method one needs to know the connection between complete and overcomplete sets of isotropic tensors by using standard Young tableaux. However, we adopt an overcomplete basis to obtain rotational averages. In the special case of $n = 5, 7$, we recover the results of Ref. [83].

To describe our method, we begin with Eq. 3.5 in the overcomplete isotropic tensor basis:

$$I^{(n)}_{i_1\cdots i_n;\lambda_1\cdots\lambda_n} = \sum_{r,\alpha} M'^{(n)}_{r\alpha} f^{(n)}_r g^{(n)}_\alpha. \tag{3.8}$$

Fortunately, the matrix $M'^{(n)}_{r\alpha}$ turns out to depend only on a small number of independent coefficients, much fewer than the size $N_n \times N_n$ of the full matrix. We aim to find these independent coefficients, and in order to achieve this goal, we first analyze the structure of 3.8 to make it a set of equations for the independent coefficients in the $M'^{(n)}_{r\alpha}$ provided certian values of $I^{(n)}_{i_1\cdots i_n;\lambda_1\cdots\lambda_n}$ on the left-hand side of expression 3.8 are given. Indeed, our other work [102] presents how $I^{(n)}_{i_1\cdots i_n;\lambda_1\cdots\lambda_n}$ can be calculated using the triple integral expression 3.4. Briefly, by using known values of $I^{(n)}_{i_1\cdots i_n;\lambda_1\cdots\lambda_n}$ we make expression 3.8 into an independent set of equations and solve it for the desired independent coefficients. Next some useful properties of $\mathbf{M}'^{(n)}$ for odd-rank tensor are presented.

For odd rank n, isotropic tensors can be classified into groups, each corresponding to a unique epsilon tensor and its members distinguished only by Kronecker deltas; for example, $\epsilon_{i_1 i_2 i_3} f^{(n-3)}_r$, $\epsilon_{i_1 i_2 i_4} f^{(n-3)}_r$ and so on. Here, $f^{(n-3)}_r$ runs over the full set of isotropic tensors of rank $n-3$. The matrix $\mathbf{M}'^{(n)}$ for odd rank has a block diagonal form

$$\mathbf{M}'^{(n)}_{r\alpha} = \begin{pmatrix} [\mathbf{A}^{(n-3)}] & 0 & \dots & 0 \\ 0 & [\mathbf{A}^{(n-3)}] & \dots & \vdots \\ \vdots & \vdots & \ddots & 0 \\ 0 & \dots & 0 & [\mathbf{A}^{(n-3)}] \end{pmatrix}, \tag{3.9}$$

and each block $\mathbf{A}^{(n-3)}$ has the same structure (but not the same coefficients) as $\mathbf{M}'^{(n-3)}$ [83]. Thus, the number of independent coefficients in $\mathbf{M}'^{(n-3)}$ equals the number of independent coefficients in $\mathbf{M}'^{(n)}$. The common value, denoted by c_n for odd n, is given by the partition function $\mathrm{p}((n-3)/2, 3)$, which counts the number of partitions of $(n-3)/2$ into at most 3 parts [83]. For example, $c_n = 1, 2, 3, 4$ for $n = 5, 7, 9, 11$. We enumerate these independent coefficients $a, b, c, \dots$ using the

first c_n letters of the alphabet.

On the left-hand side of Eq. 3.8 each of the $2n$ indices can take the values x, y, z, so the tensor $I^{(n)}_{i_1\cdots i_n;\lambda_1\cdots\lambda_n}$ has 3^{2n} components. Therefore, Eq. 3.8 can be understood as a set of 3^{2n} linear equations in the $c_n \ll 3^{2n}$ variables $a, b, \ldots$. By definition, Eq. 3.8 always has the same number of linearly independent equations as the number of independent coefficients. Moreover, Eq. 3.8 is overcomplete and there are many linearly dependent equations. A practical question arises: how to shrink the overcomplete set of equations into a *minimal* set of equations by selecting a linearly independent subset?

Here, we make the brave assumption that the diagonal terms of $I^{(n)}_{i_1\cdots i_n;\lambda_1\cdots\lambda_n}$ suffice to produce equations determining the independent coefficients. By "diagonal terms" we mean that the indices satisfy $i_1 = \lambda_1$, $i_2 = \lambda_2$, …, $i_n = \lambda_n$. The number of such terms is $3^n > c_n$, so the corresponding equations

$$I^{(n)}_{i_1\cdots i_n;i_1\cdots i_n} = \sum_{r,\alpha} M'^{(n)}_{r\alpha} f^{(n)}_r g^{(n)}_\alpha \tag{3.10}$$

are still overcomplete for the independent coefficients.

To pare down Eqs. 3.10 a final time into a minimal subset, we analyze both sides of the equations in turn.

1. Left-hand side: for convenience, we denote the diagonal terms $I^{(n)}_{i_1\cdots i_n;i_1\cdots i_n}$ by $I(q, r, s)$ in the manner

$$I(q, r, s) = \langle l^q_{xx} l^r_{yy} l^s_{zz} \rangle, \tag{3.11}$$

i.e. by collecting the indices as

$$i_1 \cdots i_n = \underbrace{x\cdots x}_{q \text{ times}}\ \underbrace{y\cdots y}_{r \text{ times}}\ \underbrace{z\cdots z}_{s \text{ times}}, \tag{3.12}$$

where $q + r + s = n$. It is important to see that $I(q, r, s)$ is invariant under the permutation of indices x, y and z, or equivalently the permutation of the powers q, r and s. For example, we can swap y and z (equivalently r and s) by simultaneously rotating the lab-fixed and

molecule-fixed frames using the 90° rotation matrix

$$R = \begin{pmatrix} -1 & 0 & 0 \\ 0 & 0 & 1 \\ 0 & 1 & 0 \end{pmatrix}. \tag{3.13}$$

We have $(RlR)_{xx} = l_{xx}$, $(RlR)_{yy} = l_{zz}$ and $(RlR)_{zz} = l_{yy}$. Then from the rotational invariance of $I^{(n)}$ we obtain the desired property:

$$\langle l_{xx}^q l_{yy}^r l_{zz}^s \rangle = \langle l_{xx}^q l_{zz}^r l_{yy}^s \rangle = \langle l_{xx}^q l_{yy}^s l_{zz}^r \rangle. \tag{3.14}$$

The proof for other indices and powers is straightforward.

The essential outcome of this invariance property is that the components of $I^{(n)}_{i_1\cdots i_n;i_1\cdots i_n}$ belonging to a particular partition of n with at most 3 parts are always equal. Accordingly, we can say that a partition of n with at most 3 parts uniquely determines a component of tensor $I^{(n)}_{i_1\cdots i_n;i_1\cdots i_n}$ of rank n. Another useful property is that the components of $I^{(n)}_{i_1\cdots i_n;i_1\cdots i_n}$ vanish if exactly one or two of q, r and s are odd. This property can be seen from invariance under 180° rotation of the lab-fixed frame about one of the coordinate axes. For example, the rotation matrix about the z-axis is $R = \mathrm{diag}(-1, -1, 1)$ and this rotation requires that $q + r$ be even to have $I(q, r, s) \neq 0$. This can be seen as follows:

$$\langle l_{xx}^q l_{yy}^r l_{zz}^s \rangle = \langle (Rl)_{xx}^q (Rl)_{yy}^r (Rl)_{zz}^s \rangle = (-1)^{q+r} \langle l_{xx}^q l_{yy}^r l_{zz}^s \rangle. \tag{3.15}$$

Likewise $q + s$ and $r + s$ must be even. Briefly, $I(q, r, s)$ can be nonzero (and indeed is, as we will calculate below) only if q, r, s are all odd or all even. As $n = q + r + s$, this is the same as requiring that q, r, s have the same parity as n. Interestingly, the number of distinct nonzero components of $I(q, r, s)$ is equal to the number of the Young frames that represent the complete set of linearly independent isotropic tensors [89, 83].

2. Right-hand side: To be nonzero, an epsilon tensor in $f_r^{(n)}$ and $g_\alpha^{(n)}$ must have different values x, y, z. Consequently, if for example, the number of x components is even then one Kronecker delta symbol must get mixed indices like δ_{xy} or δ_{xz}. Therefore, each summand on the right-hand side of Eq. 3.10 is zero unless all q, r and s are odd. Appropriately, vanishing components of $I(q, r, s)$ constantly yield the trivial identity $0 = 0$, which is useless. This tells us that we must use nonzero $I(q, r, s)$ to obtain nontrivial equations. Furthermore, for any given partition $n = q + r + s$, the right-hand side of Eq. 3.10 is the same. This follows from the equivalence of the coordinate axes x, y and z.

To sum up, all $I(q, r, s)$ of a given partition $n = q+r+s$ are equal to each other and the equations belonging to the given partition are exactly the same. On the other hand, the number of partitions that provide a nonzero component of $I(q, r, s)$ is equal to the number of independent coefficients on the $M_{r\alpha}^{\prime(n)}$. This tells us that we have the same number of independent equations as variables if we select one equation for each partition $n = q + r + s$ into odd parts (if n is odd). At this point we are done with the selection of independent equations.

Next, we have to compute $I(q, r, s)$ in explicit form. Averaging is achieved by Eq. 3.4 together with 3.2. Our interest is only in odd rank and as we explained before the powers q, r, s are all odd for odd rank n. In keeping with a desire to avoid the upper-left 2×2 block as much as possible, we note that $I(q, r, s) = -\langle l_{xx}^q l_{zy}^r l_{yz}^s \rangle$ for odd n, as follows from invariance of the average under rotation of the lab-fixed frame by R from Eq. 3.13, and it is the latter average that we explicitly compute.

Recall the elementary trigonometric integrals [103]

$$\int_0^{2\pi} \mathrm{d}x \, \sin^i x \cos^j x = \begin{cases} 2\pi \frac{(i-1)!!(j-1)!!}{(i+j)!!}, & i \text{ and } j \text{ even} \\ 0, & \text{otherwise} \end{cases} \tag{3.16}$$

$$\int_0^{\pi} \mathrm{d}x \, \sin^i x \cos^j x = \begin{cases} 2\frac{(i-1)!!(j-1)!!}{(i+j)!!}, i \text{ odd and } j \text{ even.} \\ \pi \frac{(i-1)!!(j-1)!!}{(i+j)!!}, i \text{ and } j \text{ even.} \end{cases} \tag{3.17}$$

These together with Eq. 3.4 yield

$$I(q,r,s) = \frac{(r+s)!!}{(q+r)!!(q+s)!!} \sum_{i=0}^{(q-1)/2} \binom{q}{2i+1} \frac{[(q-2i-2)!!]^3 (2i+r)!!(2i+s)!!}{(q+r+s-2i)!!}. \tag{3.18}$$

In particular,

$$I(1,r,s) = \frac{r!!s!!(r+s)!!}{(r+1)!!(s+1)!!(r+s+1)!!} = \begin{pmatrix} \frac{r}{2} & \frac{s}{2} & \frac{r+s}{2} \\ \frac{1}{2} & -\frac{1}{2} & 0 \end{pmatrix}^2 \tag{3.19}$$

and

$$I(1,1,s) = \frac{1}{2(s+2)}. \tag{3.20}$$

The $3j$ symbol in Eq. 3.19 relates to rotational averages of Wigner D-matrix elements [104, Chapter 4], though we will not pursue this interesting connection. We now apply our method on low tensor ranks, namely 5 and 7, whose rotational averages are well known.

Example 1. $\mathbf{M}'^{(5)}$. There are $N_5 = 10$ different linearly dependent isotropic tensors for rank $n = 5$, composed of 10 different epsilon tensors multiplied by a Kronecker delta symbol, which is the only isotropic tensor for rank $n = 2$, namely

$$\begin{aligned}
f_1^{(5)} &= \epsilon_{i_1 i_2 i_3}\delta_{i_4 i_5}, \quad & f_6^{(5)} &= \epsilon_{i_1 i_4 i_5}\delta_{i_2 i_3}, \\
f_2^{(5)} &= \epsilon_{i_1 i_2 i_4}\delta_{i_3 i_5}, \quad & f_7^{(5)} &= \epsilon_{i_2 i_3 i_4}\delta_{i_1 i_5}, \\
f_3^{(5)} &= \epsilon_{i_1 i_2 i_5}\delta_{i_3 i_4}, \quad & f_8^{(5)} &= \epsilon_{i_2 i_3 i_5}\delta_{i_1 i_4}, \\
f_4^{(5)} &= \epsilon_{i_1 i_3 i_4}\delta_{i_2 i_5}, \quad & f_9^{(5)} &= \epsilon_{i_2 i_4 i_5}\delta_{i_1 i_3}, \\
f_5^{(5)} &= \epsilon_{i_1 i_3 i_5}\delta_{i_2 i_4}, \quad & f_{10}^{(5)} &= \epsilon_{i_3 i_4 i_5}\delta_{i_1 i_2}.
\end{aligned} \tag{3.21}$$

For rank 5, the matrix $\mathbf{M}'^{(5)}$ is a 10×10 scalar matrix since the block matrix $\mathbf{A}^{(2)}$ is just a 1×1 matrix i.e. scalar a. That is, $\mathbf{M}'^{(5)} = a\mathbf{E}$ where $\mathbf{E}$ is the 10×10 unit matrix and a is the only coefficient that needs to be determined. Consequently, the rotational average of direction cosines

can be written as

$$I^{(5)}_{i_1\cdots i_5;\lambda_1\cdots\lambda_5} = a\sum_{r,\alpha} f^{(5)}_r g^{(5)}_\alpha \tag{3.22}$$

where r and α range from 1 to 10 and its diagonal term is

$$I^{(5)}_{i_1\cdots i_5;i_1\cdots i_5} = a(\epsilon_{i_1i_2i_3}\delta_{i_4i_5}\epsilon_{i_1i_2i_3}\delta_{i_4i_5} + \epsilon_{i_1i_2i_4}\delta_{i_3i_5}\epsilon_{i_1i_2i_4}\delta_{i_3i_5} + \ldots). \tag{3.23}$$

The diagonal term $I(1,1,3) = 1/10$ according to Eq. 3.20 and the resulting equation is

$$\frac{1}{10} = I(1,1,3) = I^{(5)}_{xyzzz;xyzzz} = 3a. \tag{3.24}$$

The coefficient a can be found as $1/30$. This solution is consistent with the result obtained by others [105, 106, 83].

Example 2. $\mathbf{M}'^{(7)}$. There are $N_7 = 105$ linearly dependent isotropic tensors of rank $n = 7$. These isotropic tensors can be classified into 35 equally divided groups. Each group has the same epsilon tensor but different Kronecker deltas. For example, the first and last groups are

$$\begin{aligned} f^{(7)}_1 &= \epsilon_{i_1i_2i_3}\delta_{i_4i_5}\delta_{i_6i_7}, & f^{(7)}_{103} &= \epsilon_{i_5i_6i_7}\delta_{i_1i_2}\delta_{i_3i_4}, \\ f^{(7)}_2 &= \epsilon_{i_1i_2i_3}\delta_{i_4i_6}\delta_{i_5i_7}, & f^{(7)}_{104} &= \epsilon_{i_5i_6i_7}\delta_{i_1i_3}\delta_{i_2i_4}, \\ f^{(7)}_3 &= \epsilon_{i_1i_2i_3}\delta_{i_4i_7}\delta_{i_5i_6}, \quad \text{and} & f^{(7)}_{105} &= \epsilon_{i_5i_6i_7}\delta_{i_1i_4}\delta_{i_2i_3}. \end{aligned} \tag{3.25}$$

Each group has the same structure for Kronecker deltas. Particularly, the product of Kronecker deltas $f^{(4)}_1$ appearing in the first member of each group has indices in ascending order. The second and third isotropic tensors are obtained by certain permutations of indices of $f^{(4)}_1$. The permutations are the same for all groups.

The matrix $\mathbf{M}'^{(7)}$ in the set of 105 linearly dependent isotropic tensors has a block diagonal form. Each block $\mathbf{A}^{(4)}$ is of dimension 3×3, and has the same structure as $\mathbf{M}'^{(4)}$ given in Ref. [83]

as

$$\mathbf{A}^{(4)} = \begin{pmatrix} a & b & b \\ b & a & b \\ b & b & a \end{pmatrix}, \tag{3.26}$$

where a and b are independent coefficients. The two admissible partitions of 7 are $1, 1, 5$ and $1, 3, 3$. The corresponding components of $I^{(7)}$ are found to be $I(1, 1, 5) = 1/14$ and $I(1, 3, 3) = 9/140$ according to formulas 3.20 and 3.19. The coupled equations for a and b are

$$\begin{aligned} \frac{1}{14} &= I(1, 1, 5) = I^{(7)}_{xyzzzzz;xyzzzzz} = 15a + 30b, \\ \frac{9}{140} &= I(1, 3, 3) = I^{(7)}_{xyyyzzz;xyyyzzz} = 9a, \end{aligned} \tag{3.27}$$

where the expressions on the right-hand side follow from Eq. 3.10. The unique solution is $(a, b) = (6/840, -1/840)$, in agreement with the result of D. L. Andrews et al. [83].

3.3 Rotational average of a ninth-rank tensor

Based on the previous discussion, the matrix $\mathbf{M}'^{(9)}$ for ninth-rank tensors has a block diagonal form in the linearly dependent set which consists of products of 84 epsilon tensors and 15 isotropic tensors of rank 6. The isotropic tensors of rank 6 are given in [83], and we use the same ordering as they did to enumerate them. Then the linearly dependent isotropic tensors of rank 9 are $\epsilon_{i_1 i_2 i_3} f^{(6)}_r$, $\epsilon_{i_1 i_2 i_4} f^{(6)}_r$, ... ,$\epsilon_{i_7 i_8 i_9} f^{(6)}_r$, where $f^{(6)}_r$ is the rth isotropic tensor of rank 6 and indices are composed of unused indices in the corresponding epsilon tensor. Therefore,

$$\mathbf{M}'^{(9)} = \mathbf{E} \otimes \mathbf{A}^{(6)} \tag{3.28}$$

where

$$\mathbf{A}^{(6)} = \begin{pmatrix}
a & b & b & b & c & c & b & c & c & c & c & b & c & c & b \\
b & a & b & c & b & c & c & c & b & b & c & c & c & b & c \\
b & b & a & c & c & b & c & b & c & c & b & c & b & c & c \\
b & c & c & a & b & b & b & c & c & c & b & c & c & b & c \\
c & b & c & b & a & b & c & b & c & b & c & c & c & c & b \\
c & c & b & b & b & a & c & c & b & c & c & b & b & c & c \\
b & c & c & b & c & c & a & b & b & b & c & c & b & c & c \\
c & c & b & c & b & c & b & a & b & c & b & c & c & c & b \\
c & b & c & c & c & b & b & b & a & c & c & b & c & b & c \\
c & b & c & c & b & c & b & c & c & a & b & b & b & c & c \\
c & c & b & b & c & c & c & b & c & b & a & b & c & b & c \\
b & c & c & c & c & b & c & c & b & b & b & a & c & c & b \\
c & c & b & c & c & b & b & c & c & b & c & c & a & b & b \\
c & b & c & b & c & c & c & c & b & c & b & c & b & a & b \\
b & c & c & c & b & c & c & b & c & c & c & b & b & b & a
\end{pmatrix} \tag{3.29}$$

has the same structure as $\mathbf{M}'^{(6)}$ given in Ref. [83]. Here, $\mathbf{E}$ is the unit matrix of dimension 84×84. There are three independent coefficients which we denote a, b and c. The system of linear equations for these coefficients can be found by computing $I(1,1,7)$, $I(1,3,5)$ and $I(3,3,3)$ and using Eq. 3.10. The resulting equations are

$$\begin{aligned}
\frac{1}{18} &= 105a + 630b + 840c, \\
\frac{1}{21} &= 45a + 90b, \\
\frac{19}{420} &= 27a
\end{aligned} \tag{3.30}$$

with the solution

$$a = \frac{38}{22680}, \qquad b = -\frac{7}{22680}, \qquad c = \frac{2}{22680}. \tag{3.31}$$

Substituting the obtained numbers Eq. 3.31 into the matrix $\mathbf{A}^{(6)}$ given by Eq. 3.29 and assembling 84 copies of $\mathbf{A}^{(6)}$ into a block diagonal matrix we find the rotational average $I^{(9)}$ in the linearly dependent set of isotropic tensors.

3.4 Rotational average of an eleventh-rank tensor

In the case of eleventh-rank tensors, there are $N_{11} = 17325$ linearly dependent isotropic tensors which can be divided into 165 groups. Each group has 105 isotropic tensors determined by eighth-rank isotropic tensors. As we did in the case of $n = 9$, the matrix $\mathbf{M}'^{(11)}$ can be written as $\mathbf{M}'^{(11)} = \mathbf{E} \otimes \mathbf{A}^{(8)}$. Here, $\mathbf{A}^{(8)}$ has the same structure as $\mathbf{M}'^{(8)}$ given by D. L. Andrews et al. [92], and $\mathbf{E}$ is the unit matrix of dimension 165×165. There are four independent coefficients a, b, c and d in the matrix $\mathbf{M}'^{(11)}$; here we cast the coefficients A, B, C and D in $\mathbf{M}'^{(8)}$ in Ref. [92] into lower case. The calculation procedure is the same as we did for the ranks $n = 5, 7, 9$ and straightforward. As a result, we obtain the equations for independent coefficients as follows:

$$\begin{aligned}
\frac{1}{22} &= 945a + 11340b + 11340c + 30240d, \\
\frac{5}{132} &= 315a + 1890b + 2520d, \\
\frac{25}{693} &= 225a + 900b + 900c, \\
\frac{97}{2772} &= 135a + 270b
\end{aligned} \tag{3.32}$$

with the solution

$$\begin{aligned}
a &= \tfrac{548}{1496880}, \qquad b = -\tfrac{80}{1496880}, \\
c &= \tfrac{3}{1496880}, \qquad d = \tfrac{14}{1496880}.
\end{aligned} \tag{3.33}$$

3.5 Conclusions

We present a new method for three-dimensional rotational averages of odd-rank tensors. The method is applied to low-rank tensors $n = 5, 7$ as an example and also applied to ninth- and eleventh-rank tensors that were not known before in explicit form. The results of our method

$I^{(n)}_{i_1\cdots i_n;\lambda_1\cdots\lambda_n}$ (rotational average of odd-rank tensors) are expressed in block diagonal form in the overcomplete set of isotropic tensors. Fortunately, the number of independent coefficients that determine $I^{(n)}_{i_1\cdots i_n;\lambda_1\cdots\lambda_n}$ is just three and four for ninth- and eleventh-rank tensors, respectively. These coefficients are found in the present work and the obtained result for ninth-rank tensor averaging is used in our next work on coherent anti-Stokes Raman spectroscopy in optically active medium [98]. The obtained three-dimensional rotational averages of odd-rank tensors can be used for calculations in various types of nonlinear spectroscopy in optically active medium.

4. PERMUTATION SYMMETRY OF SUBRADIANT STATES AND ITS APPLICATION*

4.1 Introduction

Symmetries of atoms and molecules — inversion, reflection, rotation and so on — are at the heart of selection rules in atomic and molecular physics and a rich field of study [107]. Likewise, permutation symmetry is an inevitable part of investigations of systems composed of many identical atoms, molecules or spins. Indeed, an ensemble of atoms behaves differently depending on symmetry properties of its quantum state. For example, the spontaneous emission rate of N noninteracting atoms can be N times faster than the single atomic spontaneous emission rate when these atoms are in the completely symmetric single-excited state. This phenomenon was predicted by R. H. Dicke [3] and is called superradiance [108, 109]. On the other hand, subradiant states of such a system with decreased spontaneous emission decay rates due to symmetry are potentially stable against collective spontaneous emission and are of interest in quantum information processing with low decoherence.

In recent years, much effort has been given to experimental investigation of subradiant states and their application to quantum memory. The earliest evidence of experimental demonstration of subradiance is reported in [4], where the subradiant character of a full statistical mixture of Zeeman sublevels is tested in gallium atomic vapor. Later, the experimental observation of subradiant states tends to be done with a small number of natural or artificial atoms for the purpose of quantum computing and communication. For example, two trapped ions [5, 6], plasmons [7, 8], two superconducting transmon qubits [9] and diatomic molecules in optical lattice [10, 11] are exploited for this purpose. However, we remark here the most potentially important system: superconducting quantum qubits (artificial atoms) in circuit quantum electrodynamics that enable a spatial resolution of an individual qubit in the collective superradiant and subradiant state. Consequently, a superconducting qubit system [110, 111, 112] supports the experimental realization

*Reprinted with permission from "On permutation symmetry of subradiant states and its application" by Tuguldur Kh. Begzjav, Luojia Wang, and Reed Nessler, 2019. Physica Scripta 94, 094001, Copyright [2019] IOP Publishing.

of the idea theoretically suggested by A. Beige et al. [113] and refined in [114] where a chain of N two-level systems is coherently excited by laser beams with a given relative phase for subradiant state generation. Here, we call this method the sidewise excitation method. Recent works [115, 116, 117, 9, 118] report that the sidewise excitation method is successfully tested for superconducting qubits in circuit quantum electrodynamics. Although experimental realization of subradiant states is somewhat difficult, various aspects of subradiant states are widely studied theoretically [119, 120, 121, 122, 123, 124, 125, 126].

In this work, inspired by previous works on the sidewise excitation method, we address symmetry properties of single- and double-excited subradiant states. We show how to use symmetric groups to study the single- and double-excited subradiant states. In doing so, we obtain general formulas for single- and double-excited subradiant states for an arbitrary number of two-level systems. The general formulas are extremely practical since they show a general character of relative phases between individual two-level systems and weights of each two-level system. Moreover, the obtained relative phase and weight information may determine appropriate relative phases and amplitudes of laser beams to produce a given subradiant state in the case of two-level atomic system, and also may determine circuit design in the case of superconducting qubits. This chapter is organized as follows. In the following section, permutation symmetry of subradiant states is examined and subradiant states are classified according to standard Young tableaux. The Young operator method is applied to subradiant states in section 4.3. In section 4.4, the sidewise excitation method for generating single-excited subradiant states is considered. Conclusions are given in section 4.5.

4.2 Symmetric properties of subradiant states

It is said that the nature of superradiance and subradiance is constructive and destructive interference [119] between oscillating dipoles of a number of emitters, but symmetry properties provide a deeper mathematical explanation for super- and subradiance. Specifically, selection rules of the transitions in an atomic system can be provided in an elegant way by exploiting irreducible representations of symmetric groups. This is one example of the ubiquitous applications of group theory to physics. We will briefly go through this below. Another recent application of group the-

ory is that symmetric groups are exploited to speed up a complicated — and otherwise untractable — numerical computation of dynamics of permutation-symmetric N multi-level system coupled with dissipating electromagnetic bath and external driving field [12, 13, 14, 15, 16, 17]. This is a fascinating area of research since it permits to reduce computational complexity from exponential dependence on N to polynomial scaling $\sim N^3$. This is not all, since SU(4) symmetry of quantum master equation of N two-level system coupled to single-mode photon field is also studied [18], and it provides a powerful method to solve the quantum master equation of an atomic system. With this brief remark on the group theoretical approach to superradiance and subradiance, we will continue here with the general framework of symmetry of superradiant and subradiant states which can be found elsewhere.

According to the seminal paper by Dicke [3], an ensemble of N two-level atoms exposes the same algebraic structure as an N half-spin system. Therefore, eigenstates of the total Hamiltonian of non-interacting two-level atoms can be described by two quantum numbers: Dicke's cooperation number R and the population difference $M = (N_a - N_b)/2$, where N_a and N_b are the number of atoms in the excited and ground states, respectively. The quantum numbers R and M are the two-level atomic analogy of total spin quantum number s and its z-component m of the N half-spin system. Therefore, the cooperation number R can take a value $0, 1, \ldots, N/2$ for even N and $1/2, 3/2, \ldots, N/2$ for odd N. For any given cooperation number R, the population difference M varies from $-R$ to R with step size 1. The eigenstates are denoted by $|R, M\rangle$. We note that all the eigenstates that we describe here refer to eigenstates constructed by the genealogical method [127, 128, 129]. For illustrative purposes, we give an example of genealogical eigenstates of a system with $N = 4$ atoms in Figure 4.1 and Table 4.1. It is interesting to see degeneracy for eigenstates $|1, M\rangle$. This degeneracy is an intrinsic property of our system of interest.

Since the total Hamiltonian of non-interacting two-level atoms is invariant under exchange of any pair of atoms in the system, the symmetric group S_N of degree N enables us to understand the structure of eigenstates $|R, M\rangle$ of the total Hamiltonian. Moreover, all the degenerate eigenstates $|R, M\rangle$ with given quantum numbers R and M span an irreducible subspace of the symmetric

group S_N which is associated to a Young tableau of shape $\{N/2+R, N/2-R\}$ (we will go through all details below). The dimension of the spanned irreducible subspace is described by the degeneracy of the state $|R, M\rangle$. In the case of our example $N = 4$, each state $|2, M\rangle$ of a given $M \in \{2, 1, 0, -1, -2\}$, each 3 states $|1, M\rangle$ of a given $M \in \{1, 0, -1\}$ and pair of states $|0, 0\rangle$ span respectively one-dimensional $\chi^{(1)}$, three-dimensional $\chi^{(4)}$ and two-dimensional $\chi^{(3)}$ irreducible subspaces. The notation $\chi^{(i)}$ is described in [107] page 187. To be clear, the single-excited triple degenerate eigenstates $|1, -1\rangle$ span a three-dimensional irreducible subspace $\chi^{(4)}$, i.e. a three-dimensional irreducible representation (or matrix) of S_4 (see Figure 4.1). For further information such as the character table and irreducible matrices for the S_4 group we refer readers to Ref. [107] pages 187 and 255.

As we stated above, one useful application of group theory to the problem of N identical two-level systems is to specify forbidden transitions, and consequently, to classify subradiant states. As described elsewhere, the strength of the transition from state $|R, M\rangle$ to state $|R', M'\rangle$ is proportional to the absolute square of matrix element $\langle R', M'| \sum_i \hat{d}_i |R, M\rangle$, where $\hat{d}_i$ is the ith atomic dipole moment operator. Since the total dipole moment operator $\sum_i \hat{d}_i$ is invariant under any permutation of atoms and the states belonging to different irreducible subspaces are orthogonal to each other, one can conclude here that the transitions between two different irreducible subspaces are forbidden. For example, the transitions $|1, -1\rangle \rightarrow |2, -2\rangle$ are not allowed because the states $|1, -1\rangle$ and $|2, -2\rangle$ belong to different irreducible subspaces $\chi^{(4)}$ and $\chi^{(1)}$, respectively. This is why the states $|1, -1\rangle$ are subradiant in the sense that the transitions $|1, -1\rangle \rightarrow |2, -2\rangle$ are forbidden.

There is a one-to-one correspondence between the standard Young tableaux [130, 128] of size N having not more than two rows, which are of the shape $\{N/2+R, N/2-R\}$, and the eigenstates generated by the genealogical method, which constructs the N-atom eigenstates from the $(N-1)$-atom eigenstates by subtraction or addition of the cooperation number R and using the appropriate Clebsch–Gordan coefficients (see Appendix A for details). When standard Young tableaux are used to visualize the genealogical construction, the number in each box represents the construction

scheme in each step in such a way that numbers for the addition (subtraction) process of R are arranged in the first (second) row. Therefore, subradiant states $|\frac{N}{2}-1, M\rangle$ are described by the standard Young tableaux with only one box in the second row. Then, it is easy to enumerate the subradiant states $|\frac{N}{2}-1, M\rangle$ by n, the number of boxes in the first row before the number goes to the second row. Then it is trivial that $n \in \{1, 2, \ldots, N-1\}$. For example, the standard Young tableaux for the degenerated single-excited subradiant states $|1, -1\rangle$ for $N = 4$ are shown in Figure 4.1.

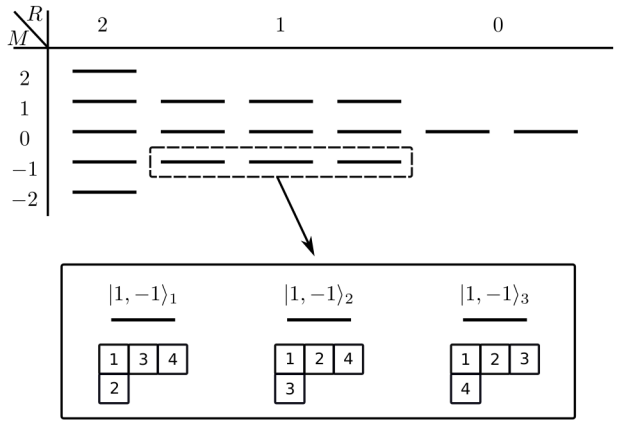

Figure 4.1: Eigenstates for four two-level atomic system. In the inset, single-excited subradiant states and corresponding standard Young tableaux are shown. Reprinted with permission from [19].

4.3 Young operator method for studying subradiant states

The Young operator is the key tool to construct an irreducible representation of the symmetric group S_N of degree N (see Appendix E). The Young operator associated to a given Young tableau is an idempotent generator of a primitive left ideal of the group algebra $\mathbb{C}S_N$ [131]. Any element u in the generated primitive left ideal maps a given trial state $|\psi\rangle$ into either the state $|\psi\rangle_{\text{ir}}$ in

irreducible subspace of S_N associated with the given Young tableau, or zero state [132], that is

$$u|\psi\rangle = |\psi\rangle_{\text{ir}} \qquad \text{or} \qquad 0. \tag{4.1}$$

For example, the Young operator E_2 associated to standard Young tableau $\begin{array}{|c|c|c|}\hline 1 & 2 & 4 \\ \hline 3 \\ \cline{1-1}\end{array}$ and single-excited subradiant state $|1,-1\rangle_2$ is given by

$$E_2 = (e + (12) + (14) + (24) + (124) + (142))\,(e - (13))\,, \tag{4.2}$$

where the parentheses denote the cyclic permutation of numbers inside. This Young operator E_2 with the trial function $|\psi\rangle = |a_1, b_2, b_3, b_4\rangle$ provides us the state

$$E_2|\psi\rangle = 2|a_1, b_2, b_3, b_4\rangle + 2|b_1, a_2, b_3, b_4\rangle + 2|b_1, b_2, b_3, a_4\rangle - 6|b_1, b_2, a_3, b_4\rangle, \tag{4.3}$$

which is contained in a three-dimensional irreducible subspace of S_4. The explicit form of Young operators of nth standard Young tableaux of given shape is given by [107]

$$E_n = \mathcal{R}_n \mathcal{C}_n, \tag{4.4}$$

where $\mathcal{R}_n$ and $\mathcal{C}_n$ are respectively symmetrizer and antisymmetrizer over row and column subgroups.

However, the Young operator described above does not provide the genealogical eigenstates of interest, e.g. the state (4.3) obtained by E_2 is not the genealogical eigenstate $|1,-1\rangle_2$. Therefore, we recall genealogically adapted Young operators $E_{g,n}$ for nth standard Young tableaux of given shape. Here, the subscript g indicates that operator is genealogically adapted. These operators map a trial state into either unnormalized genealogical eigenstates in the irreducible subspace of S_N or zero, i.e. $E_{g,n}|\psi\rangle \mapsto |R, M\rangle_n$ or 0. The operator $E_{g,n}$ of nth standard Young tableaux of given

shape is described by [133]

$$E_{g,n} = E_n^{(1)} E_n^{(2)} \cdots E_n^{(N-1)} E_n^{(N)}, \tag{4.5}$$

where $E_n^{(1)}$ is a conventional Young operator associated to the standard Young tableau of given shape without $N-1$ boxes. Thus, there is only one box with number 1 for $E_n^{(1)}$. Similarly, $E_n^{(2)}$ has only two boxes with numbers 1 and 2, and so on. For instance, $E_n^{(3)}$ for standard Young tableau $\begin{array}{|c|c|c|}\hline 1 & 2 & 4 \\ \hline 3 \\ \cline{1-1}\end{array}$ is the conventional Young operator associated to standard Young tableau $\begin{array}{|c|c|}\hline 1 & 2 \\ \hline 3 \\ \cline{1-1}\end{array}$.

Next, consider the standard Young tableau specifically given in Figure 4.2(a). The Young operator $E_{g,n}$ for this tableau is

$$E_{g,n} = \mathcal{R}_n^{(1)} \mathcal{R}_n^{(2)} \cdots \mathcal{R}_n^{(n-1)} \mathcal{R}_n^{(n)} \mathcal{R}_n^{(n+1)} \mathcal{C}_n^{(n+1)} \cdots \mathcal{R}_n^{(N)} \mathcal{C}_n^{(N)}, \tag{4.6}$$

where $\mathcal{R}_n^{(j)}$ and $\mathcal{C}_n^{(j)}$ are the symmetrizer and antisymmetrizer of the Young operator $E_n^{(j)}$, respectively. We here note that there is no column operator until $j = n+1$. Single-excited subradiant states $|\frac{N}{2}-1, -\frac{N}{2}+1\rangle_n$ are our main interest. Therefore, let $|\psi\rangle_j^{(s)} = |b_1, b_2, \ldots, b_{n+1}, \ldots, a_j, \ldots\rangle$ be the jth possible single-excited trial function to obtain the genealogical single-excited eigenstate $|\frac{N}{2}-1, -\frac{N}{2}+1\rangle_n$. Since $\mathcal{C}_n^{(N)} = (e - (1, n+1))$, the product $\mathcal{C}_n^{(N)} |\psi\rangle_j^{(s)}$ vanishes unless $j = 1$ or $j = n+1$. Then we choose $j = 1$ and

$$\begin{aligned} \mathcal{C}_n^{(N)} |\psi\rangle_1^{(s)} &= (e - (1, n+1)) |\psi\rangle_1^{(s)} \\ &= |a_1, \ldots, b_{n+1}, \ldots\rangle - |b_1, \ldots, a_{n+1}, \ldots\rangle. \end{aligned} \tag{4.7}$$

It is easy to see that

$$\begin{aligned} &\mathcal{C}_n^{(k)} R_n^{(k+1)} \left(|a_1, \ldots, b_{n+1}, \ldots\rangle - |b_1, \ldots, a_{n+1}, \ldots\rangle \right) \\ &\quad \sim \left(|a_1, \ldots, b_{n+1}, \ldots\rangle - |b_1, \ldots, a_{n+1}, \ldots\rangle \right), \end{aligned} \tag{4.8}$$

where $n+1 \leq k \leq N-1$, and we drop an unnecessary factor. Therefore, we obtain

$$\begin{aligned} E_{g,n}|\psi\rangle_1^{(s)} &\sim \mathcal{R}_n^{(1)} \cdots \mathcal{R}_n^{(n+1)} \mathcal{C}_n^{(N)} |\psi\rangle_1^{(s)} \\ &= \mathcal{R}_n^{(1)} \cdots \mathcal{R}_n^{(n+1)} \left(|a_1, \ldots, b_{n+1}, \ldots\rangle - |b_1, \ldots, a_{n+1}, \ldots\rangle \right), \end{aligned} \tag{4.9}$$

which is calculated as

$$E_{g,n}|\psi\rangle_1^{(s)} \sim \sum_{j=1}^{n} |b_1, \ldots, a_j, \ldots\rangle - n|b_1 \ldots, a_{n+1}, \ldots\rangle. \tag{4.10}$$

Finally, we obtain the normalized single-excited subradiant state as follows:

$$\begin{aligned} E_{g,n}|\psi\rangle_1^{(s)} &\sim |\frac{N}{2}-1, -\frac{N}{2}+1\rangle_n \\ &= \frac{1}{\sqrt{n(n+1)}} \sum_{j=1}^{n} |b_1, \ldots, a_j, \ldots\rangle - \sqrt{\frac{n}{n+1}} |b_1 \ldots, a_{n+1}, \ldots\rangle. \end{aligned} \tag{4.11}$$

According to the expression (4.11), the single-excited subradiant state $|\frac{N}{2}-1, -\frac{N}{2}+1\rangle_n$ is completely symmetric under any permutation within the set of the first n atoms and also the set of the last $N-n+1$ atoms. However, the subradiant state 4.11 is neither symmetric nor antisymmetric under permutations that contain the $(n+1)$th atom. In addition, the last $N-n+1$ atoms are all in the ground state $|b\rangle$. The reason for these properties of subradiant state 4.11 is clear from the standard Young tableau illustrated in Figure 4.2(a). As a result, in the case of $N=4$, it is easy to write down subradiant states just using the standard Young tableaux depicted in Figure 4.1. We illustrate the obtained three single-excited subradiant states $|1,-1\rangle$ for $N=4$ in Table 4.1. Finally, it is worth mentioning that the operator (4.6) can take the shortened form

$$E'_{g,n} = \mathcal{R}_n^{(n)} \mathcal{C}_n^{(N)}, \tag{4.12}$$

which is only valid for single-excited trial functions.

This type of analysis can be easily extended to double-excited subradiant states $|\frac{N}{2}-1, -\frac{N}{2}+2\rangle$

Subradiant states	Explicit form
$\|1,-1\rangle_1$	$\frac{1}{\sqrt{2}}(\|a_1,b_2,b_3,b_4\rangle - \|b_1,a_2,b_3,b_4\rangle$
$\|1,-1\rangle_2$	$\frac{1}{\sqrt{6}}(\|b_1,a_2,b_3,b_4\rangle + \|a_1,b_2,b_3,b_4\rangle) - \sqrt{\frac{2}{3}}\|b_1,b_2,a_3,b_4\rangle$
$\|1,-1\rangle_3$	$\frac{1}{\sqrt{12}}(\|b_1,b_2,a_3,b_4\rangle + \|a_1,b_2,b_3,b_4\rangle + \|b_1,a_2,b_3,b_4\rangle) - \sqrt{\frac{3}{4}}\|b_1,b_2,b_3,a_4\rangle$

Table 4.1: Genealogically constructed single-excited subradiant states for four two-level atoms. Reprinted with permission from [19].

that belong to the same irreducible subspace $\chi^{(4)}$ as the single-excited subradiant states $|\frac{N}{2}-1,-\frac{N}{2}+1\rangle$. Using the Young operator 4.6 and trial function $|a_1,a_2,b_3,\ldots,b_N\rangle$ we obtain a general formula for double-excited subradiant states $|\psi\rangle^{(d)}$ as

$$|\psi\rangle^{(d)}_{N-1} = \frac{1}{\sqrt{N(N-1)(N-2)}} \quad \Big(\sum_{\substack{i=1\\ i\neq j}}^{N-1}\sum_{j=1}^{N-1}|\ldots,a_i,\ldots,a_j,\ldots\rangle - (N-2)\sum_{i=1}^{N-1}|\ldots,a_i,\ldots,a_N\rangle\Big) \tag{4.13}$$

for $n=N-1$, and for other values of $1\leq n\leq N-2$

$$|\psi\rangle^{(d)}_{n} = \frac{1}{\sqrt{n(n+1)(N-2)}} \quad \Big(\sum_{\substack{i=1\\ i\neq j\\ i\neq n+1}}^{N}\sum_{j=1}^{n}|\ldots,a_i,\ldots,a_j,\ldots\rangle - (n-1)\sum_{i=1}^{n}|\ldots,a_i,\ldots,a_{n+1},\ldots\rangle - n\sum_{i=n+2}^{N}|\ldots,a_i,\ldots,a_{n+1},\ldots\rangle\Big). \tag{4.14}$$

The equations 4.13 and 4.14 are generic and valid for any number N of atoms. For example, the double-excited subradiant state $|5/2,-3/2\rangle_5$ for $N=7$ is given in Appendix F. It is not difficult to see that double-excited subradiant states 4.13 and 4.14 are also completely symmetric with respect to permutations among the first n atoms and also among the last $N-n+1$ atoms. This permutation symmetry can be easily observed by examining the corresponding standard Young tableaux.

In the next section, we will show how the permutation symmetry of single-excited subradiant states is important for the phase-controlled sidewise excitation method.

4.4 Sidewise excitation method for generation of single-excited subradiant states

Let us assume that we are able to shine spatially resolved light sources from the side upon the individual atoms of a one-dimensional array of N two-level atoms, as shown in Figure 4.2(b). Then the interaction Hamiltonian is given by [134]

$$H = \frac{1}{2}\hbar g \sum_{i=1,\ldots,N} (\hat{\sigma}_i^\dagger \hat{a}_i + \hat{a}_i^\dagger \hat{\sigma}_i), \tag{4.15}$$

where g is the atom-field coupling constant. The operator $\hat{\sigma}_i^\dagger$ ($\hat{\sigma}_i$) is ith atomic raising (lowering) operator and $\hat{a}_i^\dagger$ ($\hat{a}_i$) is a field creation (annihilation) operator in the ith arm (see Figure 4.2(b)). The Hamiltonian 4.15 is very generic since it can model any quantum two-level system from a simple atom to plasmon, exciton and superconducting qubits. Having the single-photon state of excitation in the form

$$\psi_{\text{ph}} = \sum_j c_j |0_1, 0_2, \ldots, 1_j, \ldots, 0_N\rangle, \tag{4.16}$$

where subscript j represents the photon state of light directed to the jth atom and c_j is a coefficient, the resonant interaction of the photon and atoms is governed by the unitary evolution operator [114]

$$\begin{aligned} \hat{U}(\tau)|b,1\rangle &= -i|a,0\rangle, \\ \hat{U}(\tau)|b,0\rangle &= |b,0\rangle. \end{aligned} \tag{4.17}$$

Here, interaction time τ is adjusted as $\tau = \pi/g$ to get a completely excited atom [135]. When we denote the unitary evolution operator of the kth atom–field system by $\hat{U}_k(\tau)$, the quantum state of the entire system after interaction is given by

$$\begin{aligned} &\textstyle\prod_{k=1}^N \hat{U}_k(\tau)|b_1, b_2, \ldots, b_N\rangle \sum_j c_j |0_1, 0_2, \ldots, 1_j, \ldots, 0_N\rangle \\ &\quad = -i \textstyle\sum_j c_j |b_1, b_2, \ldots, a_j, \ldots, b_N\rangle |0_1, 0_2, \ldots, 0_N\rangle, \end{aligned} \tag{4.18}$$

where initially all atoms are in the ground state $|b\rangle$. Note that the interaction results in an atomic state of the same structure as the initial single-photon state (4.16). At the same time the initial single-photon state is transformed into the vacuum state $|0_1, 0_2, \ldots, 0_N\rangle$. Therefore, once we obtain a single-photon subradiant state, the subradiant state of the atomic system can be easily produced by resonant coupling between single-photon and atomic system, and by adjusting the interaction time τ.

Next we describe our method for creating single-excited subradiant states for an N-atom system according to the above results. There are three rules as follows:

1. For standard Young tableaux shown in Figure 4.2(a), the subradiant state is symmetric under permutation of the first n atoms. This symmetry can be established by passing an incident photon through $n-1$ beam splitters (BS_2 to BS_n) and reflecting from a mirror M (see Figure 4.2(b)). The last beam splitter BS_{n+1} is for producing two terms in (4.11).

2. The reflected photon from the jth beam splitter goes to the jth atom. For the $(n+1)$th atom, $+\pi/2$ phase shifter must be applied. For other atoms $-\pi/2$ phase shifters are applied.

3. Reflectance and transmittance of the beam splitter BS_{n+1} must be $\sqrt{n/(n+1)}$ and $\sqrt{1/(n+1)}$, respectively. For the other beam splitters, the reflectance of the jth beam splitter is given by $r_j = 1/\sqrt{j}$.

Following the above rules, we present an example for a 4-atom system. There are three single-excited subradiant states for $N = 4$ shown in Table 4.1. In the case of $n = 1$, the setup is straightforward (see Figure 4.3(a)), and it is equivalent to that presented in[114]. Since the calculation is straightforward, let us only consider the case $n = 3$. The reflectance of beam splitter BS_4 is given by $\sqrt{n/(n+1)} = \sqrt{3/4}$. Beam splitters BS_3 and BS_2 have reflectance $1/\sqrt{3}$ and $1/\sqrt{2}$, respectively. Therefore, initial state $|0_1, 0_2, 1_3, 0_4\rangle$ transforms to the following state after passing BS_4:

$$\psi_{\text{BS4}} = \frac{1}{\sqrt{4}}|0_1, 0_2, 1_3, 0_4, \rangle - \sqrt{\frac{3}{4}}|0_1, 0_2, 0_3, 1_4\rangle. \tag{4.19}$$

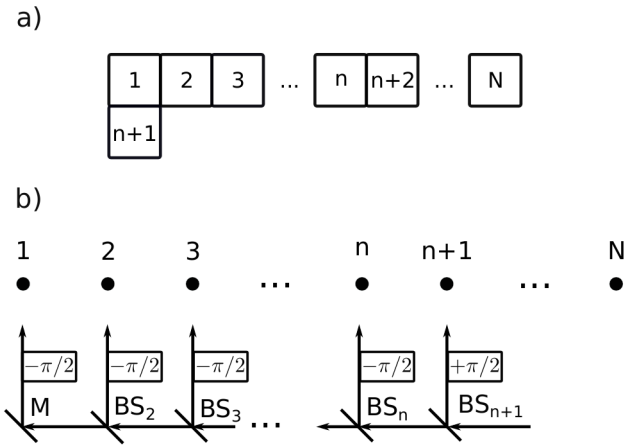

Figure 4.2: Standard Young tableau for single-excited subradiant state $|\frac{N}{2}-1,-\frac{N}{2}+1\rangle_n$ is illustrated in (a) and corresponding sidewise excitation setup with proper phase shifter ($-\pi/2$ and $+\pi/2$) is shown in (b). Atoms are depicted by black dots. BS and M stand for beam splitters and mirror, respectively. Reprinted with permission from [19].

The relative phase of the above state is determined by the $+\pi/2$ phase shifter shown in Figure 4.3(c). Transmitted light through BS_4 i.e. the first term in (4.19) is directed into BS_3. After passing through beam splitter BS_3 we obtain state of light as follows:

$$\psi_{\text{BS3}} = \tfrac{1}{\sqrt{12}}|0_1,0_2,1_3,0_4\rangle + \sqrt{\tfrac{2}{12}}|0_1,1_2,0_3,0_4\rangle - \sqrt{\tfrac{3}{4}}|0_1,0_2,0_3,1_4\rangle. \tag{4.20}$$

Again, the phase of the reflected light is changed by $-\pi/2$ phase shifter (the first term in (4.20)). In the same way, after passing through beam splitter BS_2 along with the $-\pi/2$ phase shifter we have the single photon in the following state:

$$\begin{aligned}\psi_{\text{BS2}} &= \tfrac{1}{\sqrt{12}}|0_1,0_2,1_3,0_4\rangle + \tfrac{1}{\sqrt{12}}|1_1,0_2,0_3,0_4\rangle \\ &+\tfrac{1}{\sqrt{12}}|0_1,1_2,0_3,0_4\rangle - \sqrt{\tfrac{3}{4}}|0_1,0_2,0_3,1_4\rangle.\end{aligned} \tag{4.21}$$

This is a specific example of the general state (4.11). Interaction of the atomic system with light in

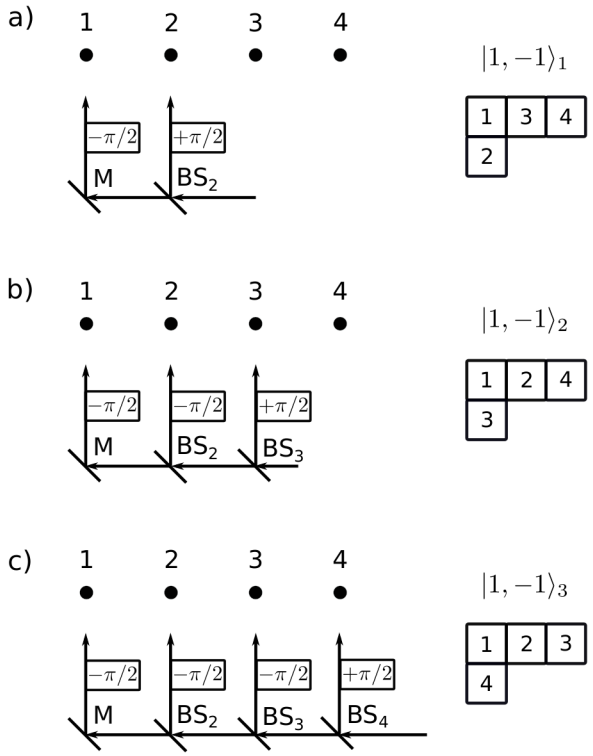

Figure 4.3: Example of four two-level atoms. Beam splitter arrangements of sidewise excitation method for creation of single-excited subradiant states $|1,-1\rangle_1$, $|1,-1\rangle_2$ and $|1,-1\rangle_3$ are shown on the left (a), (b) and (c), respectively. On the right, corresponding standard Young tableaux are depicted. Notations of elements are the same as in Figure 4.2. Reprinted with permission from [19].

the state given by (4.21) provides an atomic state

$$|1,-1\rangle_3 = -i \quad \Big[\tfrac{1}{\sqrt{12}}\left(|b_1,b_2,a_3,b_4\rangle + |a_1,b_2,b_3,b_4\rangle + |b_1,a_2,b_3,b_4\rangle\right) - \sqrt{\tfrac{3}{4}}|b_1,b_2,b_3,a_4\rangle\Big]. \tag{4.22}$$

This is our desired single-excited subradiant state $n = 3$ for the 4-atom system. We hope this technique may work also for double-excited subradiant states. Finally, we close this section by giving some discussion on experimental realization.

It is worth mentioning that experimental realization of sidewise excitation method for subradiant states has a fatal flaw in the case of a natural two-level atomic chain, namely the failure

of spatial resolution of nearly spaced two-level atoms by laser beams with larger spot sizes than inter-atomic spacing. Fortunately, in recent years it is experimentally proven that superconducting qubits in circuit quantum electrodynamics can be used for sidewise excitation method [115, 9]. There is no restriction on spatial resolution since a coplanar wave-guide resonator permits one to spatially resolve individual superconducting qubits via microwave beams. Expressions 4.11, 4.13 and 4.14 can be used for relative phase and weight determination and engineering of circuit design for superconducting qubits.

4.5 Conclusions

In summary, we give a complete mathematical treatment of symmetry properties of single- and double-excited subradiant states in this chapter. Thereby, the symmetric group on N identical atoms allows us to understand the symmetry of single- and double-excited subradiant states, and we found the general expression for those states. Furthermore, we present how to generalize the sidewise excitation method for arbitrary N in the case of single-excited subradiant states. In doing so, a simple rule for arrangement of beam splitters is derived from symmetry properties of single-excited subradiant states. The relative magnitude of the terms in subradiant states is imprinted on reflectance and transmittance of the beam splitters whereas relative phase is adjusted by applying $-\pi/2$ or $+\pi/2$ phase shifters. The proposed rule for beam splitter arrangement can be applied to any number of two-level atoms.

Even though in the current work, the sidewise excitation method is described and explained in the example of chained two-level atoms, the idea of sidewise excitation can be directly applied to a system of N superconducting qubits. Former systems failed in the sense of spatial resolution of laser beams with large spot size whereas the latter system does not. Therefore, we recommend superconducting qubits in circuit quantum electrodynamics for experimental demonstration of single- and double subradiant states, and the circuit design can be determined by our above obtained expressions 4.11, 4.13 and 4.14.

5. FANO-AGARWAL COUPLINGS AND NON-ROTATING WAVE APPROXIMATION IN SINGLE-PHOTON TIMED DICKE SUBRADIANCE*

5.1 Introduction

Cooperative spontaneous emission from an atomic ensemble has been a well-established problem of interest in quantum optics since the pioneering work of Dicke in 1954 [3]. The subject has gained renewed interest in recent years when the problem of single-photon absorption by a collection of resonant two-level atoms has been considered [41, 136, 109, 137, 138]. The consequential phenomenon of single-photon superradiance is a pure quantum many-body effect in which a system evolves into an entangled state [139] and real and virtual photons are exchanged among different atoms in the ensemble through the interaction field. The inclusion of virtual transitions and Lamb shifts in the problem turns out to bring fascinating insights related to the field of quantum electrodynamics [140, 141, 142]. Accordingly, in the last decade single-photon superradiance has witnessed a flurry of research activity with a wide range of applications in quantum optics, quantum information and condensed-matter physics [41, 143, 144, 145, 146, 147, 148, 149].

In the standard treatment of the problem a collection of N identical two-level atoms with a ground (excited) state $|b\rangle$ ($|a\rangle$) with transition frequency $E_a - E_b = \hbar\omega$ is considered. When a single photon is collectively absorbed, the system forms a superposition state in which $\beta_i(r_{ij}, t)$ describes the probability amplitude associated with the i-th member of the state ($t_{ij} = |r_i - r_j|$ is the inter-atomic separation between the i-th atom and some reference atom j). If the virtual processes, polarization of light and retardation effects are ignored, the resultant time evolution of $\beta_i(t)$ under the Markov approximation follows [150, 151, 152]:

$$\frac{\partial\beta_i(t, r_{ij})}{\partial t} = -\frac{\gamma}{N}\sum_{j=1}^{N}\frac{\sin(k_0|r_i - r_j|)}{(k_0|r_i - r_j|)}\beta_j(t, r_{ij}), \tag{5.1}$$

*Reprinted with permission from "Fano-Agarwal couplings and non-rotating wave approximation in single-photon timed Dicke subradiance" by Imran M. Mirza and Tuguldur Begzjav, 2016. Europhysics Letters 114, 24004, Copyright [2016] IOP Publishing.

where γ is the single-atom decay rate and $k_0 = \omega/c$ with c being the speed of light. The problem becomes even more richer when the virtual processes are also incorporated. In that case it is known that the time evolution of $\beta_i(t, r_{ij})$ involves an exponential kernel rather than a sine kernel [153],

$$\frac{\partial \beta_i(t, r_{ij})}{\partial t} = \frac{i\gamma}{N} \sum_{j=1}^{N} \frac{\exp(ik_0|r_i - r_j|)}{(k_0|r_i - r_j|)} \beta_j(t, r_{ij}). \tag{5.2}$$

The single-photon "timed" Dicke (TD) state $|+\rangle_{\vec{k}_0}$ was first introduced by Scully et al. in refs. [41, 154]:

$$|+\rangle_{\vec{k}_0} = \frac{1}{\sqrt{N}} \sum_{j=1}^{N} \mathrm{e}^{i\vec{k}_0 \cdot \vec{r}_j} |b_1 b_2 \ldots a_j \ldots b_N\rangle, \tag{5.3}$$

where $|b_1 b_2 \ldots a_j \ldots b_N\rangle$ is a Fock state in which an atom at the j-th location is excited and all other atoms are in the ground state. On the contrary to the ordinary Dicke (OD) state: $|+\rangle = \frac{1}{\sqrt{N}} \sum_{j=1}^{N} |b_1 b_2 \ldots a_j \ldots b_N\rangle$, in the TD states the atoms in the ensemble are excited at different times depending on their positions in the ensemble (as manifested by the phase factors which can also be interpreted as the timing factors through $t_j = \vec{k}_0 \cdot \vec{r}_j/\omega$).

Despite the extensive work on the single-photon superradiance, single-photon subradiance has been less studied essentially due to the weak interaction of subradiant states with the environment and their elevated sensitivity on non-radiative damping processes. However, recently subradiance has started to draw both theoretical and experimental attention [114, 155, 11, 156, 123] due to their promising applications in quantum information storage. In this context, Scully has introduced and analyzed a new class of TD subradiant states [114]. The first member in this class is the $|-\rangle_{\vec{k}_0}$ state which is expressed as

$$|-\rangle_{\vec{k}_0} = \frac{1}{\sqrt{2N_2}} \sum_{j,j'}^{2} \left(\mathrm{e}^{i\vec{k}_0 \cdot \vec{r}_j} |a_j b_{j'}\rangle - \mathrm{e}^{i\vec{k}_0 \cdot \vec{r}_{j'}} |b_j a_{j'}\rangle \right) |\{b_j b_{j'}\}\rangle, \tag{5.4}$$

where primed and unprimed indices mark the atoms belonging to two different sections of the sample. As emphasized in ref. [114] the basic motivation of generating the $|-\rangle_{\vec{k}_0}$ state is to

utilize it for single-photon storage on a time scale shorter than γ^{-1} . However, any kind of virtual processes and their influence on the decay of this (and other) new kind of subradiant states has not been left as an open question in that paper. In the present work, we focus on this problem in detail.

There are two types of virtual processes we shall address in this context: 1) Fano-Agarwal (FA) couplings that arise due to the interaction of discrete atomic energy levels with environmental mode continuum and 2) virtual processes arising from the non-rotating wave approximation (NRWA). In the presence of pure FA couplings, we find that the individual populations tends to achieve smaller highest values as the number of atoms in the atomic ensemble are increased; however, the summed up effect of all FA couplings remains substantial. Moreover, we notice that the dominant FA coupling between individual TD states depends on the initial state of the system. Finally, the inclusion of the scalar Lamb shift and NRW terms yields a small effect on the decay of the $|+\rangle_{\vec{k}_0}$ state, while $|-\rangle_{\vec{k}_0}$ (and other TD subradiant states) shows markedly fast decay.

In the next section, we shall begin by introducing the system model and a transformation between the Fock state basis and the TD basis is presented.

5.2 System Hamiltonian and the transformation between timed Dicke and Fock state bases

Following the paradigm model, we consider an atomic ensemble of identical two level atoms coupled to a single environment. The environment/bath is modeled to have a continuum of modes where the frequency of the k-th mode is represented by ν_k. The interaction picture Hamiltonian of the system is expressed as

$$\hat{V} = \sum_{j=1,k}^{N} g_k[(\hat{\sigma}_j \mathrm{e}^{-i\omega t} + \hat{\sigma}_j^{\dagger}\mathrm{e}^{i\omega t})(\hat{a}_{\vec{k}}^{\dagger}\mathrm{e}^{i\nu_k t - i\vec{k}\cdot\vec{r}_j} + \hat{a}_{\vec{k}}\mathrm{e}^{-i\nu_k t + i\vec{k}\cdot\vec{r}_j})], \tag{5.5}$$

where $\hbar = 1$ and $\vec{r}_j$ is the position vector of the j-th atom in the ensemble. $g_k = (\mathcal{P}/\hbar)\sqrt{\hbar\nu_k/\epsilon_0 V}$ is the atom-environment coupling rate with $\mathcal{P}$ being the dipole moment matrix element, V is the volume of the sample and ϵ_0 is the permittivity constant. The reason for not making the RWA in Eq. (5.5) is a known fact, i.e., that RWA leads to an improper treatment of the virtual processes [157, 158]. The annihilation of the photon in the k-th environmental mode is described by the

operator $\hat{a}_k$ and $\hat{\sigma}_j$ is the lowering operator for the j-th atom. Non-vanishing commutation relations are

$$[\hat{a}_k, \hat{a}_{k'}^\dagger] = \delta_{kk'}, \quad [\hat{\sigma}_j, \hat{\sigma}_l^\dagger] = \hat{\sigma}_z \delta_{jl}, \quad \forall\{j,l\} = 1, 2, \ldots, N.$$

The state describing the single excitation in the global system (atoms plus the field) in the timed Dicke (TD) basis can be expressed as

$$\begin{aligned} |\Psi(t)\rangle = &\left(\beta_+|+\rangle_{\vec{k}_0} + \beta_-|-\rangle_{\vec{k}_0} + \ldots + \beta_N|N\rangle_{\vec{k}_0}\right) \otimes |0\rangle \\ &+ \sum_{\vec{k}} \gamma_{\vec{k}}(t)|b_1, b_2, \ldots, b_N, 1_{\vec{k}}\rangle + \sum_{\vec{k},i,j} \eta_{\vec{k}}(t) \mathrm{e}^{i\vec{k}_0 \cdot \vec{r}_{ij}} |b_1, b_2, \ldots, a_i, a_j, \ldots, b_N, 1_{\vec{k}}\rangle. \end{aligned} \tag{5.6}$$

Notice that this state now includes second-order/two-photon processes as well as those exhibited by the term with amplitude $\eta_{\vec{k}}(t)$. This term describes a situation in which both atoms in the ensemble are excited and there is one (virtual) photon in the field with "negative" energy. $|0\rangle$ and $|1_{\vec{k}}\rangle$ are the environment states with zero and one photon in the k-th mode of the continuum, respectively. It turns out for an ensemble with a higher number of atoms, that the choice of TD states as a basis makes the problem intricate for both analytic and numerical solutions. In view of this, we introduce a basis transformation. Suppose we solve the present problem in a Fock (bare) basis first. The final expression of time evolution can be represented as

$$\frac{\partial \mathcal{B}}{\partial t} = \mathcal{M}\mathcal{B}_b. \tag{5.7}$$

Here $\mathcal{B}_b = (\beta_1 \beta_2 \ldots \beta_N)^T$ is the bare/Fock basis column matrix. $\mathcal{M}$ is a square matrix which depends on the system parameters (for instance inter-atomic separations). Next we introduce the transformation through the unitary matrix $\mathcal{S}$ as $\mathcal{B}_{TD} = \mathcal{S}\mathcal{B}_b$ such that

$$\frac{\partial \mathcal{B}_{TD}}{\partial t} = \mathcal{S}\mathcal{M}\mathcal{S}^{-1}\mathcal{B}_{TD}. \tag{5.8}$$

5.3 Pure Fano-Agarwal couplings

When the problem of subradiance is solved in TD basis, even in the absence of Lamb shift, there exists virtual couplings among TD states. These couplings arise fundamentally due to the interaction of discrete atomic energy states with a common environmental continuum. Such couplings were first studied by Ugo Fano in his 1961 seminal paper [159]. In the context of quantum-statistical theories of spontaneous emission these types of couplings were first pointed out by Agarwal [160]. Therefore, in view of [22], we shall refer to such interactions as the Fano-Agarwal (FA) couplings.

Decay of $|+\rangle_{\vec{k}_0}$ *and* $|-\rangle_{\vec{k}_0}$ *states.* We start with treating the full problem of the N-atom sample prepared initially in the either symmetric $|+\rangle_{\vec{k}_0}$ or first antisymmetric $|-\rangle_{\vec{k}_0}$ TD state. To analyze the influence of pure FA couplings we shall apply the RWA and neglect the presence of two excitations in the state of the system. Consequently, the N-atom Hamiltonian takes the form

$$\hat{V} = \hbar \sum_{j,k} g_k \left(\hat{a}_k \hat{\sigma}_j^{\dagger} \mathrm{e}^{i(\omega-\nu_k)t + i\vec{k}\cdot\vec{r}_j} + \hat{a}_k^{\dagger} \hat{\sigma}_j \mathrm{e}^{-i(\omega-\nu_k)t - i\vec{k}\cdot\vec{r}_j} \right). \tag{5.9}$$

The system-environment state can be expressed as

$$|\Psi(t)\rangle = \left(\beta_+ |+\rangle_{\vec{k}_0} + \beta_- |-\rangle_{\vec{k}_0} + \ldots + \beta_N |N\rangle_{\vec{k}_0}\right) \otimes |0\rangle + \sum_{\vec{k}} \gamma_{\vec{k}}(t) |b_1, b_2, \ldots, b_N, 1_{\vec{k}}\rangle. \tag{5.10}$$

The general form of the antisymmetric TD states can be presented as [136]

$$|N\rangle_{\vec{k}_0} = \frac{1}{\sqrt{N(N-1)}} \left[\sum_{j=1}^{N-1} \mathrm{e}^{i\vec{k}_0\cdot\vec{r}_j} |b_1, b_2, \ldots, a_j, \ldots, b_N\rangle - (N-1) \mathrm{e}^{i\vec{k}_0\cdot\vec{r}_N} |b_1, b_2, \ldots, a_N\rangle \right], \quad \forall N \geq 2 \tag{5.11}$$

while $|N\rangle_{\vec{k}_0}$ is equal to $|3\rangle_{\vec{k}_0}, \ldots$ for $N = 2, 3, \ldots$, respectively. Notice that the above choice of the structure of antisymmetric TD states is not unique but it can be easily extended to a many-atoms

ensemble. Following only the evolution of $\beta_{\pm}(t)$ we obtain

$$\dot{\beta}_{+} = \frac{-\gamma}{N}\left[\sum_{i,j} \mathrm{e}^{-i\vec{\mathcal{K}}_{ji}} \frac{\sin \mathcal{K}_{ji}}{\mathcal{K}_{ji}} \beta_{+} + \left(\sum_{i,j} \mathrm{e}^{-i\vec{\mathcal{K}}_{ji}} \frac{\sin \mathcal{K}_{ji}}{\mathcal{K}_{ji}} - \sum_{i',j} \mathrm{e}^{-i\vec{\mathcal{K}}_{ji'}} \frac{\sin \mathcal{K}_{ji'}}{\mathcal{K}_{ji'}}\right) \beta_{-} + \ldots + N\text{-th term}\right], \tag{5.12}$$

$$\begin{aligned}\dot{\beta}_{-} = \frac{-\gamma}{N}\Bigg[&\left(\sum_{i,j} \mathrm{e}^{-i\vec{\mathcal{K}}_{ji}} \frac{\sin \mathcal{K}_{ji}}{\mathcal{K}_{ji}} - \sum_{i',j} \mathrm{e}^{-i\vec{\mathcal{K}}_{ji'}} \frac{\sin \mathcal{K}_{ji'}}{\mathcal{K}_{ji'}}\right) \beta_{+} + \Bigg(\sum_{i,j} \mathrm{e}^{-i\vec{\mathcal{K}}_{ji}} \frac{\sin \mathcal{K}_{ji}}{\mathcal{K}_{ji}} \\ &- \sum_{i',j} \mathrm{e}^{-i\vec{\mathcal{K}}_{ji'}} \frac{\sin \mathcal{K}_{ji'}}{\mathcal{K}_{ji'}} - \sum_{i,j'} \mathrm{e}^{-i\vec{\mathcal{K}}_{j'i}} \frac{\sin \mathcal{K}_{j'i}}{\mathcal{K}_{j'i}} + \sum_{i',j'} \mathrm{e}^{-i\vec{\mathcal{K}}_{j'i'}} \frac{\sin \mathcal{K}_{j'i'}}{\mathcal{K}_{j'i'}}\Bigg) \beta_{-} + \ldots + N\text{-th term}\Bigg]\end{aligned} \tag{5.13}$$

while $\mathcal{K}_{ji} = k_0 r_{ji}$ and $\vec{\mathcal{K}}_{ji} = \vec{k}_0 \cdot \vec{r}_{ji}$. In order to further proceed with the analytic results, we notice that the general structure of coupled differential equations for the N-atom case can be written in matrix form:

$$\begin{pmatrix} \dot{\beta}_{+}(t) \\ \dot{\beta}_{-}(t) \\ \vdots \\ \dot{\beta}_{N}(t) \end{pmatrix} = \begin{pmatrix} \gamma_{11} & \gamma_{12} & \cdots & \gamma_{1N} \\ \gamma_{21} & \gamma_{22} & \cdots & \gamma_{2N} \\ \vdots & \vdots & \ddots & \vdots \\ \gamma_{N1} & \gamma_{N2} & \cdots & \gamma_{NN} \end{pmatrix} \begin{pmatrix} \beta_{+}(t) \\ \beta_{-}(t) \\ \vdots \\ \beta_{N}(t) \end{pmatrix}. \tag{5.14}$$

A general solution of the above equation can be represented as

$$\beta_i(t) = \sum_{i=1}^{N} c_i(t) V_i \mathrm{e}^{\lambda_i t}, \quad i = +, -, 3, \ldots, N, \tag{5.15}$$

V_i and λ_i are the eigenvectors and eigenvalues of the effective decay rate matrix of Eq. (5.14). From this point onwards, analytic solutions are complicated to obtain without the imposition of further approximations (for example assuming extremely dense ensembles [157]). On the other hand, we want to keep the analysis more accurate here and proceed with the numerical analysis of

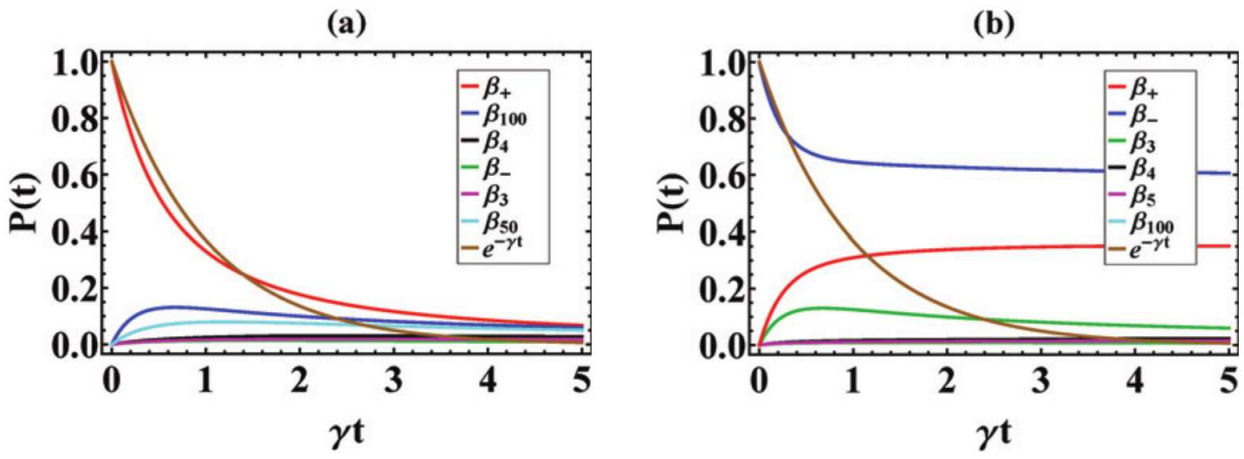

Figure 5.1: Time evolution of symmetric and antisymmetric TD states populations for an ensemble of 100 atoms in a line geometry. Part (a) ((b)) of the plots represents the case in which the system starts in a symmetric (antisymmetric) state. The lattice constant is $1k_0$ and the radiation wavelength is 2π with $\cos(\theta_0) = 1$. Reprinted with permission from [125].

the problem where the position of all atoms will be treated discretely.

To this end, we have performed the numerical simulation using the Runge-Kutta method of order 4 with time step size $\mathrm{d}t = 0.01$ and all atoms periodically placed on a line lattice with lattice constant $1\lambda_0$ ($\lambda_0 = 2\pi/k_0$). In Figure 5.1, we present the time evolution of populations for a sample made of a hundred atoms. When the system starts in the symmetric state (Figure 5.1(a)), we notice that the symmetric state shows a slightly faster decay for smaller times ($\gamma t < 2$) but still cannot be regarded as a superradiant state.

The population in the antisymmetric states achieves small maximum values; however, the number of these curves also grow. Therefore, to a good approximation one can neglect the FA contribution coming just from β_- in the evolution of β_+ (as analytically shown in ref. [114]). However, the overall effect of all FA couplings is considerable and hence cannot be omitted. On the other hand, when the ensemble starts in the first antisymmetric state (Figure 5.1(b)), the decay in the antisymmetric state population is slightly worsened. But in all cases the decay is subradiant.

FA couplings between individual TD states. The question of how an atomic ensemble initially prepared in the ordinary Dicke (OD) or symmetric TD state remains excited has already been

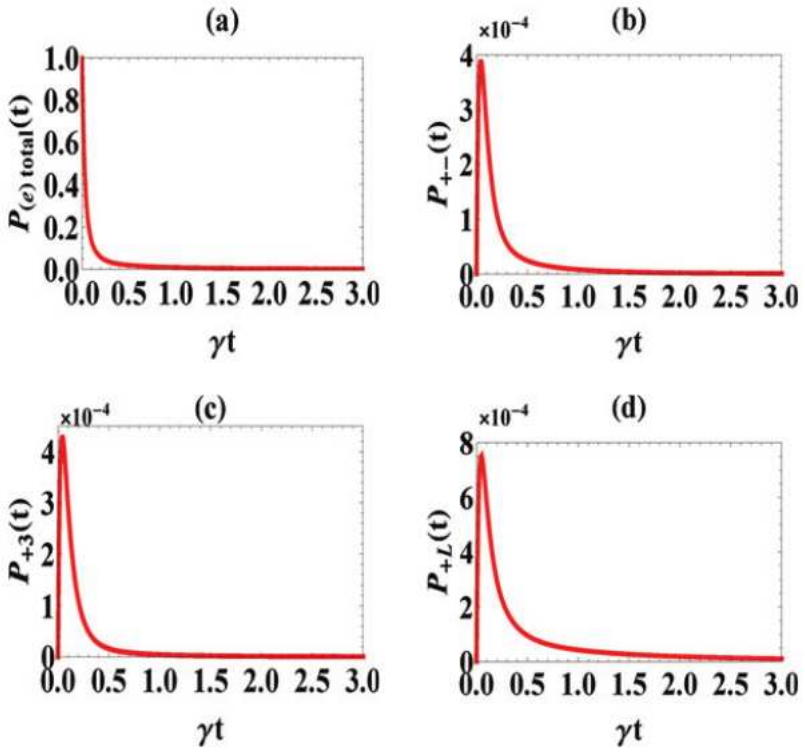

Figure 5.2: Time evolution of (a) a full sample to be excited and FA coupling between: (b) $|+\rangle_{\vec{k}_0}$ and $|-\rangle_{\vec{k}_0}$, (c) $|+\rangle_{\vec{k}_0}$, and $|3\rangle_{\vec{k}_0}$ and (d) $|+\rangle_{\vec{k}_0}$ and $|121\rangle_{\vec{k}_0}$ states. The system here begins in the symmetric TD state. For this and the next figure, we have conisered a spherical ensemble with radius $3k_0^{-1}$ and a uniform distribution of 121 atoms in the sphere. The inter-atomic separation is $1/k_0$ and the angle between $\vec{k}_0$ and $\vec{r}_{ij}$ is decided by the coordinates of each $\vec{r}_{ij}$ while $\vec{k}_0 = (1, 0, 0)$. Reprinted with permission from [125].

investigated in the past [161]. In this subsection we direct our attention to two novel questions: 1) How does the atomic ensemble decay in time if the initial preparation is in a TD subradiant state? (See the next section for the analysis of this question in the presence of the Lamb shift and NRW terms.) 2) During the decay process, how do different FA couplings between certain TD states compare?

In Figure 5.2(a) we plot the total probability of a spherical ensemble to remain excited if the initial state of the system is $|+\rangle_{\vec{k}_0}$. We notice an extremely fast (but not as fast as $N\gamma$) superradiant decay. In panels (b), (c) and (d) we have plotted the FA coupling between the $|+\rangle_{\vec{k}_0}$ and $|-\rangle_{\vec{k}_0}$,

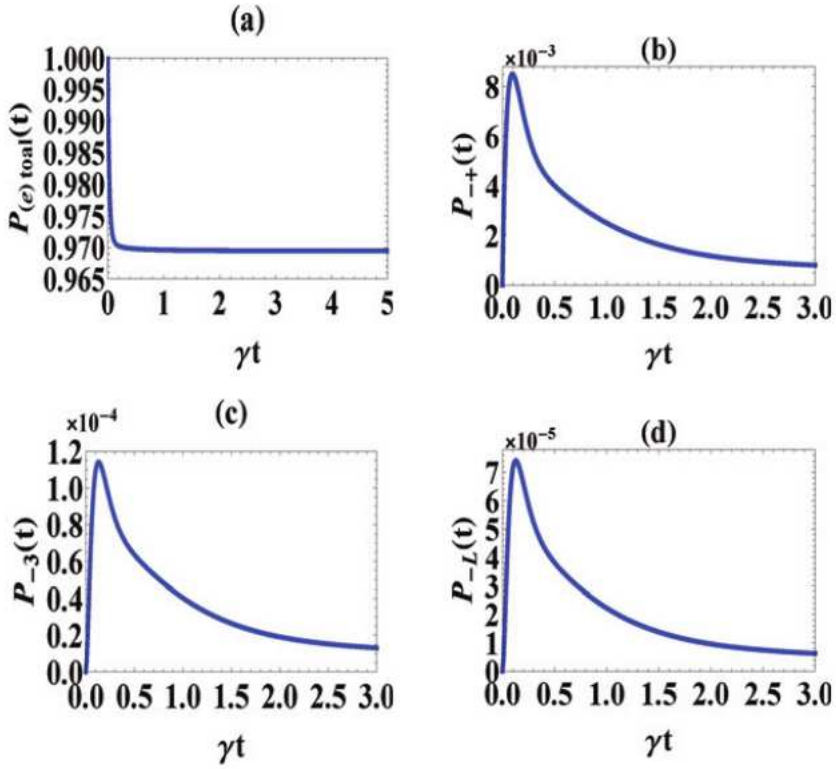

Figure 5.3: Time evolution of (a) a full sample to be in an excited state and FA coupling between: (b) $|-\rangle_{\vec{k}_0}$ and $|+\rangle_{\vec{k}_0}$, (c) $|-\rangle_{\vec{k}_0}$ and $|3\rangle_{\vec{k}_0}$, and (d) $|-\rangle_{\vec{k}_0}$ and $|121\rangle_{\vec{k}_0}$ states, when the system is initially in the $|-\rangle_{\vec{k}_0}$ TD state. Reprinted with permission from [125].

$|3\rangle_{\vec{k}_0}$ and $|121\rangle_{\vec{k}_0}$ states, respectively. We notice FA couplings to be larger between the $|+\rangle_{\vec{k}_0}$ and the TD state with largest N. This can be understood noting that for $N \gg 1$, the desired coupling probability is proportional to: $P_{+\to N} \propto |\langle +|_{\vec{k}_0} \cdot (\sum_{j=1}^{N-1} \frac{e^{i\vec{k}_0\cdot\vec{r}_j}}{N}|j\rangle - e^{i\vec{k}_0\cdot\vec{r}_N}|b_1 b_2 \ldots a_N\rangle)|$. In this probability, we find that as N tends to achieve higher values, the FA coupling of the $|+\rangle_{\vec{k}_0}$ state with larger N states starts to enhance, as for these states the first-term contribution surpasses the second-term contribution.

In Figure 5.3, we focus on the other scenario, i.e., when the system starts in the $|-\rangle_{\vec{k}_0}$ TD state. Panel (a) of the figure shows the net probability of the system to remain excited. We notice a slight but fast decay of the probability up to $t \leq 0.1\gamma^{-1}$ and after this time the probability shows an almost time-independent behavior. In panels (b), (c) and (d) we plot individual FA couplings of

the state $|-\rangle_{\vec{k}_0}$ state with the $|+\rangle_{\vec{k}_0}$, $|3\rangle_{\vec{k}_0}$ and $|121\rangle_{\vec{k}_0}$ states, respectively. We point out a contrary behavior of FA couplings in this case as compared to the $|+\rangle_{\vec{k}_0}$ state situation (Figure 5.2). Now $|-\rangle_{\vec{k}_0}$ maximally couples with the $|+\rangle_{\vec{k}_0}$ state and as we go further away (i.e. higher N values in $|N\rangle_{\vec{k}_0}$) FA couplings become smaller. This trend can again be attributed to the desired coupling probabilities. There are two relevant probabilities now: 1) between symmetric and minus TD state $P_{-\rightarrow+} \propto |\langle -|_{\vec{k}_0} \cdot \sum_{j=1}^{N-1} \frac{\mathrm{e}^{i\vec{k}_0\cdot\vec{r}_j}}{\sqrt{N}}|j\rangle|$ and 2) between minus and any other $N \geq 3$ subradiant state $|N\rangle_{\vec{k}_0}$ TD state which is proportional to $P_{-\rightarrow N} \propto |\langle -|_{\vec{k}_0} \cdot (\sum_{j=1}^{N-1} \frac{\mathrm{e}^{i\vec{k}_0\cdot\vec{r}_j}}{N}|j\rangle - \mathrm{e}^{i\vec{k}_0\cdot\vec{r}_N}|b_1 b_2 \ldots a_N\rangle)|$, for $N > 1$. We note that if in the $|-\rangle_{\vec{k}_0}$ state, only atoms at positions $\vec{r}_1$ and $\vec{r}_2$ participate in defining the antisymmetry, then the second term in $|N\rangle_{\vec{k}_0}$ (in which the last (N-th) atom is excited) never participates in the desired probability. In this situation, as N becomes larger, the contribution from the first term in $P_{-\rightarrow N}$ becomes smaller as compared to the overlap of $|-\rangle_{\vec{k}_0}$ with the $|+\rangle_{\vec{k}_0}$ state. Interestingly, we notice that even when two atoms that are defining the antisymmetry in the $|-\rangle_{\vec{k}_0}$ state are placed at arbitrary positions in the respective atomic bins (the situation actually plotted in Figures 5.2 and 5.3), the same pattern of decay holds.

5.4 Inclusion of the Lamb shift (scalar theory) and non-rotating wave terms

We now examine the effect of the Lamb shift and the non-rotating wave terms on the evolution of symmetric ($|+\rangle_{\vec{k}_0}$) and new kind of subradiant TD states ($|-\rangle_{\vec{k}_0}$, $|3\rangle_{\vec{k}_0}$,. . ., $|N\rangle_{\vec{k}_0}$). We apply a scalar theory for simplicity here (for a comparison between a scalar and vector theory of electromagnetic modes decay from a spherical sample we refer the reader to [162]). We make use of the full Hamiltonian presented in Eq. (5.5) along with the global system-environment state presented in Eq. (5.6). The equations of motion for $\beta_+(t)$ and $\beta_-(t)$ amplitudes now take the form

$$\dot{\beta}_+ = \frac{i\gamma}{N}\left[\sum_{i,j} \mathrm{e}^{-i\vec{\mathcal{K}}_{ji}} \frac{\mathrm{e}^{i\mathcal{K}_{ji}}}{\mathcal{K}_{ji}}\beta_+ + \left(\sum_{i,j} \mathrm{e}^{-i\vec{\mathcal{K}}_{ji}} \frac{\mathrm{e}^{i\mathcal{K}_{ji}}}{\mathcal{K}_{ji}} - \sum_{i',j} \mathrm{e}^{-i\vec{\mathcal{K}}_{ji'}} \frac{\mathrm{e}^{i\mathcal{K}_{ji'}}}{\mathcal{K}_{ji'}}\right)\beta_- + \ldots + N\text{-th term}\right], \tag{5.16}$$

$$\dot{\beta}_- = \frac{i\gamma}{N}\Bigg[\left(\sum_{i,j} \mathrm{e}^{-i\vec{\mathcal{K}}_{ji}}\frac{\mathrm{e}^{i\mathcal{K}_{ji}}}{\mathcal{K}_{ji}} - \sum_{i',j} \mathrm{e}^{-i\vec{\mathcal{K}}_{ji'}}\frac{\mathrm{e}^{i\mathcal{K}_{ji'}}}{\mathcal{K}_{ji'}}\right)\beta_+ + \Bigg(\sum_{i,j} \mathrm{e}^{-i\vec{\mathcal{K}}_{ji}}\frac{\mathrm{e}^{i\mathcal{K}_{ji}}}{\mathcal{K}_{ji}}$$
$$- \sum_{i',j} \mathrm{e}^{-i\vec{\mathcal{K}}_{ji'}}\frac{\mathrm{e}^{i\mathcal{K}_{ji'}}}{\mathcal{K}_{ji'}} - \sum_{i,j'} \mathrm{e}^{-i\vec{\mathcal{K}}_{j'i}}\frac{\mathrm{e}^{i\mathcal{K}_{j'i}}}{\mathcal{K}_{j'i}} + \sum_{i',j'} \mathrm{e}^{-i\vec{\mathcal{K}}_{j'i'}}\frac{\mathrm{e}^{i\mathcal{K}_{j'i'}}}{\mathcal{K}_{j'i'}}\Bigg)\beta_- + \ldots + N\text{-th term}\Bigg]. \quad (5.17)$$

To arrive at these equations we have performed the integration by the method of contours, where we have set $k_0 \to k_0 + i\epsilon$ (while $\epsilon \ll 1$) and identified $\frac{1}{x\mp i\epsilon} = \mathbf{P}[\frac{1}{x}] \pm i\pi\delta(x)$. Note that the appearance of additional timing factors ($\mathrm{e}^{-i\vec{k}_0\cdot\vec{r}_{ij}}$ and similar primed exponential kernel) factors makes our results different from the one obtained by using the Fock state basis (see Eq. (5.2) in the introduction section).

We now present the results both with and without the presence of the Lamb shift in Figure 5.4. We notice that the effect of the Lamb shift on the decay of the symmetric (superradiant) state is small and the Lamb shift slightly slows down the decay. Our result here is consistent with ref. [161] where the effect of the Lamb shift on the collective decay of a spherical dense ensemble prepared initially either in the $|+\rangle$ or $|+\rangle_{\vec{k}_0}$ state was investigated.

However, the effect of the Lamb shift is marked on the decay of antisymmetric subradiant TD states (up to $\sim$40% faster decay when Lamb shifts are included). This behavior, which, to our knowledge, has not been reported before, can be understood as a consequence of enhanced couplings between the $|-\rangle_{\vec{k}_0}$, $|3\rangle_{\vec{k}_0}$ and $|+\rangle_{\vec{k}_0}$ states in the presence of virtual processes. This feature points out that along with the FA couplings, now there are additional coupling channels available among the single- and two-excitation states through virtual interactions. A small enhanced coupling of fragile subradiant states with the superradiant state causes a marked effect on the decay of the subradiant state as opposed to when the superradiant state is elevatedly coupled with the subradiant states. Hence, the effect of the Lamb shift is more pronounced for the subradiant states.

5.5 Conclusions

The proposal of utilizing atomic ensembles prepared in single-photon subradiant states [114, 156] for quantum information storage purposes crucially relies on how these states decay. Consequently, in this work we have investigated the effects of virtual processes on the time evolution of

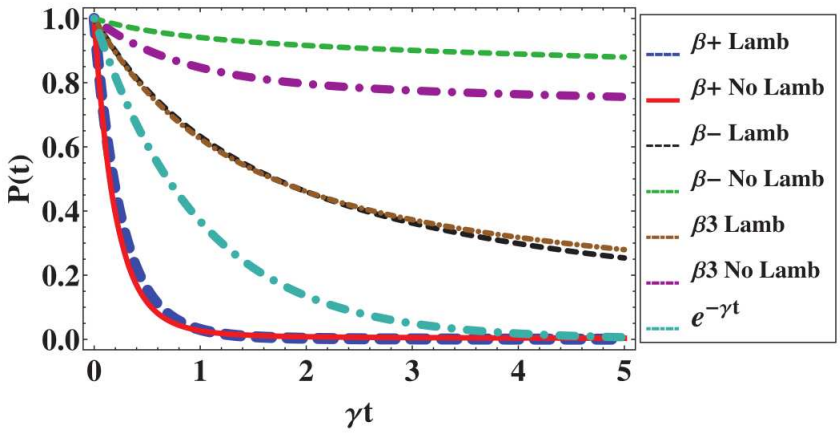

Figure 5.4: Lamb shift influencing the decay of an atomic ensemble initially prepared either in the $|+\rangle_{\vec{k}_0}$ or $|-\rangle_{\vec{k}_0}$ or $|3\rangle_{\vec{k}_0}$ state. Here we consider an ensemble in spherical geometry with diameter $5\lambda_0$ (λ_0 is the wavelength of a single photon in resonance with the atomic transition frequency). The ensemble consists of 1000 periodically and uniformity distributed atoms with inter-atomic separation equal to λ_0. For the $|-\rangle_{\vec{k}_0}$ and $|3\rangle_{\vec{k}_0}$ states we have divided the ensemble into two and three sections, respectively, with each section having an equal number of atoms. Reprinted with permission from [125].

a new kind of TD subradiant states introduced in ref. [114]. We concluded that, in the case of pure FA couplings, the symmetric TD state decay tends to slow down without any superradiance, while the subradiant states remain no more frozen (unlike OD case). Additionally, the overall (summed up) effect of FA couplings remained substantial and hence cannot be neglected. The analysis of the individual FA couplings among different TD states revealed that if we start in the $|+\rangle_{\vec{k}_0}$ state, then the FA couplings are highest with largest-N TD state. On the contrary, if the ensemble in prepared initially in $|-\rangle_{\vec{k}_0}$, then the coupling diminishes for the TD states with larger N. Finally, the inclusion of the scalar Lamb shift and NRW terms yields a small effect on the decay of the $|+\rangle_{\vec{k}_0}$ state; however, $|-\rangle_{\vec{k}_0}$ (and other TD subradiant states) shows up to 40% swift decay.

6. ACCELERATION RADIATION ENHANCED BY SUPERRADIANCE: DICKE MEETS UNRUH*

6.1 Introduction

The most intriguing outcome of quantum field theory in curved spacetime is the ambiguity of particle definition. Its simplest manifestation is the Unruh effect, first introduced by S. Fulling, P. Davies, and W. Unruh in the late '70s [43, 44, 42]. The Unruh effect is a phenomenon where field particles can be detected in an accelerating frame even when the corresponding field is in its vacuum state in the inertial frame of reference. This effect has received much attention in the last 50 years due to its strong theoretical importance and connections with cosmology, particle physics, and even quantum optics [163, 47, 45, 164, 165]. To overcome the difficulty in particle definition, one can use model detector in curved spacetime and count detector clicks. This is the approach that Unruh and DeWitt developed in the late '70s. Indeed, a uniformly accelerating detector sees a thermal-like bath with temperature $T_{\rm U} = a/2\pi$, called Unruh temperature. We call this thermal-like bath "the Unruh bath".

In the current work, we study acceleration radiation of accelerated two-level atoms placed in a short line whose linear size is much smaller than the transition wavelength of atoms. The same problem for inertial atoms — Dicke superradiance where inertial two-level atoms confined in small volume whose size is much shorter than transition wavelength has been well studied last 70 years [3, 109]. Certainly, inertial two-level atoms exhibit super- and subradiant properties depending on the symmetry of their initial state. However, if atoms are uniformly accelerated, the super- and subradiant behaviors do not change too much. In particular, inertial and accelerated atoms exhibit the same feature in the limiting cases $R_{jl} \to 0$ and $R_{jl} \to \infty$, and in between these cases, a small difference exists. Here R_{jl} is a distance between jth and lth atoms. Therefore, as inertial superradiant emission, we show that the energy of acceleration radiation per unit time is N times

*"Acceleration radiation enhanced by superradiance: Dicke meets Unruh" by Tuguldur Begzjav, Jonathan Ben-Benjamin, Marlan O. Scully and William G. Unruh, 2020 in preparation.

larger than one for single accelerated two-level atoms when $R_{jl} \to 0$. We call this enhanced acceleration radiation via Dicke superradiance. Since enhanced acceleration radiation is intense and its intensity goes like N^2 it could be exploited for an experimental test of the Unruh effect.

Moreover, we compare the Unruh bath with Minkowski thermal bath and observe a small difference between density matrix elements of two-level atoms in the Unruh and Minkowski thermal baths in a short proper time scale. However, in the long proper time scale, there is no difference between stationary density matrix elements of atoms surrounded by the Unruh and Minkowski thermal baths. This feature is also pointed out by Uliana Lima et al [166].

6.2 Co-accelerating atoms interacting with Minkowski vacuum of massless scalar field

Detector can be any physical system that can absorb and emit field particles resulting in the transition between energy levels of the system. Then, it is safe to choose a two-level atom as a detector. Therefore, we consider co-accelerating two-level atoms with the same constant acceleration (see Figure 6.1). In the course of their motion, the atoms interact with a massless scalar field initially in the Minkowski vacuum state. The atoms move along z direction and are apart from one another in the x-direction by a distance $R_{ij} = x_i - x_j$. Thus, the atomic coordinates x_i and y_i are all constant. The explicit form of the trajectory of uniformly accelerating atoms is

$$\begin{aligned} t(\tau) &= \frac{1}{a}\sinh(a\tau), \\ z_i(\tau) &= \frac{1}{a}\cosh(a\tau), \quad y_i(\tau) = 0, \quad x_i(\tau) = x_i \end{aligned} \tag{6.1}$$

where a is a constant acceleration, τ is the proper time of atoms (they have a common proper time).

Atomic free Hamiltonian in the atomic rest frame is

$$H_A(\tau) = \frac{1}{2}\omega \sum_j \hat{\sigma}_{z,j}, \tag{6.2}$$

where $\hat{\sigma}_{z,j} = |a_j\rangle\langle a_j| - |b_j\rangle\langle b_j|$ is jth atoms population operator, atomic excited and ground levels are $|a_j\rangle$ and $|b_j\rangle$ and ω is transition frequency of atoms. On the other hand free Hamiltonian of

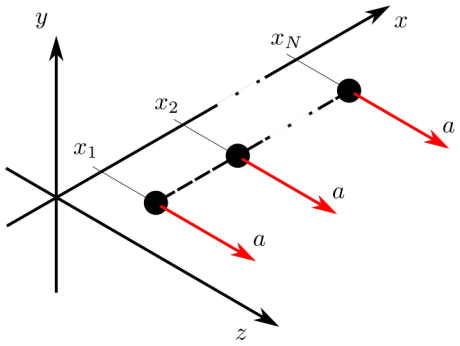

Figure 6.1: Geometry of N co-accelerating two-level atoms.

massless scalar field in Minkowski frame is given by

$$H_F(t) = \int d^3\mathbf{k}\, \nu_k \hat{a}_k^\dagger \hat{a}_k, \tag{6.3}$$

where $\hat{a}_k^\dagger$ and $\hat{a}_k$ are bosonic creation and annihilation operators of the mode $\mathbf{k}$, and ν_k is field frequency. Here, Minkowski time is denoted by t.

The interaction Hamiltonian between massless scalar field and two-level atoms is

$$H_I = \mu \sum_j \hat{\sigma}_{x,j} \hat{\phi}(\mathbf{r}_j), \tag{6.4}$$

where $\hat{\sigma}_{x,j} = |a_j\rangle\langle b_j| + |b_j\rangle\langle a_j|$, and μ is a coupling constant. Field operator $\hat{\phi}(\mathbf{r})$ at Minkowski position vector $\mathbf{r}$ is given by

$$\hat{\phi}(\mathbf{r}) = \int d^3\mathbf{k}\, g_k \left(\hat{a}_k \mathrm{e}^{i\mathbf{k}\cdot\mathbf{r}} + \hat{a}_k^\dagger \mathrm{e}^{-i\mathbf{k}\cdot\mathbf{r}} \right), \tag{6.5}$$

where $g_k = (2\nu_k(2\pi)^3)^{-1/2}$ is a frequency-dependent normalization constant. With the help of

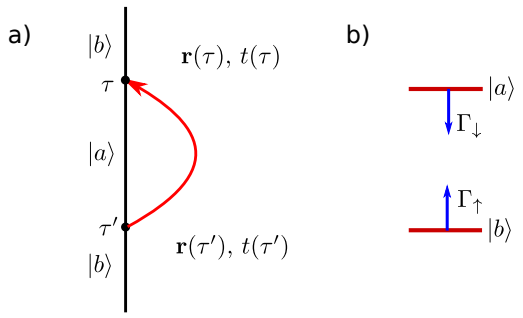

Figure 6.2: (a) Feynman diagram that explains the emission and absorption of Minkowski virtual photon. The vertical black line is proper time axis. Atom initially in the $|b\rangle$ state emits a Minkowski virtual photon at proper time τ' leaving the atom in the excited state $|a\rangle$. Later, at proper time τ the emitted Minkowski virtual photon reabsorbed by the atom and atom goes to its ground state $|b\rangle$. (b) Level scheme of two level-atom and its decay and excitation rates.

Eqs. (6.2), (6.3) and (6.4), Hamiltonian in the interaction picture is given by

$$\hat{V}(\tau) = \int d^3\mathbf{k}\, g_k \mu \sum_j (\hat{a}_k \mathrm{e}^{i\mathbf{k}\cdot\mathbf{r}_j(\tau) - i\nu_k t_j(\tau)} + \hat{a}_k^\dagger \mathrm{e}^{-i\mathbf{k}\cdot\mathbf{r}_j(\tau) + i\nu_k t_j(\tau)})(\hat{\sigma}_{+j}\mathrm{e}^{i\omega\tau} + \hat{\sigma}_{-j}\mathrm{e}^{-i\omega\tau}), \tag{6.6}$$

where field is evaluated along the atom's worldline (the atom-field interaction is local).

6.2.1 Single accelerating two-level atom

Before we proceed with co-accelerating two-level atoms, we present here how quantum field theory helps us to understand what happens when an atom is accelerating. To achieve this goal, we solve a non-relativistic Schrödinger equation for the system composed of accelerating two-level atom and massless scalar field. Initial conditions are Minkowski vacuum state $|0\rangle$ for field and ground state $|b\rangle$ for atom. There is a nonzero excitation probability of the atom due to its acceleration. Therefore, the transitions from lower energy state to the higher energy state of the full atom-field system are only due to counter-rotating term $\hat{a}_k^\dagger \sigma_+$ in the interaction Hamiltonian which is usually ignored via the rotating wave approximation. Let state vector of the system at

proper time τ be expressed in the basis of $|b\rangle|0\rangle$ and $|a\rangle|1_{\mathbf{k}}\rangle$ as follows:

$$|\Psi(\tau)\rangle = \beta(\tau)|b\rangle|0\rangle + \int d^3\mathbf{k}\alpha_k(\tau)|a\rangle|1_{\mathbf{k}}\rangle, \tag{6.7}$$

where $\beta(\tau)$ and $\alpha_k(\tau)$ are probability amplitudes at proper time τ and $|1_{\mathbf{k}}\rangle$ represents virtual photon in Minkowski spacetime since it is created and annihilated by Minkowski operators $\hat{a}^\dagger$ and $\hat{a}$, respectively. Plugging Eq. 6.7 into Schrödinger equation $i\partial|\Psi(\tau)\rangle/\partial\tau = \hat{V}(\tau)|\Psi(\tau)\rangle$ we obtain a set of integro-differential equations for probability amplitudes as below:

$$\frac{d\beta(\tau)}{d\tau} = -i\mu \int d^3\mathbf{k} g_k \mathrm{e}^{-i\omega\tau}\mathrm{e}^{i\mathbf{k}\cdot\mathbf{r}(\tau)-i\nu_k t(\tau)}\alpha_k(\tau), \tag{6.8a}$$

$$\frac{d\alpha_k(\tau)}{d\tau} = -i\mu g_k \mathrm{e}^{i\omega\tau}\mathrm{e}^{-i\mathbf{k}\cdot\mathbf{r}(\tau)+i\nu_k t(\tau)}\beta(\tau). \tag{6.8b}$$

These equations have deep physical meaning. Particularly, Eq. (6.8b) implies the emission of a single photon of wavevector $\mathbf{k}$ at time $t(\tau)$ and at spatial point $\mathbf{r}(\tau)$ whereas Eq. (6.8a) indicates absorption of a single photon of the same wavenumber $\mathbf{k}$ again at time $t(\tau)$ and at spatial point $\mathbf{r}(\tau)$. Until now, there is no connection between absorption and emission times and places. However, keeping in mind that the initial state of the system is $|b\rangle|0\rangle$, then emission must be first and absorption must be later. Integrating Eq. (6.8b) and substituting it into Eq. (6.8a) we obtain

$$\frac{d\beta(\tau)}{d\tau} = -\mu^2 \int d^3\mathbf{k} g_k^2 \mathrm{e}^{-i\omega\tau}\mathrm{e}^{i\mathbf{k}\cdot\mathbf{r}(\tau)-i\nu_k t(\tau)} \times \int_0^\tau d\tau' \mathrm{e}^{i\omega\tau'}\mathrm{e}^{-i\mathbf{k}\cdot\mathbf{r}(\tau')+i\nu_k t(\tau')}\beta(\tau'). \tag{6.9}$$

Interpretation of this equation is illustrated in Figure 6.2. Atom emits a single photon at time $t(\tau')$ and at point $\mathbf{r}(\tau')$ followed by excitation to the excited state $|a\rangle$ and absorbs the emitted photon at later time $t(\tau)$ and at the point $\mathbf{r}(\tau)$ followed by transition to the ground state $|b\rangle$. It is worth noticing that rates of flowing time for atom and field are different; it is τ for atom whereas t for field. That means the atom experiences the different frequency than Minkowski frequency of field ν_k and resonance condition is not simple as $\nu_k = \omega$ (Indeed, this phenomenon is neither

Doppler effect nor redshift). This is the main reason why accelerating atom in its ground state gets excited due to interaction with the Minkowski vacuum. To make this reason clear, consider inertial (non-accelerating) atom where proper time τ is just Minkowski time t. According to Eq. (6.9) resonance condition reads as $\nu_k = -\omega$ and since ω is positive, resonance peak is out of integration range $0 \leq \nu_k \leq \infty$ that yields $d\beta(t)/dt = 0$. Hence, inertial atom in its ground state interacting with the Minkowski vacuum stays in the ground state all the time. On the other hand, if you accelerate atom with uniform acceleration, resonance condition is not simple as inertial atom as long as $\mathrm{e}^{i\mathbf{k}\cdot\mathbf{r}(\tau)}$ term makes the situation complicated. Fortunately, the final result of the integration of Eq. (6.9) is transparent and it has the following form

$$\frac{d\beta(\tau)}{d\tau} = -\frac{\Gamma_\uparrow}{2}\beta(\tau), \tag{6.10}$$

where $\Gamma_\uparrow = \Gamma_0 \left(\mathrm{e}^{2\pi\omega/a} - 1\right)^{-1}$ is excitation rate from the ground state to the excited state. Here, the spontaneous decay rate of inertial atom in the excited state is denoted by $\Gamma_0 = \mu^2\omega/2\pi$. Equation (6.10) indicates that accelerating atom in the ground state interacting with the Minkowski vacuum is excited exactly the same as inertial atom interacting with the thermal reservoir of temperature T_U. Two remarks must be given for the calculation of Eq. (6.10). First, when we evaluate the integral in Eq. (6.9), well-known Markovian approximation is applied. In particular, $\beta(\tau')$ is replaced by $\beta(\tau)$ allowing us to take it out of the integral and the upper limit of integration over τ is extended to ∞. Second, because of the complicated nature of the integrals in Eq. (6.9), we omit the Cauchy principal part of diverging integral with respect to $\mathbf{k}$ which can lead us to Lamb shift of the ground state.

As we stated above, $|1_\mathbf{k}\rangle$ is Minkowski virtual photon. As a consequence of continuous emission and reabsorption of Minkowski virtual photon, $\beta(\tau)$ decreases with the rate $\Gamma_\uparrow/2$ as we have shown above. However, after long enough time compared to virtual photon timescale $\alpha_k(\tau)$ becomes nonzero and then we interpret the second term of Eq. (6.7) as real Minkowski photon. In other words, accelerating two-level atom radiates into Minkowski spacetime. Therefore, this cal-

culation supports acceleration radiation predicted by Unruh and Wald [48].

According to the similar calculation as previous, accelerating atom initially in the excited state decays to the ground state with decay rate:

$$\frac{d\alpha(\tau)}{d\tau} = -\frac{\Gamma_{\downarrow}}{2}\alpha(\tau), \tag{6.11}$$

where $\alpha(\tau)$ is a probability amplitude as a function of proper time τ for atom in the excited state $|a\rangle$ and no photon is present $|0\rangle$. Decay rate is given by $\Gamma_{\downarrow} = \Gamma_0 \left(1 + \left[\mathrm{e}^{2\pi\omega/a} - 1\right]^{-1}\right)$.

6.2.2 Two co-accelerating two-level atoms

In the same manner as a single accelerating atom, we can easily continue our discussion with two detectors (co-accelerating two-level atoms). Atomic trajectories and interaction Hamiltonian are the specific case of Eqs. (6.1) and (6.6). We start with atoms in the ground states $|b, b\rangle$. Then, time state vector of the system at proper time τ can be written as

$$\begin{aligned} |\Psi(\tau)\rangle &= \beta(\tau)|b,b\rangle|0\rangle \\ &\quad + \int d^3\mathbf{k}\, \eta_{k\pm}(\tau)\frac{1}{\sqrt{2}}\left(|a,b\rangle \pm |b,a\rangle\right)|1_k\rangle, \end{aligned} \tag{6.12}$$

where $\beta(\tau)$ and $\eta_{k\pm}(\tau)$ are probability amplitudes. Plugging the state vector (6.12) into Schrödinger equation, we obtain the coupled integro-differential equations for transition amplitudes $\beta(\tau)$ and $\eta_{k\pm}(\tau)$

$$\begin{aligned} \frac{d\beta(\tau)}{d\tau} &= -\frac{i\mu}{\sqrt{2}}\int d^3\mathbf{k}\, g_k \mathrm{e}^{-i\omega\tau}\mathrm{e}^{i\mathbf{k}\cdot\mathbf{r}_1(\tau)-i\nu_k t_1(\tau)}\eta_{k\pm}(\tau) \\ &\quad \mp \frac{i\mu}{\sqrt{2}}\int d^3\mathbf{k}\, g_k \mathrm{e}^{-i\omega\tau}\mathrm{e}^{i\mathbf{k}\cdot\mathbf{r}_2(\tau)-i\nu_k t_2(\tau)}\eta_{k\pm}(\tau), \end{aligned} \tag{6.13a}$$

$$\begin{aligned} \frac{d\eta_{k\pm}(\tau)}{d\tau} &= -\frac{i\mu g_k}{\sqrt{2}}\left(\mathrm{e}^{i\omega\tau}\mathrm{e}^{-i\mathbf{k}\cdot\mathbf{r}_1(\tau)+i\nu_k t_1(\tau)}\right. \\ &\quad \left. \pm \mathrm{e}^{i\omega\tau}\mathrm{e}^{-i\mathbf{k}\cdot\mathbf{r}_2(\tau)+i\nu_k t_2(\tau)}\right)\beta(\tau). \end{aligned} \tag{6.13b}$$

By integrating Eq. (6.13b) and plugging it into Eq. (6.13a) we obtain

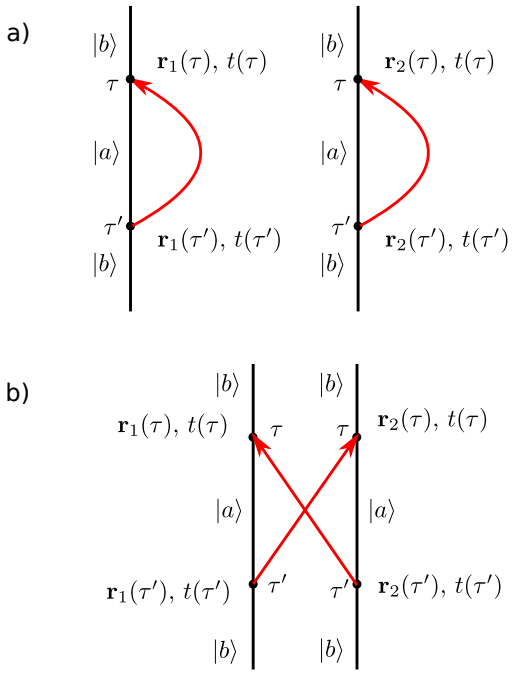

Figure 6.3: (a) Feynman diagram of individual emission and absorption processes. The explanation of this Feynman diagrams is similar to Figure 6.2. Left Feynman diagram is associated with the atom 1 and the right one is associated with the atom 2. (b) Feynman diagram of collective emission and absorption processes. In contrast to Feynman diagrams (a), atomic states are Dicke states. At proper time τ a Minkowski virtual photon is emitted leaving the atomic system in the symmetric or antisymmetric state because we do not know which atom emits. Then the emitted Minkowski virtual photon is reabsorbed by the atomic system at proper time τ'. We also do not know which atom absorbed the Minkowski virtual photon. After the reabsorption, the atomic system remains in the ground state $|b, b\rangle$. In this way total energy is conserved before and after the processes.

$$
\begin{aligned}
\frac{d\beta(\tau)}{d\tau} =& -\frac{\mu^2}{2}\int d^3\mathbf{k}\, g_k^2 \mathrm{e}^{-i\omega\tau}\mathrm{e}^{i\mathbf{k}\cdot\mathbf{r}_1(\tau)-i\nu_k t_1(\tau)} \\
&\times \int_0^\tau d\tau' \mathrm{e}^{i\omega\tau'}\mathrm{e}^{-i\mathbf{k}\cdot\mathbf{r}_1(\tau')+i\nu_k t_1(\tau')}\beta(\tau') \\
&\mp \frac{\mu^2}{2}\int d^3\mathbf{k}\, g_k^2 \mathrm{e}^{-i\omega\tau}\mathrm{e}^{i\mathbf{k}\cdot\mathbf{r}_1(\tau)-i\nu_k t_1(\tau)} \\
&\times \int_0^\tau d\tau' \mathrm{e}^{i\omega\tau'}\mathrm{e}^{-i\mathbf{k}\cdot\mathbf{r}_2(\tau')+i\nu_k t_2(\tau')}\beta(\tau') \\
&\mp \frac{\mu^2}{2}\int d^3\mathbf{k}\, g_k^2 \mathrm{e}^{-i\omega\tau}\mathrm{e}^{i\mathbf{k}\cdot\mathbf{r}_2(\tau)-i\nu_k t_2(\tau)} \\
&\times \int_0^\tau d\tau' \mathrm{e}^{i\omega\tau'}\mathrm{e}^{-i\mathbf{k}\cdot\mathbf{r}_1(\tau')+i\nu_k t_1(\tau')}\beta(\tau') \\
&- \frac{\mu^2}{2}\int d^3\mathbf{k}\, g_k^2 \mathrm{e}^{-i\omega\tau}\mathrm{e}^{i\mathbf{k}\cdot\mathbf{r}_2(\tau)-i\nu_k t_2(\tau)} \\
&\times \int_0^\tau d\tau' \mathrm{e}^{i\omega\tau'}\mathrm{e}^{-i\mathbf{k}\cdot\mathbf{r}_2(\tau')+i\nu_k t_2(\tau')}\beta(\tau'). \qquad (6.14)
\end{aligned}
$$

The first and fourth terms in Eq. (6.14) represent individual processes where atoms emit virtual photon at time $t_i(\tau')$ at point $\mathbf{r}_i(\tau')$ and reabsorb it $t_i(\tau)$ at point $\mathbf{r}_i(\tau)$, where i can be either 1 or 2 (see Figure 6.3(a)). It is nothing to do with collective processes. On the other hand, the second and third terms represent the collective process. Explicitly it means, the atom emits a virtual photon but the emitted virtual photon is absorbed by another atom rather than being absorbed by the original atom. This circumstance is depicted in the Figure 6.3(b).

After integrating with respect to τ' and performing the Markovian approximation, we obtain a simple equation for the probability amplitude $\beta(\tau)$

$$
\frac{d\beta(\tau)}{d\tau} = -\frac{\Gamma_\uparrow}{2}(1 \pm S)\beta(\tau) \qquad (6.15)
$$

where the factor S is given by

$$
S = \frac{\sin\left(\omega\frac{2}{a}\sinh^{-1}\frac{Ra}{2}\right)}{\omega R\sqrt{1+\frac{R^2a^2}{4}}}, \qquad (6.16)
$$

R is interatomic separation defined as $x_2 - x_1$ and $\Gamma_\uparrow$ is the same excitation rate as we defined in

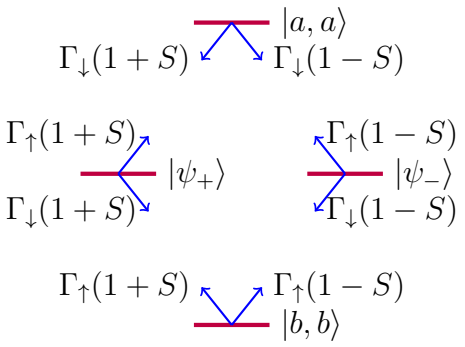

Figure 6.4: All possible transition paths for accelerated pair of two-level atoms and its decay and excitation rates.

the previous section. As a result, the excitation rates from ground state $|b,b\rangle$ to the symmetric state ψ_+ and to the anti-symmetric state ψ_- are respectively, $\Gamma_\uparrow(1+S)$ and $\Gamma_\uparrow(1-S)$ (see Figure 6.4).

The physical interpretation of the above result is fascinating. Indeed, nonzero probability amplitude $\eta_{k\pm}(\tau)$ in Eq. (6.12) implies acceleration radiation into Minkowski spacetime but with increased rate $\Gamma_\uparrow(1+S)$. When $R \to 0$ the rate is doubled as $2\Gamma_\uparrow$. This means two co-accelerating atoms radiate faster than single accelerating atom. This result is easy to be extended for N co-accelerating atoms and we will do it in the next section using the master equation method.

Until now we find only the excitation rate of co-accelerating atoms interacting with the Minkowski vacuum. Similarly, it is easy to obtain the decay and excitation rates for all possible transitions between stationary energy levels of two co-accelerating atoms. These rates are illustrated in Figure 6.4. As it is shown, decay and excitation rates for each transition are multiplied by the same collective term represented by either $1+S$ or $1-S$ depending on transition paths. This means, as we expected, the energy distribution of the accelerating atomic system in the equilibrium state is the same as that for the atoms at rest in a thermal bath with a temperature $a/2\pi$.

6.2.3 Population dynamics of two co-accelerating two-level atoms

The obtained decay and excitation rates shown in Figure 6.4 allow us to write a system of differential equations for the atomic level populations as follows

$$\begin{aligned}
\frac{dP_a(\tau)}{d\tau} =& -2\Gamma_{\downarrow}P_a(\tau) + \Gamma_{\uparrow}(1+S)P_+(\tau) \\
&+ \Gamma_{\uparrow}(1-S)P_-(\tau), \\
\frac{dP_b(\tau)}{d\tau} =& -2\Gamma_{\uparrow}P_b(\tau) + \Gamma_{\downarrow}(1+S)P_+(\tau) \\
&+ \Gamma_{\downarrow}(1-S)P_-(\tau), \\
\frac{dP_+(\tau)}{d\tau} =& -(\Gamma_{\uparrow}+\Gamma_{\downarrow})(1+S)P_+(\tau) \\
&+ \Gamma_{\uparrow}(1+S)P_b(\tau) + \Gamma_{\downarrow}(1+S)P_a(\tau), \\
\frac{dP_-(\tau)}{d\tau} =& -(\Gamma_{\uparrow}+\Gamma_{\downarrow})(1-S)P_-(\tau) \\
&+ \Gamma_{\uparrow}(1-S)P_b(\tau) + \Gamma_{\downarrow}(1-S)P_a(\tau)
\end{aligned} \tag{6.17}$$

where $P_a(\tau) = |\langle a, a|\Psi(\tau)\rangle|^2$, $P_b(\tau) = |\langle b, b|\Psi(\tau)\rangle|^2$ and $P_{\pm} = |\langle \psi_{\pm}|\Psi(\tau)\rangle|^2$. We see that total population is conserved

$$P_a(\tau) + P_b(\tau) + P_+(\tau) + P_-(\tau) = 1. \tag{6.18}$$

Note that the Eq. (6.17) is only valid for pure state without any coherence since it is derived from Schrödinger equation. The total energy rate, calculated using $dE(\tau)/d\tau = \omega d(P_a - P_b)/d\tau$ results in

$$\begin{aligned}
\frac{dE(\tau)}{d\tau} =& -\Gamma_0\omega - \Gamma_0\left(1 + \frac{2}{\mathrm{e}^{2\pi\omega/a}-1}\right)E(\tau) \\
&- \Gamma_0\omega S(P_+(\tau) - P_-(\tau)).
\end{aligned} \tag{6.19}$$

Finally, it is interesting to analyze the stationary solution of the rate Eq. (6.17); we find that it has a steady-state solution as

$$P_a(\infty) = \frac{1}{(\mathrm{e}^{2\pi\omega/a}+1)^2}, \quad P_b(\infty) = \frac{(\mathrm{e}^{2\pi\omega/a})^2}{(\mathrm{e}^{2\pi\omega/a}+1)^2}$$
$$P_+(\infty) = \frac{\mathrm{e}^{2\pi\omega/a}}{(\mathrm{e}^{2\pi\omega/a}+1)^2}, \quad \text{and} \quad P_-(\infty) = P_+(\infty). \tag{6.20}$$

This result can be found from Fermi-Dirac statistics of two two-level atoms. Particularly, each of two atoms satisfies Fermi-Dirac statistics as $p_a = 1/(\mathrm{e}^{2\pi\omega/a}+1)$ and $p_b = \mathrm{e}^{2\pi\omega/a}/(\mathrm{e}^{2\pi\omega/a}+1)$ where p_a and p_b are probabilities of an atom to be in its excited and ground state, respectively. Then using simple probability theory, we obtain Eq. (6.20). Therefore, this simple analysis shows Unruh bath does not differ from a thermal bath of temperature $a/2\pi$ when we consider only the probability distribution of atoms at equilibrium state with the Unruh bath. Furthermore, total atomic energy at steady-state to be as

$$\begin{aligned} E(\infty) &= \omega P_a(\infty) - \omega P_b(\infty) \\ &= -\omega + \frac{2\omega}{\mathrm{e}^{2\pi\omega/a}+1} \end{aligned} \tag{6.21}$$

which also shows a Fermi-Dirac distribution of Unruh temperature $T_{\mathrm{U}} = a/2\pi$.

6.3 Master equation for co-accelerating atoms

Now we apply the master equation approach to our problem. Unlike the previous method, here, we extend the problem to N co-accelerating atoms rather than just two atoms. In the course of the derivation of the master equation, we follow the standard method given in Refs. [160, 167]. Using the second order perturbation theory with Markovian approximation we find

$$\frac{d\hat{\rho}(\tau)}{d\tau} = -\mathrm{Tr}_F \int_0^\tau d\tau' [\hat{V}(\tau), [\hat{V}(\tau'), \hat{\rho}(\tau) \otimes \hat{\rho}_F(0)]] \tag{6.22}$$

where $\hat{\rho}(\tau)$ and $\hat{\rho}_F(0)$ are atomic and field density operators and Tr_F denotes trace with respect to field variables. We take initial Minkowski vacuum state for field as $\hat{\rho}_F(0) = |0\rangle\langle 0|$. Here, the distance between the jth and lth atoms is denoted by R_{jl}. The final result is given by the master equation

$$\begin{aligned}\frac{d\hat{\rho}(\tau)}{d\tau} =& -\frac{\Gamma_\downarrow}{2}\sum_{j,l} S_{jl}(\hat{\sigma}_{+j}\hat{\sigma}_{-l}\hat{\rho} - \hat{\sigma}_{-l}\hat{\rho}\hat{\sigma}_{+j} \\ & - \hat{\sigma}_{-j}\hat{\rho}\hat{\sigma}_{+l} + \hat{\rho}\hat{\sigma}_{+l}\hat{\sigma}_{-j}) \\ & -\frac{\Gamma_\uparrow}{2}\sum_{j,l} S_{jl}(\hat{\sigma}_{-j}\hat{\sigma}_{+l}\hat{\rho} - \hat{\sigma}_{+l}\hat{\rho}\hat{\sigma}_{-j} \\ & - \hat{\sigma}_{+j}\hat{\rho}\hat{\sigma}_{-l} + \hat{\rho}\hat{\sigma}_{-l}\hat{\sigma}_{+j}),\end{aligned} \tag{6.23}$$

where

$$S_{jl} = \frac{\sin\left(\omega\frac{2}{a}\sinh^{-1}\frac{R_{jl}a}{2}\right)}{\omega R_{jl}\sqrt{1+\frac{R_{jl}^2a^2}{4}}}. \tag{6.24}$$

Here, we also omit Cauchy principal parts which are responsible for Lamb shift and Van der Waals force. In the derivation of master equation (6.23) we neglect the mixed terms with co- and counter-rotating transitions due to their violation of energy conservation law. For example, the term $\hat{\sigma}_{+j}\hat{a}\hat{\sigma}_{+l}\hat{a}^\dagger\hat{\rho}$ is omitted.

6.3.1 Comparison of accelerating atoms through Minkowski vacuum and inertial atoms in a thermal bath

The master equation (6.23) is very similar to the master equation of two-level atoms in a thermal bath with a temperature $T_U = a/2\pi$. The only difference is the factor S_{jl}. For co-accelerating two-level atoms, this factor is given by Eq. (6.24) whereas for atoms at rest in the thermal bath, it is

given by

$$S_{jl}^{th} = \frac{\sin(\omega R_{jl})}{\omega R_{jl}}. \tag{6.25}$$

Therefore, it is interesting to discuss the difference between Unruh and thermal baths in terms of the time evolution of density matrix elements of co-accelerating atoms. To do that, we take co-

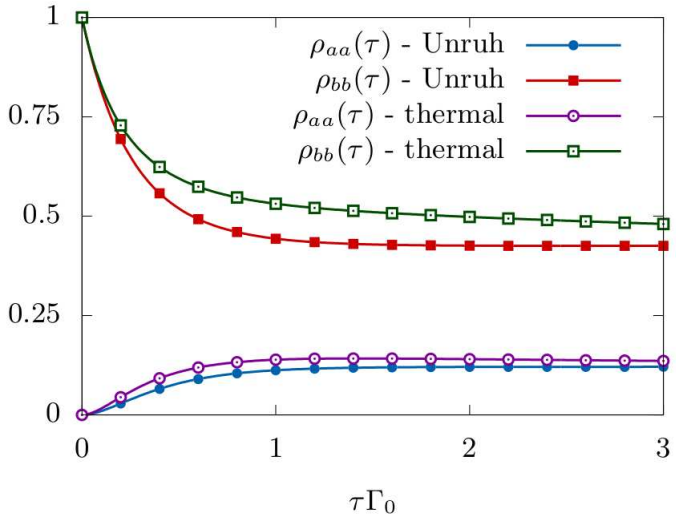

Figure 6.5: Probabilities of excited $|a, a\rangle$ and ground $|b, b\rangle$ states as a function of proper time τ. In the master equation (6.23), the factors S and S_{jl}^{th} are used to compare Unruh and thermal baths. We use the following parameter values: $a = 10\omega$ and $R = 0.1\lambda$.

accelerating two two-level atoms and plot the excited $|a, a\rangle$ and ground $|b, b\rangle$ state probabilities ρ_{aa} and ρ_{bb} as a function of atomic proper time τ. As shown in Figure 6.5, a significant difference is present between $\rho_{bb}(\tau)$ for Unruh (red line with filled square) and Minkowski thermal (green line with hollow square) baths. Similarly, for $\rho_{aa}(\tau)$, small difference is observed. This difference is due to the different factors S_{jl} and S_{jl}^{th} for Unruh and thermal baths, respectively. Here, we choose the case with a large acceleration $a = 10\omega$ and small interatomic distance $R = 0.1\lambda$ to exaggerate the difference. However, the difference is negligible in the limits of $R = 0$ or $a = 0$. The difference is also small when $R \to \infty$ since atoms behave like individual systems. This result

is also consistent with the local character of the Unruh effect [168, 166] which states two-point correlation functions for Unruh and thermal baths are equivalent only if the distance between two points is zero.

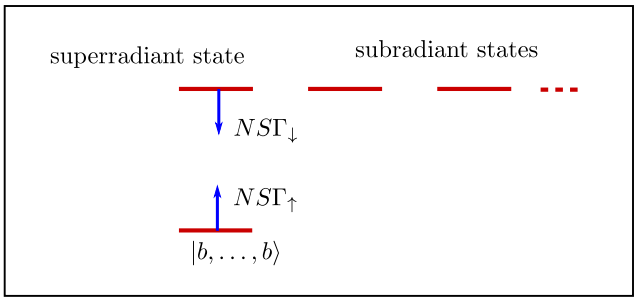

Figure 6.6: Ground state $|b,\ldots,b\rangle$ and single excited super and subradiant states of N two-level atoms. Only allowed transition is between ground and superradiant states. Enhanced decay and excitation rates are shown by blue arrows.

6.3.2 Enhanced acceleration radiation

Now we study acceleration radiation for N co-accelerating two-level atoms in the limit $R \to 0$. We assume all two-level atoms are initially in their ground state e.g. $|b,\ldots,b\rangle$. Then, at the beginning of time evolution, intensity of acceleration radiation is approximately proportional to rate $d\rho_g(\tau)/d\tau$ where $\rho_g(\tau)$ is density matrix element of the ground state $|b,\ldots,b\rangle$. The rate $d\rho_g(\tau)/d\tau$ can be easily derived from master equation (6.23) assuming $R \to 0$ ($S \to 1$) and given by

$$\left.\frac{d\rho_g(\tau)}{d\tau}\right|_{R\to 0} = \left.-NS\Gamma_{\uparrow}\rho_g(\tau) + NS\Gamma_{\downarrow}\rho_+(\tau)\right|_{S\to 1} \tag{6.26}$$

(cf. with Eq. (6.17)). Here, $\rho_+(\tau)$ is density matrix element of single excited symmetric state (or superradiant state as shown in Figure 6.6). In the beginning of the evolution, $\rho_g \approx 1$ and $\rho_+ \approx 0$ therefore the rate of $\rho_g(\tau)$ is approximately $N\Gamma_{\uparrow}$ which is N times larger than that of single two-level atom (we assume $S = 1$). With that, we conclude that intensity of acceleration

radiation from N two-level atoms confined in small volume is much stronger than the intensity of acceleration radiation emitted from a single two-level atom (see Figure 6.6). We call it enhanced acceleration radiation and its dependence on N is quadratic. We hope this enhanced acceleration radiation will be exploited as a direct or indirect tool to experimentally observe the Unruh effect.

6.4 Conclusions

In this work, we consider uniformly co-accelerating two-level atoms interacting with the Minkowski vacuum of a massless scalar field. Since our interest is the collective phenomena of the system we place the atoms in line whose length is much shorter than the transition wavelength of atoms. Our calculation demonstrates that decay and excitation rates of single-excited superradiant state are proportional to the number of atoms N both for co-accelerating and inertial two-level atoms in the case of Dicke limit $R \to 0$. Thus, two-level atoms are excited with the enhanced rate in Rindler spacetime and this excitation could be seen by Minkowski observer as enhanced acceleration radiation via Dicke superradiance. In this manner, we claim that the intensity of acceleration radiation emitted from co-accelerating atoms has a quadratic dependence on the number of atoms ($\sim N^2$) and therefore, the enhanced acceleration radiation could be considerably useful for the experimental demonstration of the Unruh effect.

7. SUMMARY AND CONCLUSIONS

Theoretical studies of quantum coherence and its implication on a variety of physical systems, in particular Dicke superradiance, Fano-Agarwal couplings in timed Dicke subradiance, uniformly accelerating two-level atoms, have been presented in this dissertation. Furthermore, enhancing the spectroscopic signal of CARS-ROA using quantum coherence is also explored in this dissertation. The main results and achievements are summarized as follows.

1. It is shown that the chiral sample can emit 10^4 times strong CARS-ROA signal in comparison with ROA. But for the heterodyne detection scheme, the enhancement factor is estimated as 10^2. Essentially, we show that molecular coherence plays an equally important role in higher-order optically active processes which involve magnetic dipole and electric quadrupole moments.

2. We developed a new method for finding the rotational average of odd-rank tensors. The method is tested in the case of 5th and 7th rank tensors and applied to 9th and 11th rank tensors. Rotational averages of 9th and 11th rank tensors are obtained in the linearly dependent basis for the first time.

3. Using genealogically adapted Young operators, the explicit forms of single- and double-excited Dicke subradiant states are obtained for an arbitrary number of molecules for the first time. The obtained formula of single-excited subradiant Dicke states much helps to design the sidewise excitation method.

4. We revealed a substantial effect of Fano-Agarwal couplings on the spontaneous decay of timed Dicke states. In particular, the decay rate of the symmetric timed Dicke state slows down while those of the subradiant timed Dicke states speed up due to Fano-Agarwal couplings. Moreover, the inclusion of scalar Lamb shift results in a huge effect on timed Dicke subradiant states (about 40%) but has no significant effect on symmetric timed Dicke state.

Finally, this study shows that Fano-Agarwal coupling should not be simply ignored when applications of subradiant states are concerned.

5. We demonstrated that the coherence effects of co-accelerating atoms are not the same as those of inertial atoms interacting with the thermal field of Unruh temperature. Furthermore, due to Dicke superradiance and quantum coherence, it is concluded that the intensity of acceleration radiation of N co-accelerating atoms is N times stronger than the intensity of radiation coming from a single atom. We expect this enhanced acceleration radiation can provide a new way to experimentally demonstrate the Unruh effect.

Finally, we expect this research works can be of substantial interest of the physical community.

REFERENCES

[1] M. O. Scully, G. W. Kattawar, R. P. Lucht, T. Opatrný, H. Pilloff, A. Rebane, A. V. Sokolov, and M. S. Zubairy, "FAST CARS: Engineering a laser spectroscopic technique for rapid identification of bacterial spores," *Proc. Natl. Acad. Sci. U.S.A.*, vol. 99, pp. 10994–11001, Aug 2002.

[2] A. J. Traverso, B. Hokr, Z. Yi, L. Yuan, S. Yamaguchi, M. O. Scully, and V. V. Yakovlev, "Two-photon infrared resonance can enhance coherent Raman scattering," *Phys. Rev. Lett.*, vol. 120, p. 063602, Feb 2018.

[3] R. H. Dicke, "Coherence in spontaneous radiation processes," *Phys. Rev.*, vol. 93, pp. 99–110, Jan 1954.

[4] D. Pavolini, A. Crubellier, P. Pillet, L. Cabaret, and S. Liberman, "Experimental evidence for subradiance," *Phys. Rev. Lett.*, vol. 54, pp. 1917–1920, Apr 1985.

[5] R. G. DeVoe and R. G. Brewer, "Observation of superradiant and subradiant spontaneous emission of two trapped ions," *Phys. Rev. Lett.*, vol. 76, pp. 2049–2052, Mar 1996.

[6] C. Hettich, C. Schmitt, J. Zitzmann, S. Kúhn, I. Gerhardt, and V. Sandoghdar, "Nanometer resolution and coherent optical dipole coupling of two individual molecules," *Science*, vol. 298, pp. 385–389, Oct 2002.

[7] Y. Sonnefraud, N. Verellen, H. Sobhani, G. A. Vandenbosch, V. V. Moshchalkov, P. Van Dorpe, P. Nordlander, and S. A. Maier, "Experimental realization of subradiant, superradiant, and Fano resonances in ring/disk plasmonic nanocavities," *ACS Nano*, vol. 4, pp. 1664–1670, Feb 2010.

[8] W. Zhou and T. W. Odom, "Tunable subradiant lattice plasmons by out-of-plane dipolar interactions," *Nat. Nanotechnol.*, vol. 6, pp. 423–427, May 2011.

[9] S. Filipp, A. F. van Loo, M. Baur, L. Steffen, and A. Wallraff, "Preparation of subradiant states using local qubit control in circuit QED," *Phys. Rev. A*, vol. 84, p. 061805, Dec 2011.

[10] Y. Takasu, Y. Saito, Y. Takahashi, M. Borkowski, R. Ciuryło, and P. S. Julienne, "Controlled production of subradiant states of a diatomic molecule in an optical lattice," *Phys. Rev. Lett.*, vol. 108, p. 173002, Apr 2012.

[11] B. McGuyer, M. McDonald, G. Iwata, M. Tarallo, W. Skomorowski, R. Moszynski, and T. Zelevinsky, "Precise study of asymptotic physics with subradiant ultracold molecules," *Nat. Phys.*, vol. 11, pp. 32–36, Jan 2015.

[12] S. Sarkar and J. S. Satchell, "Optical bistability with small numbers of atoms," *Europhys. Lett.*, vol. 3, pp. 797–801, Apr 1987.

[13] S. Sarkar and J. S. Satchell, "Solution of master equations for small bistable systems," *J. Phys. A: Math. Gen.*, vol. 20, pp. 2147–2157, Jun 1987.

[14] N. Shammah, N. Lambert, F. Nori, and S. De Liberato, "Superradiance with local phase-breaking effects," *Phys. Rev. A*, vol. 96, p. 023863, Aug 2017.

[15] M. Gegg and M. Richter, "PsiQuaSP–a library for efficient computation of symmetric open quantum systems," *Sci. Rep.*, vol. 7, p. 16304, Jul 2017.

[16] M. Gegg, A. Carmele, A. Knorr, and M. Richter, "Superradiant to subradiant phase transition in the open system Dicke model: dark state cascades," *New J. Phys.*, vol. 20, p. 013006, Jan 2018.

[17] P. Kirton and J. Keeling, "Superradiant and lasing states in driven-dissipative Dicke models," *New J. Phys.*, vol. 20, p. 015009, Jan 2018.

[18] M. Xu, D. A. Tieri, and M. J. Holland, "Simulating open quantum systems by applying SU(4) to quantum master equations," *Phys. Rev. A*, vol. 87, p. 062101, Jun 2013.

[19] T. K. Begzjav, L. Wang, and R. Nessler, "On permutation symmetry of subradiant states and its application," *Phys. Scr.*, vol. 94, p. 094001, Jun 2019.

[20] J. O. Bjarnason, H. C. Andersen, and B. S. Hudson, "Quantum theory of coherent Raman scattering by optically active isotropic materials," *J. Chem. Phys.*, vol. 72, pp. 4132–4140, Apr 1980.

[21] J. Oudar, C. Minot, and B. A. Garetz, "Polarization spectroscopy as a probe of Raman optical activity," *J. Chem. Phys.*, vol. 76, pp. 2227–2237, Mar 1982.

[22] K. Hiramatsu, M. Okuno, H. Kano, P. Leproux, V. Couderc, and Hiro-o. Hamaguchi, "Observation of Raman optical activity by heterodyne-detected polarization-resolved coherent anti-Stokes Raman scattering," *Phys. Rev. Lett.*, vol. 109, p. 083901, Aug 2012.

[23] K. Hiramatsu, H. Kano, and T. Nagata, "Raman optical activity by coherent anti-Stokes Raman scattering spectral interferometry," *Opt. Express*, vol. 21, pp. 13515–13521, Jun 2013.

[24] K. Hiramatsu, P. Leproux, V. Couderc, T. Nagata, and H. Kano, "Raman optical activity spectroscopy by visible-excited coherent anti-Stokes Raman scattering," *Opt. Lett.*, vol. 40, pp. 4170–4173, Sep 2015.

[25] T. Kh. Begzjav, Z. Zhang, M. O. Scully, and G. S. Agarwal, "Enhanced signals from chiral molecules via molecular coherence," *Opt. Express*, vol. 27, pp. 13965–13977, May 2019.

[26] J. Marino, A. Noto, and R. Passante, "Thermal and nonthermal signatures of the Unruh effect in Casimir-Polder forces," *Phys. Rev. Lett.*, vol. 113, p. 020403, Jul 2014.

[27] L. Rizzuto, M. Lattuca, J. Marino, A. Noto, S. Spagnolo, W. Zhou, and R. Passante, "Nonthermal effects of acceleration in the resonance interaction between two uniformly accelerated atoms," *Phys. Rev. A*, vol. 94, p. 012121, Jul 2016.

[28] J. Marino and R. Passante, *Casimir-Polder forces between two accelerating atoms and the Unruh effect*, pp. 328–333. World Scientific, 2010.

[29] W. Zhou, R. Passante, and L. Rizzuto, "Resonance dipole-dipole interaction between two accelerated atoms in the presence of a reflecting plane boundary," *Symmetry*, vol. 10, May 2018.

[30] T. K. Begzjav, J. Ben-Benjamin, M. O. Scully, and W. G. Unruh, "Acceleration radiation enhanced by superradiance: Dicke meets Unruh." to be published.

[31] M. O. Scully, S.-Y. Zhu, and A. Gavrielides, "Degenerate quantum-beat laser: Lasing without inversion and inversion without lasing," *Phys. Rev. Lett.*, vol. 62, pp. 2813–2816, Jun 1989.

[32] O. Kocharovskaya, "Amplification and lasing without inversion," *Phys. Rep.*, vol. 219, pp. 175–190, Oct 1992.

[33] K.-J. Boller, A. Imamoğlu, and S. E. Harris, "Observation of electromagnetically induced transparency," *Phys. Rev. Lett.*, vol. 66, pp. 2593–2596, May 1991.

[34] R. Bonifacio and L. A. Lugiato, "Cooperative radiation processes in two-level systems: Superfluorescence," *Phys. Rev. A*, vol. 11, pp. 1507–1521, May 1975.

[35] G. O. Ariunbold, V. A. Sautenkov, and M. O. Scully, "Temporal coherent control of superfluorescent pulses," *Opt. Lett.*, vol. 37, pp. 2400–2402, Jun 2012.

[36] T. Ritz, S. Adem, and K. Schulten, "A model for photoreceptor-based magnetoreception in birds," *Biophysical Journal*, vol. 78, pp. 707–718, Feb 2000.

[37] C. T. Rodgers and P. J. Hore, "Chemical magnetoreception in birds: The radical pair mechanism," *Proc. Natl. Acad. Sci. U. S. A.*, vol. 106, pp. 353–360, Jan 2009.

[38] G. S. Engel, T. R. Calhoun, E. L. Read, T.-K. Ahn, T. Mančal, Y.-C. Cheng, R. E. Blankenship, and G. R. Fleming, "Evidence for wavelike energy transfer through quantum coherence in photosynthetic systems," *Nature*, vol. 446, pp. 782–786, Apr 2007.

[39] G. I. Petrov, R. Arora, V. V. Yakovlev, X. Wang, A. V. Sokolov, and M. O. Scully, "Comparison of coherent and spontaneous Raman microspectroscopies for noninvasive detection of single bacterial endospores," *Proc. Natl. Acad. Sci. U.S.A.*, vol. 104, pp. 7776–7779, May 2007.

[40] J. P. Ogilvie, M. Cui, D. Pestov, A. V. Sokolov, and M. O. Scully, "Time-delayed coherent Raman spectroscopy," *Mol. Phys.*, vol. 106, no. 2–4, pp. 587–594, 2008.

[41] M. O. Scully, E. S. Fry, C. H. R. Ooi, and K. Wódkiewicz, "Directed spontaneous emission from an extended ensemble of N atoms: Timing is everything," *Phys. Rev. Lett.*, vol. 96, p. 010501, Jan 2006.

[42] W. G. Unruh, "Notes on black-hole evaporation," *Phys. Rev. D*, vol. 14, pp. 870–892, Aug 1976.

[43] S. A. Fulling, "Nonuniqueness of canonical field quantization in Riemannian space-time," *Phys. Rev. D*, vol. 7, pp. 2850–2862, May 1973.

[44] P. C. W. Davies, "Scalar production in Schwarzschild and Rindler metrics," *J. Phys. A: Math. Gen.*, vol. 8, no. 4, pp. 609–616, 1975.

[45] M. O. Scully, S. Fulling, D. M. Lee, D. N. Page, W. P. Schleich, and A. A. Svidzinsky, "Quantum optics approach to radiation from atoms falling into a black hole," *Proc. Natl. Acad. Sci. U. S. A.*, vol. 115, pp. 8131–8136, Aug 2018.

[46] V. Mukhanov and S. Winitzki, *Introduction to quantum effects in gravity*. Cambridge University Press, 2007.

[47] A. Belyanin, V. V. Kocharovsky, F. Capasso, E. Fry, M. S. Zubairy, and M. O. Scully, "Quantum electrodynamics of accelerated atoms in free space and in cavities," *Phys. Rev. A*, vol. 74, p. 023807, Aug 2006.

[48] W. G. Unruh and R. M. Wald, "What happens when an accelerating observer detects a Rindler particle," *Phys. Rev. D*, vol. 29, pp. 1047–1056, Mar 1984.

[49] V. L. Ginzburg and V. P. Frolov, "Vacuum in a homogeneous gravitational field and excitation of a uniformly accelerated detector," *Soviet Physics - Uspekhi*, vol. 30, pp. 1073–1095, Dec 1987.

[50] A. O. Barut and J. P. Dowling, "Quantum electrodynamics based on self-fields: On the origin of thermal radiation detected by an accelerating observer," *Phys. Rev. A*, vol. 41, pp. 2277–2283, Mar 1990.

[51] G. Ford and R. O'Connell, "Is there Unruh radiation?," *Phys. Lett. A*, vol. 350, pp. 17–26, Jan 2006.

[52] D. J. Raine, D. W. Sciama, and P. G. Grove, "Does a uniformly accelerated quantum oscillator radiate?," *Proc. R. Soc. London, Ser. A*, vol. 435, pp. 205–215, Oct 1991.

[53] J. Bell and J. Leinaas, "Electrons as accelerated thermometers," *Nucl. Phys. B*, vol. 212, pp. 131–150, Feb 1983.

[54] J. Bell and J. Leinaas, "The Unruh effect and quantum fluctuations of electrons in storage rings," *Nucl. Phys. B*, vol. 284, pp. 488–508, 1987.

[55] N. Rad and D. Singleton, "A test of the circular Unruh effect using atomic electrons," *Eur. Phys. J. D*, vol. 66, p. 258, Oct 2012.

[56] E. Yablonovitch, "Accelerating reference frame for electromagnetic waves in a rapidly growing plasma: Unruh-Davies-Fulling-Dewitt radiation and the nonadiabatic Casimir effect," *Phys. Rev. Lett.*, vol. 62, pp. 1742–1745, Apr 1989.

[57] P. Chen and T. Tajima, "Testing Unruh radiation with ultraintense lasers," *Phys. Rev. Lett.*, vol. 83, pp. 256–259, Jul 1999.

[58] G. Cozzella, A. G. S. Landulfo, G. E. A. Matsas, and D. A. T. Vanzella, "Proposal for observing the Unruh effect using classical electrodynamics," *Phys. Rev. Lett.*, vol. 118, p. 161102, Apr 2017.

[59] L. Barron and A. Buckingham, "Rayleigh and Raman scattering from optically active molecules," *Mol. Phys.*, vol. 20, no. 6, pp. 1111–1119, 1971.

[60] L. D. Barron, M. P. Bogaard, and A. D. Buckingham, "Raman scattering of circularly polarized light by optically active molecules," *J. Am. Chem. Soc.*, vol. 95, pp. 603–605, Jan 1973.

[61] W. Hug, "Virtual enantiomers as the solution of optical activity's deterministic offset problem," *Appl. Spectrosc.*, vol. 57, pp. 1–13, Jan 2003.

[62] L. D. Barron, *Molecular Light Scattering and Optical Activity*. Cambridge University, 2 ed., 2004.

[63] L. A. Nafie, *Vibrational Optical Activity: Principles and Applications*. A John Wiley & Sons, Ltd, 1 ed., 2011.

[64] V. Parchaňský, J. Kapitán, and P. Bouř, "Inspecting chiral molecules by Raman optical activity spectroscopy," *RSC Adv.*, vol. 4, pp. 57125–57136, Oct 2014.

[65] L. D. Barron, "The development of biomolecular Raman optical activity spectroscopy," *Biomedical Spectroscopy and Imaging*, vol. 4, no. 3, pp. 223–253, 2015.

[66] N. I. Koroteev, "BioCARS — a novel nonlinear optical technique to study vibrational spectra of chiral biological molecules in solution," *Biospectroscopy*, vol. 1, no. 5, pp. 341–350, 1995.

[67] L. A. Nafie, "Theory of resonance Raman optical activity: the single electronic state limit," *Chem. Phys.*, vol. 205, pp. 309 – 322, May 1996.

[68] A. M. Zheltikov and A. N. Naumov, "Waveguide solution of the Koroteev problem in the nonlinear optics of media with broken mirror symmetry: collinear three- and five-wave mixing schemes in planar waveguides," *Quantum Electron.*, vol. 29, no. 7, pp. 607–612, 1999.

[69] C. Merten, H. Li, X. Lu, A. Hartwig, and L. A. Nafie, "Observation of resonance electronic and non-resonance-enhanced vibrational natural Raman optical activity," *J. Raman Spectrosc.*, vol. 41, pp. 1563–1565, Dec 2010.

[70] J.-X. Cheng and X. S. Xie, "Coherent anti-Stokes Raman scattering microscopy:âĂL'instrumentation, theory, and applications," *J. Phys. Chem. B*, vol. 108, pp. 827–840, Dec 2003.

[71] J.-x. Cheng, A. Volkmer, L. D. Book, and X. S. Xie, "An epi-detected coherent anti-Stokes Raman scattering (E-CARS) microscope with high spectral resolution and high sensitivity," *J. Phys. Chem. B*, vol. 105, no. 7, pp. 1277–1280, 2001.

[72] A. Volkmer, L. D. Book, and X. S. Xie, "Time-resolved coherent anti-Stokes Raman scattering microscopy: Imaging based on Raman free induction decay," *Appl. Phys. Lett.*, vol. 80, pp. 1505–1507, Feb 2002.

[73] D. Pestov, X. Wang, G. O. Ariunbold, R. K. Murawski, V. A. Sautenkov, A. Dogariu, A. V. Sokolov, and M. O. Scully, "Single-shot detection of bacterial endospores via coherent Raman spectroscopy," *Proc. Nat. Acad. Sci. U.S.A.*, vol. 105, pp. 422–427, Jan 2008.

[74] S. E. Harris and A. V. Sokolov, "Subfemtosecond pulse generation by molecular modulation," *Phys. Rev. Lett.*, vol. 81, pp. 2894–2897, Oct 1998.

[75] A. V. Sokolov, K. K. Lehmann, M. O. Scully, and D. Herschbach, "Orienting molecules via an ir and uv pulse pair: Implications for coherent Raman spectroscopy," *Phys. Rev. A*, vol. 79, p. 053805, May 2009.

[76] S. A. Malinovskaya and V. S. Malinovsky, "Chirped-pulse adiabatic control in coherent anti-Stokes Raman scattering for imaging of biological structure and dynamics," *Opt. Lett.*, vol. 32, pp. 707–709, Mar 2007.

[77] D. A. Long, *The Raman Effect: A Unified Treatment of the Theory of Raman Scattering by Molecules*. A John Wiley & Sons, Ltd, 2002.

[78] F. Lu, W. Zheng, and Z. Huang, "Heterodyne polarization coherent anti-Stokes Raman scattering microscopy," *Appl. Phys. Lett.*, vol. 92, p. 123901, Mar 2008.

[79] D. Che and L. A. Nafie, "Isolation of Raman optical activity invariants," *Chem. Phys. Lett.*, vol. 189, pp. 35–42, Jan 1992.

[80] D. Craig and T. Thirunamachandran, *Molecular Quantum Electrodynamics: An Introduction to Radiation-molecule Interactions*. Dover Books on Chemistry Series, Dover Publications, 1998.

[81] L. Gårding and B. Nordén, "Simple formulas for rotation averages of spectroscopic intensities," *Chem. Phys.*, vol. 41, no. 3, pp. 431 – 437, 1979.

[82] S. J. Cyvin, J. E. Rauch, and J. C. Decius, "Theory of hyper-Raman effects (nonlinear inelastic light scattering): Selection rules and depolarization ratios for the second-order polarizability," *J. Chem. Phys.*, vol. 43, pp. 4083–4095, Dec 1965.

[83] D. L. Andrews and T. Thirunamachandran, "On three-dimensional rotational averages," *J. Chem. Phys.*, vol. 67, pp. 5026–5033, Dec 1977.

[84] D. L. Andrews and T. Thirunamachandran, "The hyper-Raman effect: A new approach to vibrational mode classification and assignment of spectral lines," *J. Chem. Phys.*, vol. 68, pp. 2941–2951, Mar 1978.

[85] W. M. McClain, "Polarization dependence of three-photon phenomena for randomly oriented molecules," *J. Chem. Phys.*, vol. 57, pp. 2264–2272, Sep 1972.

[86] D. L. Andrews and P. J. Wilkes, "Irreducible tensors and selection rules for three-frequency absorption," *J. Chem. Phys.*, vol. 83, pp. 2009–2014, Sep 1985.

[87] J. R. Cable and A. C. Albrecht, "Theory of three-photon photoselection with application to the hexagonal point groups," *J. Chem. Phys.*, vol. 85, pp. 3145–3154, Sep 1986.

[88] J. S. Ford and D. L. Andrews, "Molecular tensor analysis of third-harmonic scattering in liquids," *J. Phys. Chem. A*, vol. 122, no. 2, pp. 563–573, 2018.

[89] G. F. Smith, "On isotropic tensors and rotation tensors of dimension m and order n," *Tensor, N. S.*, vol. 19, pp. 79–88, 1968.

[90] L. L. Boyle, "Fifth-rank molecular polarization tensors," *Int. J. Quantum Chem.*, vol. 4, pp. 413–425, Jul 1970.

[91] L. L. Boyle and P. S. C. Matthews, "The isotropic invariants of fifth-rank cartesian tensors," *Int. J. Quantum Chem.*, vol. 5, pp. 381–386, Jul 1971.

[92] D. L. Andrews and W. A. Ghoul, "Eighth rank isotropic tensors and rotational averages," *J. Phys. A: Math. Gen.*, vol. 14, no. 6, pp. 1281–1290, 1981.

[93] G. Wagnière, "The evaluation of three-dimensional rotational averages," *J. Chem. Phys.*, vol. 76, pp. 473–480, Jan 1982.

[94] D. L. Andrews and N. P. Blake, "Three-dimensional rotational averages in radiation-molecule interactions: an irreducible cartesian tensor formulation," *J. Phys. A: Math. Gen.*, vol. 22, no. 1, pp. 49–60, 1989.

[95] S. N. A. Smith and D. L. Andrews, "Three-dimensional ensemble averages for tensorial interactions in partially oriented, multi-particle systems," *J. Phys. A: Math. Theor.*, vol. 44, p. 395001, Sep 2011.

[96] P. P. Man, "Cartesian and spherical tensors in NMR Hamiltonians," *Concepts Magn. Reson., Part A*, vol. 42, pp. 197–244, Feb 2014.

[97] D. H. Friese, M. T. P. Beerepoot, and K. Ruud, "Rotational averaging of multiphoton absorption cross sections," *J. Chem. Phys.*, vol. 141, p. 204103, Nov 2014.

[98] T. Kh. Begzjav, M. O. Scully, and G. S. Agarwal, "Coherent Anti-Stokes Raman scattering in optically active medium," *arXiv e-prints*, p. arXiv:1901.00459, Jan. 2019.

[99] T. K. Begzjav and R. Nessler, "On three-dimensional rotational averages of odd-rank tensors," *Phys. Scr.*, vol. 94, p. 105504, Aug 2019.

[100] H. Goldstein, *Classical Mechanics*. Addison-Wesley Publishing Company, Inc., 2 ed., 1980.

[101] H. Weyl, *The Classical Groups: Their Invariants and Representations*. Princeton mathematical series, Princeton University Press, 1939.

[102] R. Nessler and T. Begzjav, "A general method for rotational averages," *arXiv e-prints*, p. arXiv:1902.02396, Feb 2019.

[103] M. Abramowitz and I. A. Stegun, *Handbook of Mathematical Functions with Formulas, Graphs, and Mathematical Tables*. New York: Dover, 1972.

[104] A. R. Edmonds, *Angular Momentum in Quantum Mechanics*. Investigations in physics, Princeton University Press, 1957.

[105] E. A. Power and T. Thirunamachandran, "Circular dichroism: A general theory based on quantum electrodynamics," *J. Chem. Phys.*, vol. 60, pp. 3695–3701, May 1974.

[106] I. Tinoco, "Two-photon circular dichroism," *J. Chem. Phys.*, vol. 62, pp. 1006–1009, Feb 1975.

[107] M. Hamermesh, *Group Theory and Its Application to Physical Problems*. Addison Wesley Series in Physics, Dover Publications, 1989.

[108] M. Gross and S. Haroche, "Superradiance: An essay on the theory of collective spontaneous emission," *Phys. Rep.*, vol. 93, pp. 301–396, Dec 1982.

[109] M. O. Scully and A. A. Svidzinsky, "The super of superradiance," *Science*, vol. 325, pp. 1510–1511, Sep 2009.

[110] A. Wallraff, D. I. Schuster, A. Blais, L. Frunzio, R.-S. Huang, J. Majer, S. Kumar, S. M. Girvin, and R. J. Schoelkopf, "Strong coupling of a single photon to a superconducting qubit using circuit quantum electrodynamics," *Nature*, vol. 431, pp. 162–167, Sep 2004.

[111] J. Majer, J. M. Chow, J. M. Gambetta, J. Koch, B. R. Johnson, J. A. Schreier, L. Frunzio, D. I. Schuster, A. A. Houck, A. Wallraff, A. Blais, M. H. Devoret, S. M. Girvin, and R. J. Schoelkopf, "Coupling superconducting qubits via a cavity bus," *Nature*, vol. 449, pp. 443–447, Sep 2007.

[112] A. A. Houck, D. I. Schuster, J. M. Gambetta, J. A. Schreier, B. R. Johnson, J. M. Chow, L. Frunzio, J. Majer, M. H. Devoret, S. M. Girvin, and R. J. Schoelkopf, "Generating single microwave photons in a circuit," *Nature*, vol. 449, pp. 328–331, Sep 2007.

[113] A. Beige, S. F. Huelga, P. L. Knight, M. B. Plenio, and R. C. Thompson, "Coherent manipulation of two dipole-dipole interacting ions," *J. Mod. Opt.*, vol. 47, no. 2–3, pp. 401–414, 2000.

[114] M. O. Scully, "Single photon subradiance: Quantum control of spontaneous emission and ultrafast readout," *Phys. Rev. Lett.*, vol. 115, p. 243602, Dec 2015.

[115] J. M. Fink, R. Bianchetti, M. Baur, M. Göppl, L. Steffen, S. Filipp, P. J. Leek, A. Blais, and A. Wallraff, "Dressed collective qubit states and the Tavis-Cummings model in circuit QED," *Phys. Rev. Lett.*, vol. 103, p. 083601, Aug 2009.

[116] P. C. de Groot, J. Lisenfeld, R. N. Schouten, S. Ashhab, A. Lupascu, C. J. P. M. Harmans, and J. E. Mooij, "Selective darkening of degenerate transitions demonstrated with two superconducting quantum bits," *Nat. Phys.*, vol. 6, pp. 763–766, Aug 2010.

[117] J. M. Chow, A. D. Córcoles, J. M. Gambetta, C. Rigetti, B. R. Johnson, J. A. Smolin, J. R. Rozen, G. A. Keefe, M. B. Rothwell, M. B. Ketchen, and M. Steffen, "Simple all-microwave entangling gate for fixed-frequency superconducting qubits," *Phys. Rev. Lett.*, vol. 107, p. 080502, Aug 2011.

[118] S. Filipp, M. Göppl, J. M. Fink, M. Baur, R. Bianchetti, L. Steffen, and A. Wallraff, "Multimode mediated qubit-qubit coupling and dark-state symmetries in circuit quantum electrodynamics," *Phys. Rev. A*, vol. 83, p. 063827, Jun 2011.

[119] A. Crubellier and D. Pavolini, "Superradiance and subradiance. II. Atomic systems with degenerate transitions," *J. Phys. B: At. Mol. Phys.*, vol. 19, pp. 2109–2138, Jul 1986.

[120] A. Crubellier, "Superradiance and subradiance. III. Small samples," *J. Phys. B: At. Mol. Phys.*, vol. 20, pp. 971–996, Mar 1987.

[121] A. Crubellier and D. Pavolini, "Superradiance and subradiance. IV. Atomic cascades between degenerate levels," *J. Phys. B: At. Mol. Phys.*, vol. 20, pp. 1451–1470, Apr 1987.

[122] D. Petrosyan and G. Kurizki, "Scalable solid-state quantum processor using subradiant two-atom states," *Phys. Rev. Lett.*, vol. 89, p. 207902, Oct 2002.

[123] V. V. Temnov and U. Woggon, "Superradiance and subradiance in an inhomogeneously broadened ensemble of two-level systems coupled to a low-Q cavity," *Phys. Rev. Lett.*, vol. 95, p. 243602, Dec 2005.

[124] P. A. Vetter, L. Wang, D.-W. Wang, and M. O. Scully, "Single photon subradiance and superradiance revisited: a group theoretic analysis of subradiant states," *Phys. Scr.*, vol. 91, p. 023007, Jan 2016.

[125] I. M. Mirza and T. Begzjav, "Fano-Agarwal couplings and non-rotating wave approximation in single-photon timed Dicke subradiance," *Europhys. Lett.*, vol. 114, p. 24004, May 2016.

[126] H. Cai, D.-W. Wang, A. A. Svidzinsky, S.-Y. Zhu, and M. O. Scully, "Symmetry-protected single-photon subradiance," *Phys. Rev. A*, vol. 93, p. 053804, May 2016.

[127] T. Yamanouchi, "On the construction of unitary irreducible representations of the symmetric group," *Proc. Phys.-Math. Soc. Jap.*, vol. 19, pp. 436–450, Apr 1937.

[128] R. Pauncz, *Spin eigenfunctions: construction and use*. Plenum Press, 1979.

[129] R. Pauncz, *The Construction of Spin Eigenfunctions: An Exercise Book*. Springer US, 2000.

[130] A. Young, "On quantitative substitutional analysis," *Proc. London Math. Soc.*, vol. s1-33, pp. 97–145, Nov 1900. see p. 133.

[131] P.-o. Löwdin, "Group algebra, convolution algebra, and applications to quantum mechanics," *Rev. Mod. Phys.*, vol. 39, pp. 259–287, Apr 1967.

[132] H. V. McIntosh, "Symmetry-adapted functions belonging to the symmetric groups," *J. Math. Phys.*, vol. 1, pp. 453–460, Nov 1960.

[133] W. I. Salmon, "Genealogical electronic spin eigenfunctions and antisymmetric many-electron wavefunctions generated directly from Young diagrams," vol. 8 of *Adv. Quantum Chem.*, pp. 37–94, Academic Press, 1974.

[134] M. Tavis and F. W. Cummings, "Exact solution for an N-molecule—radiation-field Hamiltonian," *Phys. Rev.*, vol. 170, pp. 379–384, Jun 1968.

[135] L. Allen and J. Eberly, *Optical Resonance and Two-level Atoms*. Dover books on physics and chemistry, Dover, 1987.

[136] A. A. Svidzinsky, J.-T. Chang, and M. O. Scully, "Dynamical evolution of correlated spontaneous emission of a single photon from a uniformly excited cloud of N atoms," *Phys. Rev. Lett.*, vol. 100, p. 160504, Apr 2008.

[137] E. A. Sete, A. A. Svidzinsky, H. Eleuch, Z. Yang, R. D. Nevels, and M. O. Scully, "Correlated spontaneous emission on the Danube," *J. Mod. Opt.*, vol. 57, pp. 1311–1330, Mar 2010.

[138] A. A. Svidzinsky, X. Zhang, and M. O. Scully, "Quantum versus semiclassical description of light interaction with atomic ensembles: Revision of the Maxwell-Bloch equations and single-photon superradiance," *Phys. Rev. A*, vol. 92, p. 013801, Jul 2015.

[139] R. Wiegner, J. von Zanthier, and G. S. Agarwal, "Quantum-interference-initiated superradiant and subradiant emission from entangled atoms," *Phys. Rev. A*, vol. 84, p. 023805, Aug 2011.

[140] M. O. Scully, "Collective Lamb shift in single photon Dicke superradiance," *Phys. Rev. Lett.*, vol. 102, p. 143601, Apr 2009.

[141] M. O. Scully and A. A. Svidzinsky, "The Lamb Shift—yesterday, today, and tomorrow," *Science*, vol. 328, pp. 1239–1241, Jun 2010.

[142] R. Friedberg and J. T. Manassah, "Effects of including the counterrotating term and virtual photons on the eigenfunctions and eigenvalues of a scalar photon collective emission theory," *Phys. Lett. A*, vol. 372, pp. 2514–2521, Mar 2008.

[143] M. D. Eisaman, L. Childress, A. André, F. Massou, A. S. Zibrov, and M. D. Lukin, "Shaping quantum pulses of light via coherent atomic memory," *Phys. Rev. Lett.*, vol. 93, p. 233602, Nov 2004.

[144] A. Kalachev, "Quantum storage on subradiant states in an extended atomic ensemble," *Phys. Rev. A*, vol. 76, p. 043812, Oct 2007.

[145] A. A. Svidzinsky, L. Yuan, and M. O. Scully, "Quantum amplification by superradiant emission of radiation," *Phys. Rev. X*, vol. 3, p. 041001, Oct 2013.

[146] A. Kuzmich, W. P. Bowen, A. D. Boozer, A. Boca, C. W. Chou, L.-M. Duan, and H. J. Kimble, "Generation of nonclassical photon pairs for scalable quantum communication with atomic ensembles," *Nature*, vol. 423, pp. 731–734, Jun 2003.

[147] D.-W. Wang, R.-B. Liu, S.-Y. Zhu, and M. O. Scully, "Superradiance lattice," *Phys. Rev. Lett.*, vol. 114, p. 043602, Jan 2015.

[148] D. Porras and J. I. Cirac, "Collective generation of quantum states of light by entangled atoms," *Phys. Rev. A*, vol. 78, p. 053816, Nov 2008.

[149] D.-W. Wang, H. Cai, L. Yuan, S.-Y. Zhu, and R.-B. Liu, "Topological phase transitions in superradiance lattices," *Optica*, vol. 2, pp. 712–715, Aug 2015.

[150] A. A. Svidzinsky, "Nonlocal effects in single-photon superradiance," *Phys. Rev. A*, vol. 85, p. 013821, Jan 2012.

[151] V. Ernst, "Coherent emission of a photon by many atoms," *Z. Phys.*, vol. 218, pp. 111–128, Apr 1969.

[152] W. Feng, Y. Li, and S.-Y. Zhu, "Effect of atomic distribution on cooperative spontaneous emission," *Phys. Rev. A*, vol. 89, p. 013816, Jan 2014.

[153] R. Friedberg, S. Hartmann, and J. Manassah, "Frequency shifts in emission and absorption by resonant systems ot two-level atoms," *Phys. Rep.*, vol. 7, pp. 101–179, Mar 1973.

[154] M. O. Scully, "Correlated spontaneous emission on the Volga," *Laser Phys.*, vol. 17, pp. 635–646, May 2007.

[155] W. Guerin, M. O. Araújo, and R. Kaiser, "Subradiance in a large cloud of cold atoms," *Phys. Rev. Lett.*, vol. 116, p. 083601, Feb 2016.

[156] T. Bienaimé, N. Piovella, and R. Kaiser, "Controlled Dicke subradiance from a large cloud of two-level systems," *Phys. Rev. Lett.*, vol. 108, p. 123602, Mar 2012.

[157] A. A. Svidzinsky and M. O. Scully, "On the evolution of N-atom state prepared by absorption of a single photon," *Opt. Commun.*, vol. 283, pp. 753–757, Mar 2010.

[158] Y. Li, J. Evers, H. Zheng, and S.-Y. Zhu, "Collective spontaneous emission beyond the rotating-wave approximation," *Phys. Rev. A*, vol. 85, p. 053830, May 2012.

[159] U. Fano, "Effects of configuration interaction on intensities and phase shifts," *Phys. Rev.*, vol. 124, pp. 1866–1878, Dec 1961.

[160] G. S. Agarwal, *Quantum statistical theories of spontaneous emission and their relation to other approaches*, pp. 1–128. Berlin, Heidelberg: Springer Berlin Heidelberg, 1974.

[161] A. A. Svidzinsky and M. O. Scully, "Evolution of collective n atom states in single photon superradiance: Effect of virtual lamb shift processes," *Opt. Commun.*, vol. 282, pp. 2894–2897, Jul 2009.

[162] R. Friedberg and J. T. Manassah, "Electromagnetic decay modes in a spherical sample of two-level atoms," *Phys. Lett. A*, vol. 372, pp. 6833–6842, Nov 2008.

[163] M. O. Scully, V. V. Kocharovsky, A. Belyanin, E. Fry, and F. Capasso, "Enhancing acceleration radiation from ground-state atoms via cavity quantum electrodynamics," *Phys. Rev. Lett.*, vol. 91, p. 243004, Dec 2003.

[164] R. Lopp, E. Martín-Martínez, and D. Page, "Relativity and quantum optics: Accelerated atoms in optical cavities," *Classical Quantum Gravity*, vol. 35, Oct 2018.

[165] A. Svidzinsky, J. Ben-Benjamin, S. Fulling, and D. Page, "Excitation of an atom by a uniformly accelerated mirror through virtual transitions," *Phys. Rev. Lett.*, vol. 121, Aug 2018.

[166] C. A. Uliana Lima, F. Brito, J. A. Hoyos, and D. A. Turolla Vanzella, "Probing the Unruh effect with an accelerated extended system," *Nat. Commun.*, vol. 10, July 2019.

[167] M. O. Scully and M. S. Zubairy, *Quantum Optics*. Cambridge University Press, 1997.

[168] C. Anastopoulos and N. Savvidou, "Coherences of accelerated detectors and the local character of the Unruh effect," *J. Math. Phys.*, vol. 53, no. 1, p. 012107, 2012.

[169] J. Jackson, *Classical electrodynamics*. Wiley, 1975.

APPENDIX A

INITIAL MOLECULAR COHERENCE

For completeness and the convenience of the reader, details of derivation of Eq. (2.8) are presented in this appendix. Problem is to find time dependent molecular coherence $\rho_{21}(t)$ created by pump $\mathbf{E}_p(t)$ and Stokes $\mathbf{E}_s(t)$ pulses. Using semiclassical light matter Hamiltonian $H^{(I)}(t)$ in the interaction picture we obtain molecular density operator $\hat{\rho}^{(I)}(t)$ and its matrix element $\rho_{21}^{(I)}(t)$ in the interaction picture as follow

$$\hat{\rho}^{(I)}(t) \simeq \left(-\frac{i}{\hbar}\right)^2 \int_{t_0}^{t} \mathrm{d}t'' \int_{t_0}^{t''} \mathrm{d}t' \, [\hat{H}^{(I)}(t''), [\hat{H}^{(I)}(t'), \hat{\rho}^{(I)}(t')]] \tag{A.1}$$

and

$$\rho_{21}^{(I)}(t) \simeq \left(-\frac{i}{\hbar}\right)^2 \langle 2|\hat{\mu}_\beta|3\rangle\langle 3|\hat{\mu}_\alpha|1\rangle \int_{t_0}^{t} \mathrm{d}t'' \int_{t_0}^{t''} \mathrm{d}t' \, \mathrm{e}^{i\omega_{23}t''} \mathrm{e}^{i\omega_{31}t'} E_{s,\beta}(t'') E_{p,\alpha}(t'). \tag{A.2}$$

Here, initial condition for density matrix is $\rho_{11}(t_0) = 1$. New variables t_1 and t_2 defined in Figure A.1 can simplify double integral in Eq. (A.2) to

$$\begin{aligned} \rho_{21}(t) \simeq & \left(-\frac{i}{\hbar}\right)^2 \langle 2|\hat{\mu}_\beta|3\rangle\langle 3|\hat{\mu}_\alpha|1\rangle \\ & \times \int_{-\infty}^{\infty} \mathrm{d}t_2 \, \theta(t_2) \mathrm{e}^{-i\omega_{21}t_2} E_{s,\beta}(t - t_2) \int_{-\infty}^{\infty} \mathrm{d}t_1 \, \theta(t_1) \mathrm{e}^{-i\omega_{31}t_1} E_{p,\alpha}(t - t_1 - t_2), \end{aligned} \tag{A.3}$$

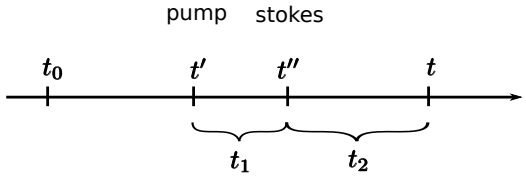

Figure A.1: New time variables t_1 and t_2 used in Eq. (A.3). Reprinted with permission from [25].

where $\theta(t)$ is Heaviside step function. With the standard definition of Fourier transform of a function $F(t)$ as

$$F(t) = \frac{1}{\sqrt{2\pi}} \int_{-\infty}^{\infty} \mathrm{d}\omega \, F(\omega) \mathrm{e}^{-i\omega t},$$
$$F(\omega) = \frac{1}{\sqrt{2\pi}} \int_{-\infty}^{\infty} \mathrm{d}t \, F(t) \mathrm{e}^{i\omega t} \tag{A.4}$$

and using convolution theorem, finally, we obtain dynamics of molecular coherence as follows

$$\rho_{21}(t) \simeq \frac{\langle 2|\hat{\mu}_\beta|3\rangle\langle 3|\hat{\mu}_\alpha|1\rangle}{2\pi\hbar^2} \int_{-\infty}^{\infty} \mathrm{d}\omega_p \int_{-\infty}^{\infty} \mathrm{d}\Omega \, \frac{\mathrm{e}^{-i\Omega t} E_{s,\beta}(\Omega - \omega_p) E_{p,\alpha}(\omega_p)}{(\omega_p - \omega_{31} + i\Gamma_3)(\Omega - \omega_{21} + i\Gamma)}. \tag{A.5}$$

When pump and Stokes pulses are nearly in two-photon resonance with transition ω_{21} the factor $1/(\Omega - \omega_{21} + i\Gamma)$ in Eq. (A.5) yields $-i\pi\delta(\Omega - \omega_{21})$, and consequently, Eq. (A.5) with summation over all possible excited states $\{|3\rangle\}$ provides us Eq. (2.8).

APPENDIX B

POLARIZABILITY AND OPTICAL ACTIVITY TENSORS

Our starting point is the field-matter interaction Hamiltonian Eq. (2.1). Once we calculate the polarizability tensor with electric dipole interactions, the procedure for derivation of optical activity tensors is straightforward.

The induced polarization of a single molecule is given by

$$\boldsymbol{\mu}(t) = \mathrm{Tr}[\hat{\boldsymbol{\mu}}\hat{\rho}(t)] = \sum_{\{3\}} \left(\mu_{13}\rho_{31}(t) + \mu_{23}\rho_{32}(t) + \mu_{31}\rho_{13}(t) + \mu_{32}\rho_{23}(t)\right), \tag{B.1}$$

where $\hat{\rho}(t)$ is a density matrix of a single molecule. The time evolution of $\hat{\rho}(t)$ is governed by the von Neumann equation $d\hat{\rho}(t)/dt = (-i/\hbar)[\hat{H}(t), \hat{\rho}(t)]$, and exploiting first-order perturbation theory, the density matrix elements $\rho_{31}(t)$ and $\rho_{32}(t)$ at time t are found to be

$$\begin{aligned}
\rho_{31}(t) &= \mathrm{e}^{-i\omega_{31}t}\left(-\frac{i}{\hbar}\right)\int_0^t \mathrm{d}t'\, H_{32}^{(I)}(t')\rho_{21}(0), \\
\rho_{23}(t) &= \mathrm{e}^{-i\omega_{23}t}\left(\frac{i}{\hbar}\right)\int_0^t \mathrm{d}t'\, \rho_{21}(0)H_{13}^{(I)}(t').
\end{aligned} \tag{B.2}$$

Here, we keep only anti-Stokes Raman terms. Matrix elements of the Hamiltonian in the interaction picture are denoted by $H_{32}^{(I)}(t')$ and $H_{31}^{(I)}(t')$ and their explicit form is given by

$$H_{32}^{(I)}(t') = -\langle 3|\hat{\mu}_\alpha|2\rangle E_{l,\alpha}(t')\mathrm{e}^{-\Gamma|t'|}\mathrm{e}^{i\omega_{32}t'}, \tag{B.3}$$

$$H_{13}^{(I)}(t') = -\langle 1|\hat{\mu}_\alpha|3\rangle E_{l,\alpha}(t')\mathrm{e}^{-\Gamma|t'|}\mathrm{e}^{i\omega_{13}t'}, \tag{B.4}$$

where dephasing constant Γ is introduced as a part of electric field as $E_{l,\alpha}(t')\exp(-\Gamma|t'|)$. Then

spectral decomposition of electric field is given by

$$E_{l,\alpha}(t')\mathrm{e}^{-\Gamma|t'|} = \frac{1}{\sqrt{2\pi}}\int_{-\infty}^{\infty}\mathrm{d}\omega_l\left[\frac{1}{\sqrt{2\pi}}\int_{-\infty}^{\infty}\mathrm{d}\omega'\,E_{l,\alpha}(\omega')\frac{\sqrt{2/\pi}\Gamma}{\Gamma^2+(\omega_l-\omega')^2}\right]\mathrm{e}^{-i\omega_l t'}. \tag{B.5}$$

Furthermore, Eqs. (B.2) yield

$$\begin{aligned}
\rho_{31}(t) &= \frac{1}{2\pi\hbar}\int_{-\infty}^{\infty}\mathrm{d}\omega_l\,\frac{\langle 3|\hat{\mu}_\alpha|2\rangle}{\omega_{32}-\omega_l-i\Gamma_3}\int_{-\infty}^{\infty}\mathrm{d}\omega'\,E_{l,\alpha}(\omega')\frac{\sqrt{2/\pi}\Gamma}{\Gamma^2+(\omega_l-\omega')^2}\rho_{21}(0)\mathrm{e}^{-i(\omega_{21}+\omega_l)t},\\
\rho_{23}(t) &= \frac{1}{2\pi\hbar}\int_{-\infty}^{\infty}\mathrm{d}\omega_l\,\frac{\langle 1|\hat{\mu}_\alpha|3\rangle}{\omega_{31}+\omega_l+i\Gamma_3}\int_{-\infty}^{\infty}\mathrm{d}\omega'\,E_{l,\alpha}(\omega')\frac{\sqrt{2/\pi}\Gamma}{\Gamma^2+(\omega_l-\omega')^2}\rho_{21}(0)\mathrm{e}^{-i(\omega_{21}+\omega_l)t},
\end{aligned} \tag{B.6}$$

Plugging $\rho_{31}(t)$ and $\rho_{23}(t)$ into Eq. (B.1), we obtain βth component of induced electric dipole moment due to electric dipole perturbation as follows:

$$\mu_\beta^{(e)}(t) = \frac{1}{2\pi}\int_{-\infty}^{\infty}\mathrm{d}\omega_l\,\tilde{\alpha}_{\beta\alpha}(\omega_l)\int_{-\infty}^{\infty}\mathrm{d}\omega'\,E_{l,\alpha}(\omega')\frac{\sqrt{2/\pi}\Gamma}{\Gamma^2+(\omega_l-\omega')^2}\mathrm{e}^{-i\omega_l t}\rho_{21}(0)\mathrm{e}^{-i\omega_{21}t}. \tag{B.7}$$

Here, superscript (e) indicates that the electric dipole moment is induced by electric dipole perturbation. The polarizability tensor is defined by

$$\tilde{\alpha}_{\beta\alpha}(\omega_l) = \frac{1}{\hbar}\sum_{\{3\}}\left(\frac{\langle 1|\hat{\mu}_\beta|3\rangle\langle 3|\hat{\mu}_\alpha|2\rangle}{\omega_{32}-\omega_l-i\Gamma_3}+\frac{\langle 1|\hat{\mu}_\alpha|3\rangle\langle 3|\hat{\mu}_\beta|2\rangle}{\omega_{31}+\omega_l+i\Gamma_3}\right), \tag{B.8}$$

where summation over all possible excited states $\{|3\rangle\}$ is taken. In the same way, βth component of induced electric dipole moments $\mu_\beta^{(m)}(t)$ due to magnetic dipole perturbation, $\mu_\beta^{(q)}(t)$ due to electric quadrupole perturbation, induced magnetic dipole $m_\beta(t)$ and electric quadrupole $q_{\gamma\beta}(t)$

moments due to electric dipole perturbation are, respectively

$$\mu_{\beta}^{(m)}(t) = \frac{1}{2\pi}\int_{-\infty}^{\infty} \mathrm{d}\omega_l\, \tilde{G}_{\beta\alpha}(\omega_l) \int_{-\infty}^{\infty} \mathrm{d}\omega'\, B_{l,\alpha}(\omega') \frac{\sqrt{2/\pi}\Gamma}{\Gamma^2 + (\omega_l - \omega')^2} \mathrm{e}^{-i\omega_l t} \rho_{21}(0) \mathrm{e}^{-i\omega_v t},$$
$$m_{\beta}(t) = \frac{1}{2\pi}\int_{-\infty}^{\infty} \mathrm{d}\omega_l\, \tilde{\mathscr{G}}_{\beta\alpha}(\omega_l) \int_{-\infty}^{\infty} \mathrm{d}\omega'\, E_{l,\alpha}(\omega') \frac{\sqrt{2/\pi}\Gamma}{\Gamma^2 + (\omega_l - \omega')^2} \mathrm{e}^{-i\omega_l t} \rho_{21}(0) \mathrm{e}^{-i\omega_v t},$$
$$\mu_{\beta}^{(q)}(t) = \frac{1}{2\pi}\int_{-\infty}^{\infty} \mathrm{d}\omega_l\, \frac{i}{3}\tilde{A}_{\beta,\gamma\alpha}(\omega_l) k_{\gamma} \int_{-\infty}^{\infty} \mathrm{d}\omega'\, E_{l,\alpha}(\omega') \frac{\sqrt{2/\pi}\Gamma}{\Gamma^2 + (\omega_l - \omega')^2} \mathrm{e}^{-i\omega_l t} \rho_{21}(0) \mathrm{e}^{-i\omega_v t},$$
$$q_{\gamma\beta}(t) = \frac{1}{2\pi}\int_{-\infty}^{\infty} \mathrm{d}\omega_l\, \tilde{\mathscr{A}}_{\alpha,\gamma\beta}(\omega_l) \int_{-\infty}^{\infty} \mathrm{d}\omega'\, E_{l,\alpha}(\omega') \frac{\sqrt{2/\pi}\Gamma}{\Gamma^2 + (\omega_l - \omega')^2} \mathrm{e}^{-i\omega_l t} \rho_{21}(0) \mathrm{e}^{-i\omega_v t}, \quad \text{(B.9)}$$

where superscripts m and q denote magnetic dipole and electric quadrupole perturbations, respectively, and k_γ is the γth component of wave-vector of the incident laser pulse. In Eq. (B.9), the electric dipole-magnetic dipole optical activity tensors $\{\tilde{\boldsymbol{G}}, \tilde{\boldsymbol{\mathscr{G}}}\}$ and electric dipole-electric quadrupole optical activity tensors $\{\tilde{\boldsymbol{A}}, \tilde{\boldsymbol{\mathscr{A}}}\}$ are defined as follows:

$$\tilde{G}_{\beta\alpha} = \frac{1}{\hbar}\sum_{\{3\}} \left(\frac{\langle 1|\hat{\mu}_{\beta}|3\rangle\langle 3|\hat{m}_{\alpha}|2\rangle}{\omega_{32} - \omega_l - i\Gamma_3} + \frac{\langle 1|\hat{m}_{\alpha}|3\rangle\langle 3|\hat{\mu}_{\beta}|2\rangle}{\omega_{31} + \omega_l + i\Gamma_3} \right), \quad \text{(B.10)}$$

$$\tilde{\mathscr{G}}_{\beta\alpha} = \frac{1}{\hbar}\sum_{\{3\}} \left(\frac{\langle 1|\hat{m}_{\beta}|3\rangle\langle 3|\hat{\mu}_{\alpha}|2\rangle}{\omega_{32} - \omega_l - i\Gamma_3} + \frac{\langle 1|\hat{\mu}_{\alpha}|3\rangle\langle 3|\hat{m}_{\beta}|2\rangle}{\omega_{31} + \omega_l + i\Gamma_3} \right), \quad \text{(B.11)}$$

$$\tilde{A}_{\beta,\gamma\alpha} = \frac{1}{\hbar}\sum_{\{3\}} \left(\frac{\langle 1|\hat{\mu}_{\beta}|3\rangle\langle 3|\hat{q}_{\gamma\alpha}|2\rangle}{\omega_{32} - \omega_l - i\Gamma_3} + \frac{\langle 1|\hat{q}_{\gamma\alpha}|3\rangle\langle 3|\hat{\mu}_{\beta}|2\rangle}{\omega_{31} + \omega_l + i\Gamma_3} \right), \quad \text{(B.12)}$$

$$\tilde{\mathscr{A}}_{\alpha,\gamma\beta} = \frac{1}{\hbar}\sum_{\{3\}} \left(\frac{\langle 1|\hat{q}_{\gamma\beta}|3\rangle\langle 3|\hat{\mu}_{\alpha}|2\rangle}{\omega_{32} - \omega_l - i\Gamma_3} + \frac{\langle 1|\hat{\mu}_{\alpha}|3\rangle\langle 3|\hat{q}_{\gamma\beta}|2\rangle}{\omega_{31} + \omega_l + i\Gamma_3} \right). \quad \text{(B.13)}$$

In the frequency domain, induced dipole moment due to electric dipole perturbation is determined

by Fourier transform of Eq. (B.7) as follows:

$$\mu_{\beta}^{(e)}(\omega_{as}) = \frac{1}{\pi}\int_{-\infty}^{\infty} \mathrm{d}\omega_l\, \tilde{\alpha}_{\beta\alpha}(\omega_{as}-\omega_v)\frac{\mathcal{E}_{l,\alpha}(\omega_l-\omega_l^{(0)})\mathrm{e}^{i(\omega_l-\omega_l^{(0)})\tau}}{\Gamma^2+(\omega_{as}-\omega_v-\omega_l)^2}\Gamma\rho_{21}(0), \tag{B.14}$$

where vibrational frequency $\omega_v = \omega_{21}$ and the electric field of the laser pulse in time domain is defined as $E_{l,\alpha}(t) = \mathcal{E}_{l,\alpha}(t-\tau)\mathrm{e}^{-i\omega_l^{(0)}t}$ and its Fourier transform is given by $E_{l,\alpha}(\omega_l) = \mathcal{E}_{l,\alpha}(\omega_l-\omega_l^{(0)})\mathrm{e}^{i(\omega_l-\omega_l^{(0)})\tau}$. Similarly, other induced dipole and quadrupole moments are written in the frequency domain as follows:

$$\begin{aligned}
\mu_{\beta}^{(m)}(\omega_{as}) &= \frac{1}{\pi}\int_{-\infty}^{\infty} \mathrm{d}\omega_l\, \tilde{G}_{\beta\alpha}(\omega_{as}-\omega_v)\frac{\mathcal{B}_{l,\alpha}(\omega_l-\omega_l^{(0)})\mathrm{e}^{i(\omega_l-\omega_l^{(0)})\tau}}{\Gamma^2+(\omega_{as}-\omega_v-\omega_l)^2}\Gamma\rho_{21}(0),\\
m_{\beta}(\omega_{as}) &= \frac{1}{\pi}\int_{-\infty}^{\infty} \mathrm{d}\omega_l\, \tilde{\mathscr{G}}_{\beta\alpha}(\omega_{as}-\omega_v)\frac{\mathcal{E}_{l,\alpha}(\omega_l-\omega_l^{(0)})\mathrm{e}^{i(\omega_l-\omega_l^{(0)})\tau}}{\Gamma^2+(\omega_{as}-\omega_v-\omega_l)^2}\Gamma\rho_{21}(0),\\
\mu_{\beta}^{(q)}(\omega_{as}) &= \frac{ik_\gamma}{3\pi}\int_{-\infty}^{\infty} \mathrm{d}\omega_l\, \tilde{A}_{\beta,\gamma\alpha}(\omega_{as}-\omega_v)\frac{\mathcal{E}_{l,\alpha}(\omega_l-\omega_l^{(0)})\mathrm{e}^{i(\omega_l-\omega_l^{(0)})\tau}}{\Gamma^2+(\omega_{as}-\omega_v-\omega_l)^2}\Gamma\rho_{21}(0),\\
q_{\gamma\beta}(\omega_{as}) &= \frac{1}{\pi}\int_{-\infty}^{\infty} \mathrm{d}\omega_l\, \tilde{\mathscr{A}}_{\alpha,\gamma\beta}(\omega_{as}-\omega_v)\frac{\mathcal{E}_{l,\alpha}(\omega_l-\omega_l^{(0)})\mathrm{e}^{i(\omega_l-\omega_l^{(0)})\tau}}{\Gamma^2+(\omega_{as}-\omega_v-\omega_l)^2}\Gamma\rho_{21}(0),
\end{aligned} \tag{B.15}$$

where $\mathcal{B}_{l,\alpha}(\omega-\omega_l^{(0)})$ is a Fourier transform of envelope function of magnetic field. Here, $|1\rangle$, $|2\rangle$ and $|3\rangle$ are ground and excited electro-vibrational states of a molecule. Generally, the tensors Eqs. (B.8) and (B.10)–(B.13) are complex valued (tilde of these tensors means that they are complex), but commonly used assumptions are: (a) the Born–Oppenheimer approximation, where each molecular state is a direct product of electronic and vibrational wavefunctions; and (b) we can always choose real wavefunctions in the absence of external magnetic field, so allowing us to assume the electric dipole and quadrupole moment operators are purely real and the magnetic dipole moment operator is purely imaginary. With these two assumptions, we have only three tensors (without tilde), namely real-valued tensors $(\alpha_{\beta\alpha})_{12}$ and $(A_{\beta,\gamma\alpha})_{12} = (\mathscr{A}_{\beta,\gamma\alpha})_{12}$, and imaginary-valued tensor $(G_{\beta\alpha})_{12} = (\mathscr{G}^*_{\alpha\beta})_{12}$. Moreover, we exclude the imaginary unit i from $(G_{\beta\alpha})_{12}$ by introducing the purely real tensor $(G_{\beta\alpha})'_{12} = i(G_{\beta\alpha})_{12}$.

The scattered electric fields $\mathbf{E}_\mu$, $\mathbf{E}_m$ and $\mathbf{E}_q$ at point $r\mathbf{n}$ in radiation zone due to electric dipole,

magnetic dipole and electric quadrupole moments, respectively, are given by [169]

$$\begin{aligned}
\mathbf{E}_{\mu} &= Z_0 \frac{ck_{as}^2}{4\pi} \frac{\mathrm{e}^{ik_{as}r}}{r} (\mathbf{n} \times \boldsymbol{\mu}) \times \mathbf{n}, \\
\mathbf{E}_{m} &= Z_0 \frac{k_{as}^2}{4\pi} \frac{\mathrm{e}^{ik_{as}r}}{r} (\mathbf{m} \times \mathbf{n}), \\
\mathbf{E}_{q} &= Z_0 \frac{ick_{as}^3}{12\pi} \frac{\mathrm{e}^{ik_{as}r}}{r} (\mathbf{q} \times \mathbf{n}) \times \mathbf{n},
\end{aligned} \tag{B.16}$$

where $Z_0 = \sqrt{\mu_0/\epsilon_0}$, $(\mathbf{q})_\alpha = q_{\alpha\beta} n_\beta$ and $\mathbf{n}$ is direction of emission. The wave-number for oscillating dipole and quadrupole moments is denoted by k_{as}. Next, we calculate the electric fields of scattered emission for several different pulse configurations using Eq. (B.16) along with the induced moments Eqs. (B.14) and (B.15).

APPENDIX C

LIN-CIR CARS-ROA

Lin-Cir CARS-ROA refers to difference between right- and left-circularly polarized components of the scattered pulse when the incident probe pulse is linearly polarized. Let us choose x-polarized incident laser pulse $E_{l,x}(t)$ propagating along z direction; then after squaring the Eq. (2.6) and averaging over random orientations of the molecules, we obtain intensities of circularly polarized components of scattered anti-Stokes emission as follows:

$$I^x_{R/L} \propto (E^x_{R/L} + E_{LO})(E^x_{R/L} + E_{LO})^* \propto \frac{45a^2 + 7\gamma^2(\alpha)}{90} N^2|F|^2 \pm \frac{180aG' + 4\gamma^2(G')}{90c} N^2|F|^2$$
$$\mp \frac{6\gamma^2(A)}{90c} N^2|F|^2 \pm \frac{\omega_{as}}{\omega_l} \frac{2\gamma^2(A)}{90c} N^2|F|^2 + \sqrt{2}aN\,\mathrm{Re}(FE^*_{LO}) \pm \frac{4}{\sqrt{2}c} G'N\,\mathrm{Re}(FE^*_{LO}), \tag{C.1}$$

where $E_{LO} = E_{LO,R/L} = (1/\sqrt{2})(\mathbf{e}_x \pm i\mathbf{e}_y) \cdot \mathbf{E}_{LO}$ is circular components of local oscillator at frequency ω_{as}.

APPENDIX D

CIR-LIN CARS-ROA

Cir-Lin CARS-ROA refers to measurement of linearly polarized component of scattered emission provided right- and left-circularly polarized incident pulses are present. Thus, we consider a circularly polarized incident laser pulse propagating along z direction whose field components are

$$E_{l,x}(t) = \frac{E_l(t)}{\sqrt{2}}, \quad E_{l,y}(t) = \mp i\frac{E_l(t)}{\sqrt{2}}, \quad B_{l,x}(t) = \pm i\frac{E_l(t)}{\sqrt{2}c}, \quad B_{l,y}(t) = \frac{E_l(t)}{\sqrt{2}c}, \tag{D.1}$$

where sign at the top indicates right-circularly polarized incident light whereas sign in the bottom indicates left-circularly polarized incident light. In the same manner as Lin-Cir CARS-ROA, we obtain x and y components of scattered emission at forward direction $\mathbf{n} = \mathbf{e}_z$ as follows:

$$\begin{aligned} E_x^{R/L} &\propto \frac{N}{\sqrt{2}}\left(\alpha_{xx} \mp i\alpha_{xy} + \frac{ik_l}{3}A_{x,zx} - \frac{ik_{as}}{3}A_{x,zx} \pm \frac{1}{c}G'_{xx} \pm \frac{k_l}{3}A_{x,zy} \pm \frac{1}{c}G'_{yy} \mp \frac{k_{as}}{3}A_{y,xz}\right)F, \\ E_y^{R/L} &\propto \frac{N}{\sqrt{2}}\left(\alpha_{yx} \mp i\alpha_{yy} \pm \frac{k_l}{3}A_{y,zy} \mp \frac{k_{as}}{3}A_{y,yz} - \frac{i}{c}G'_{yy} + \frac{ik_l}{3}A_{y,zx} - \frac{i}{c}G'_{xx} - \frac{ik_{as}}{3}A_{x,yz}\right)F. \end{aligned} \tag{D.2}$$

After averaging over random molecular orientations, the intensity is found to be

$$\begin{aligned} I_x^{R/L} \propto &\left(\frac{45a^2 + 7\gamma^2(\alpha)}{90} \pm \frac{180aG' + 4\gamma^2(G')}{90c} \mp \frac{\omega_{as}}{\omega_l}\frac{6\gamma^2(A)}{90c} \pm \frac{2\gamma^2(A)}{90c}\right)N^2|F|^2 \\ &+ \sqrt{2}aN\,\mathrm{Re}(FE_{LO}^*) \pm \frac{4}{\sqrt{2}c}G'N\,\mathrm{Re}(FE_{LO}^*), \end{aligned} \tag{D.3}$$

where $E_{LO} = \mathbf{e}_x \cdot \mathbf{E}_{LO}$.

APPENDIX E

STANDARD YOUNG TABLEAUX AND IRREDUCIBLE REPRESENTATIONS

Young tableaux are one of the most intriguing devices in group theory providing as they do an explicit construction of the irreducible representations of the symmetric group S_N. Since rigorous mathematical proof of the connection between Young tableaux and irreducible representations of S_N is given in many places, here we present some crucial understanding of irreducible representations from a physicist's point of view.

Let us take N identical non-interacting two-level atoms as an example. Then, any permutation in the group S_N can be represented by a $2^N \times 2^N$ matrix in Hilbert space $\mathcal{H}_{2^N}$ in which quantum states of the system are defined. We denote the representation matrix of element r of group S_N by $D(r)$. Forms of these representation matrices vary depending on the basis vectors in $\mathcal{H}_{2^N}$. If it were possible, it would be desirable to find simultaneous diagonal representation matrices for *all* elements in the group S_N. Then, it is easy to see that any single basis vector for these diagonal representation matrices would transform into itself with unimportant factor under any group operation of S_N. For our particular example, quantum state of the system would not change under any permutation of two-level atoms. However, this is not possible in general unless we consider an abelian group. Of course, the group S_N is nonabelian for $N > 2$.

In general, we can find basis states that diagonalize the representation matrix of one specific group element r but not of all group elements in S_N at the same time. Fortunately, we can partially and simultaneously diagonalize all representation matrices $D(r)$ and afterwards, all these matrices $D(r)$ have the same block diagonal form. In this case, the blocks on the diagonal of the matrix $D(r)$ represent subspaces whose elements transform only among the subspace under any group operation. When the sizes of these subspaces, i.e. sizes of blocks on the diagonal of representation matrices, $D(r)$ are minimal, the representation matrices and subspaces are called irreducible. For example, the single-excited subradiant states $|1,-1\rangle_1$, $|1,-1\rangle_2$ and $|1,-1\rangle_3$ form an irreducible

subspace and transform within this subspace under any group action of S_4, i.e. any group element of S_4 can be represented by 3×3 matrices in the bases of the single-excited subradiant states. Young tableaux are inevitable tools for analysis of these irreducible representations.

The modern approach introduces the group algebra for dealing with irreducible representations. Formal linear combinations of the group elements of S_N in the complex field form a vector space called the group algebra $\mathbb{C}(S_N)$. It follows that an irreducible subspace W is not only closed under the group action but also under the action of the group algebra, i.e. for any $u \in \mathbb{C}(S_N)$ and $|\psi\rangle \in W$,

$$u|\psi\rangle \in W. \tag{E.1}$$

To understand the irreducible representation in terms of the group algebra, we consider the subset $\mathcal{L}$ of elements s in $\mathbb{C}(S_N)$ that map any state $|\psi\rangle$ in $\mathcal{H}_{2^N}$ into the irreducible subspace W of $\mathcal{H}_{2^N}$ i.e. for any $s \in \mathcal{L}$ and $|\psi\rangle \in \mathcal{H}_{2^N}$, $s|\psi\rangle \in W$. Then, for all u in group algebra $\mathbb{C}(S_N)$ it is true that

$$(us)|\psi\rangle = u(s|\psi\rangle) \in W. \tag{E.2}$$

The last equation means that $\mathcal{L}$ is closed under the left multiplication by u of the whole group algebra. This defines a left ideal of the group algebra. In our specific case, $\mathcal{L}$ forms a primitive left ideal of the group algebra $\mathbb{C}(S_N)$. Therefore, once we find the primitive left ideals of the group algebra it is straightforward to find irreducible subspaces in $\mathcal{H}_{2^N}$. Actually the Young operator is a generator of a primitive left ideal of the group algebra $\mathbb{C}(S_N)$ and can be found by introducing Young tableaux.

APPENDIX F

AN EXAMPLE OF DOUBLE-EXCITED SUBRADIANT STATES

According to the formula 4.14 double-excited subradiant state $|5/2,-3/2\rangle_5$ is given by

$$
\begin{aligned}
|5/2,-3/2\rangle_5 = \frac{1}{\sqrt{150}} \quad & (2|a_1a_2\rangle + 2|a_1a_3\rangle + 2|a_1a_4\rangle + 2|a_1a_5\rangle \\
& +2|a_2a_3\rangle + 2|a_2a_4\rangle + 2|a_2a_5\rangle + 2|a_3a_4\rangle \\
& +2|a_3a_5\rangle + 2|a_4a_5\rangle + |a_1a_7\rangle + |a_2a_7\rangle \\
& +|a_3a_7\rangle + |a_4a_7\rangle + |a_5a_7\rangle \\
& -4|a_1a_6\rangle - 4|a_2a_6\rangle - 4|a_3a_6\rangle - 4|a_4a_6\rangle \\
& -4|a_5a_6\rangle - 5|a_6a_7\rangle)\,, \qquad \text{(F.1)}
\end{aligned}
$$

where the shortened notation is defined as $|a_1a_2\rangle = |a_1, a_2, b_3, b_4, b_5, b_6, b_7\rangle$, $|a_1a_3\rangle = |a_1, b_2, a_3, b_4, b_5, b_6, b_7\rangle$ and so forth.

APPENDIX G

MAGNUS EXPANSION METHOD FOR TWO-LEVEL ATOM INTERACTING WITH FEW-CYCLE PULSE*

Introduction

Simple models are at the heart of fundamental physics. The harmonic oscillator in classical mechanics, the ideal gas in statistical physics, and the two-level system in quantum mechanics are prime examples of such models. A two-level system (e.g. spin up–spin down system) driven by an electromagnetic pulse is the quintessential problem in nuclear magnetic resonance, laser physics, and quantum information theory [1, 2]. However, simple analytical solutions are only readily available for the exactly solvable model of a square pulse interacting with a two-level system treated within the rotating wave approximation (RWA). In the RWA the key terms that depend on the difference between the atomic frequency ω and the field carrier frequency ν, i.e. $\omega - \nu$, are kept while the counter-rotating terms expressed in terms of the frequency sum $\omega + \nu$ are neglected. The usual extension of the analytical solution for the two-level atom was to include non-RWA terms. A number of powerful methods have been developed that treat two-level systems beyond the RWA.

Recently, a remarkably accurate analytic solution in the case of a two-level system interacting with a far off-resonant pulse has been found [3] and applied to analyze the system's behavior due to different driving fields [4, 5]. Another way to solve the two-level problem analytically is proposed in [6]. It is based on the transformation of the scattering problem into a two-level atom, since several approximate analytical methods for the stationary Schrödinger equation have shown their validity [7, 8, 9, 10, 11, 12, 13, 14, 15, 16]. However, this approach gives practical expressions only in limited cases; in general, very complicated expressions are generated. Here, we obtain a new class of analytical solutions for a two-level system pumped by an arbitrarily time-

*Reprinted with permission from "Magnus expansion method for two-level atom interacting with few-cycle pulse" by Tuguldur Begzjav, Jonathan S. Ben-Benjamin, Hichem Eleuch, Reed Nessler, Yuri Rostovtsev and Gavriil Shchedrin, 2018. Journal of Modern Optics 65, 1378-84, Copyright [2018] Taylor & Francis.

dependent field of a few-cycle pulse. The present class of solutions is based on the evolution operator technique, employing an approximation that preserves its unitarity. More precisely, we derive analytical expressions for the population dynamics of a two-level atomic system, pumped by an external field, using the Magnus expansion method. This method generates simple and surprisingly accurate solutions. The Magnus expansion, introduced by outstanding mathematician Wilhelm Magnus in 1954 [17], was applied shortly after in a variety of fields of physics, for example, for studying nuclear spectroscopy [18], nuclear collisions [19], crystal structure [20], and averaging effects in magnetic resonance [21]. Nowadays, the Magnus expansion has wide applications in several fields of physics and mathematics [22, 23, 24].

Model and calculation

Our system of interest is a two-level atom, consisting of an excited state $|a\rangle$ and a ground state $|b\rangle$, having an atomic transition frequency ω and interacting with an electric field. The pulse has a frequency ν and a time-dependent Rabi frequency $\Omega(t) = \wp E(t)/\hbar$, where $E(t)$ represents the amplitude of the electric field and $\wp$ is the transition dipole moment.

In the interaction picture, the atomic state is given by

$$|\Psi(t)\rangle = a(t)|a\rangle + b(t)|b\rangle. \tag{G.1}$$

The dynamical evolution of the wavefunction $|\Psi(t)\rangle$ is described by the Schrödinger equation

$$i\hbar\frac{d}{dt}|\Psi(t)\rangle = H(t)|\Psi(t)\rangle, \tag{G.2}$$

where the Hamiltonian $H(t)$ for the two-level system in the interaction picture has the following expression:

$$H(t) = -\hbar\Omega(t)\Big(\exp[i\omega t]|a\rangle\langle b| + \text{h.c.}\Big). \tag{G.3}$$

Here, without loss of generality and for simplicity, $\Omega(t)$ is assumed to be real.

If the initial state at $t = 0$ is defined by $|\Psi(0)\rangle$, the formal solution at a later time $t > 0$ can be written as

$$|\Psi(t)\rangle = U(t,0)|\Psi(0)\rangle, \tag{G.4}$$

where the time-evolution operator satisfies a similar equation as the state $|\Psi(t)\rangle$,

$$i\hbar\frac{d}{dt}U(t,0) = H(t)U(t,0), \tag{G.5}$$

and has the initial condition $U(0,0) = 1$. To simplify notation, we suppress the initial time $t = 0$ in $U(t,0)$, and simply write $U(t)$.

From a mathematical point of view, Eq. (G.5) is a linear ordinary differential matrix equation on the complex field $\mathbb{C}$. If the Hamiltonian $H(t)$ commutes with itself at different times ($[H(t_1), H(t_2)] = 0$), then the time-evolution operator for Eq. (G.5) is

$$U(t) = \exp\left(-\frac{i}{\hbar}\int_0^t H(t')\,dt'\right). \tag{G.6}$$

However, the situation becomes more complicated if the Hamiltonian does *not* commute with itself at different times. Using standard perturbation theory, the general solution for the time-evolution operator is

$$U(t) = 1 + \sum_{n=1}^{\infty}\left(-\frac{i}{\hbar}\right)^n \int_0^t dt_n \int_0^{t_n} dt_{n-1}\cdots\int_0^{t_2} dt_1 H(t_n)H(t_{n-1})\cdots H(t_1). \tag{G.7}$$

A more compact, equivalent expression, named after Freeman John Dyson, is given by [25]

$$U(t) = \mathscr{T}\exp\left(-\frac{i}{\hbar}\int_0^t H(t_1)\,dt_1\right), \tag{G.8}$$

where $\mathscr{T}$ is the time-ordering operator.

In his seminal paper of 1954 [17], Magnus claims that the general solution of the linear ordinary differential matrix equation (G.5) can be written as

$$U(t) = \exp\left[\sum_{n=1}^{\infty} S_n(t,0)\right], \tag{G.9}$$

and we refer to the sum in the exponent as "the Magnus expansion". However, as we will mention in the next section, this expansion has a limited range of validity. The Magnus expansion method attracts great interest among mathematicians, physicists, and chemists. It is worth mentioning that the Magnus expansion preserves the unitarity and symplectic property of the $U(t)$ matrix, which is a great advantage for numerical integration methods of linear ordinary differential equations. The first few terms of the expansion are

$$S_1 = \frac{1}{(i\hbar)1!}\int_0^t dt_1 H(t_1), \tag{G.10a}$$

$$S_2 = \frac{1}{(i\hbar)^2 2!}\int_0^t dt_1 \int_0^{t_1} dt_2 [H(t_1), H(t_2)], \tag{G.10b}$$

$$S_3 = \frac{1}{(i\hbar)^3 3!}\int_0^t dt_1 \int_0^{t_1} dt_2 \int_0^{t_2} dt_3 \{[H(t_1), [H(t_2), H(t_3)]] + [H(t_3), [H(t_2), H(t_1)]]\}, \tag{G.10c}$$

$$\begin{aligned} S_4 = \frac{1}{(i\hbar)^4 4!}\int_0^t dt_1 \int_0^{t_1} dt_2 \int_0^{t_2} dt_3 \int_0^{t_3} dt_4 \\ \{[[[H(t_1), H(t_2)], H(t_3)], H(t_4)] + [H(t_1), [[H(t_2), H(t_3)], H(t_4)]] \\ + [H(t_1), [H(t_2), [H(t_3), H(t_4)]]] + [H(t_2), [H(t_3), [H(t_4), H(t_1)]]]\}. \end{aligned} \tag{G.10d}$$

The explicit expression for the operators (matrices) S_n of higher order in n are much more complicated, and an explicit formula of the fifth-order Magnus expansion term is presented in [26]. From an algorithmic point of view, the reference [26] provides a formula for finding the nth expansion

term from the previous terms:

$$S_n = \frac{1}{i\hbar}\int_0^t dt_1 \left(H(t_1) - \frac{1}{2}[S_{n-1}, H(t_1)] + \frac{1}{12}[S_{n-1}, [S_{n-1}, H(t_1)]] + \cdots \right) \tag{G.11}$$

Notice that when the matrices $H(t)$ at different times commute, the only nonzero term is S_1, and the solution reduces to the well-known Eq. (G.6).

Motivated by [24] we apply the Magnus expansion method to solve the Schrödinger equation with the Hamiltonian given in Eq. (G.3). Since this Hamiltonian is off-diagonal, and since S_n involves only the summation and integration of products of n Hamiltonians at different times, for even n, the S_n are diagonal

$$S_{2n} = \begin{pmatrix} -i\phi^{(2n)}(t) & 0 \\ 0 & i\phi^{(2n)}(t) \end{pmatrix}, \tag{G.12}$$

and for odd n, the S_n terms are are off-diagonal

$$S_{2n+1} = \begin{pmatrix} 0 & i\theta^{(2n+1)}(t) \\ i[\theta^{(2n+1)}]^*(t) & 0 \end{pmatrix}. \tag{G.13}$$

Therefore, we write

$$U(t) = \exp\left\{ \left[\sum_{n=1}^{\infty} S_n(t) \right] \right\} = \exp\left\{ \left[-i \begin{pmatrix} \phi(t) & -\theta(t) \\ -\theta^*(t) & -\phi(t) \end{pmatrix} \right] \right\}. \tag{G.14}$$

Here, the real-valued phase shift $\phi(t)$ is given by

$$\phi(t) = \phi^{(2)}(t) + \phi^{(4)}(t) + \cdots, \tag{G.15}$$

and the complex-valued pulse area $\theta(t)$ is

$$\theta(t) = \theta^{(1)}(t) + \theta^{(3)}(t) + \cdots . \tag{G.16}$$

Note that $\phi(t)$ and $\theta(t)$ are sums of even and odd terms, since S_n alternates its symmetry consecutively. By using the formula

$$\exp[i(\mathbf{a}\cdot\sigma)] = \mathbf{1}\cos|\mathbf{a}| + i(\mathbf{a}\cdot\sigma)\frac{\sin|\mathbf{a}|}{|\mathbf{a}|}, \tag{G.17}$$

where σ is the Pauli vector and $|\mathbf{a}| = \sqrt{a_1^2 + a_2^2 + a_3^2}$, we arrive at the final expression of the time-evolution operator

$$U(t) = \begin{pmatrix} \cos\beta(t) - i\dfrac{\phi(t)}{\beta(t)}\sin\beta(t) & i\dfrac{\theta(t)}{\beta(t)}\sin\beta(t) \\ i\dfrac{\theta^*(t)}{\beta(t)}\sin\beta(t) & \cos\beta(t) + i\dfrac{\phi(t)}{\beta(t)}\sin\beta(t) \end{pmatrix}, \tag{G.18}$$

where $\beta(t)$ is the real-valued magnitude

$$\beta(t) = \sqrt{|\theta(t)|^2 + \phi^2(t)}. \tag{G.19}$$

Using the Hamiltonian of interest, Eq. (G.3), and the Magnus expansion (Eqs. (G.10)), we obtain the first two non-vanishing terms of the complex pulse area $\theta(t)$ ($\theta^{(1)}$ and $\theta^{(3)}$) as

$$\theta^{(1)}(t) = \int_0^t \Omega(t_1)\exp[i\omega t_1]\,dt_1, \tag{G.20a}$$

and

$$\begin{aligned}\theta^{(3)}(t) =& \frac{1}{3}\int_0^t dt_1 \int_0^{t_1} dt_2 \int_0^{t_2} dt_3 \Omega(t_1)\Omega(t_2)\Omega(t_3) \\ & \left(\mathrm{e}^{i\omega(t_2+t_3-t_1)} + \mathrm{e}^{i\omega(t_1+t_2-t_3)} - 2\mathrm{e}^{i\omega(t_1+t_3-t_2)}\right),\end{aligned} \tag{G.20b}$$

while the first two non-vanishing contributions to the phase shift ($\phi^{(2)}$ and $\phi^{(4)}$) can be written as

$$\phi^{(2)}(t) = \int_0^t dt_1 \int_0^{t_1} dt_2\, \Omega(t_1)\Omega(t_2)\sin[\omega(t_1 - t_2)], \tag{G.21a}$$

and

$$\phi^{(4)}(t) = -\frac{2}{3}\int_0^t dt_1 \int_0^{t_1} dt_2 \int_0^{t_2} dt_3 \int_0^{t_3} dt_4$$
$$\Omega(t_1)\Omega(t_2)\Omega(t_3)\Omega(t_4)\cos(\omega(t_4 - t_1)\sin(\omega(t_3 - t_2))). \tag{G.21b}$$

In order to develop an analytical approximation for the two-level system, we truncate the Magnus expansion $\sum S_n$ to both second order and fourth order. We insert the truncated Magnus expansions into Eq. (G.14) to find two approximations for the time-evolution operator, $U^{(2)}(t)$ and $U^{(4)}(t)$, respectively. We use our approximate time-evolution operators to evolve the state $|\Psi(0)\rangle$, and we will compare in the next section the results with those obtained by fourth-order perturbation theory, and with those obtained by numerics.

Using our $U^{(2)}(t)$, and placing the atomic wavefunction initially in the ground state $|\Psi(0)\rangle = |b\rangle$, we obtain

$$|\Psi^{(2)}(t)\rangle \approx \left[i\frac{\theta^{(1)}(t)}{\beta^{(2)}(t)}\sin\beta^{(2)}(t)\right]|a\rangle$$
$$+ \left[\cos\beta^{(2)}(t) + i\frac{\theta^{(1)}(t)}{\beta^{(2)}(t)}\sin\beta^{(2)}(t)\right]|b\rangle. \tag{G.22}$$

Applying instead our $U^{(4)}(t)$ we find that

$$|\Psi^{(4)}(t)\rangle \approx \left[i\frac{\theta^{(1)}(t) + \theta^{(3)}(t)}{\beta^{(4)}(t)}\sin\beta^{(4)}(t)\right]|a\rangle$$
$$+ \left[\cos\beta^{(4)}(t) + i\frac{\theta^{(1)}(t) + \theta^{(3)}(t)}{\beta^{(4)}(t)}\sin\beta^{(4)}(t)\right]|b\rangle. \tag{G.23}$$

Here, the β's are

$$\beta^{(2)}(t) = \sqrt{|\theta^{(1)}(t)|^2 + (\phi^{(2)}(t))^2} \tag{G.24}$$

and

$$\beta^{(4)}(t) = \sqrt{|\theta^{(1)}(t) + \theta^{(3)}(t)|^2 + (\phi^{(2)}(t) + \phi^{(4)}(t))^2}. \tag{G.25}$$

These are the approximate solutions of the two-level atom interacting with a laser pulse of an arbitrary shape. Before proceeding to our numerical analysis, we discuss here the convergence, and implications of our results. In Magnus's original paper, the issue of convergence is not considered. But it has attracted great attention and has been extensively studied for the past half-century. In general, the Magnus expansion converges only in a limited time interval. The interval of convergence, $0 \leq t \leq T$, depends on the Frobenius norm [27] of the Hamiltonian $H(t)$, and can be deduced from the inequality [23]

$$\int_0^T \| -\frac{i}{\hbar} H(t) \| \, dt < r_c, \tag{G.26}$$

where $\|\cdot\|$ stands for the Frobenius norm and r_c is a real number.

To find the convergence criterion for our situation, we use the Hamiltonian Eq. (G.3) and Eq. (G.26) and find that the inequality

$$\int_0^T |\Omega(t)| \, dt < \frac{r_c}{\sqrt{2}}, \tag{G.27}$$

must be satisfied. This raises an obvious question: how is r_c calculated? Several values for r_c are found in the literature. For example, Pechukas and Light [28] have found that $r_c = \log 2$, while S. Blanes et al. [29] calculate $r_c = 1.08686$. Later, Moan and Niesen [30] provide $r_c = \pi$, and show that the restriction in Eq. (G.26) is not strict; in other words, it gives only an approximate value

for convergence domain. From a physical point of view, if we use the value $r_c = \pi$, the restriction in Eq. (G.27) means that the solutions in Eqs. (G.22) and (G.23) are valid for weak pulse areas of roughly less than $\pi/\sqrt{2}$, though it is unclear whether there is a strict limit on the pulse area.

Numerical analysis

In this section we apply our approximate solutions, Eqs. (G.22) and (G.23), to a Gaussian pulse driving the two-level system described as

$$\Omega(t) = \Omega_0 \exp\big(-a(t-\tau)^2\big)\cos(\nu(t-\tau)), \tag{G.28}$$

where ν represents the frequency of the pulse and Ω_0 is its amplitude. In order to test the convergence of the Magnus expansion and its dependence on the pulse area, we consider three pulses of different areas: one weak pulse of an area $A = \pi/20$, according to

$$A = \int_{-\infty}^{\infty} dt\,|\Omega(t)| \tag{G.29}$$

which is less than the boundary value $\pi/\sqrt{2}$ for the Magnus method, and pulses of area $\pi/2$ and $\pi/\sqrt{2}$, and compute the time evolution of the two-level system for each pulse.

Weak pulse

First, for a weak Gaussian pulse with pulse area $\pi/20$, the excited-state population is calculated using both 4th order Magnus expansion method and standard 4th order Runge–Kutta integration method. The results are shown in Figure G.1. Frequency and time units are in atomic transition frequency ω and its inverse ω^{-1} respectively. We choose parameters which are from usual experimental situations. We take the atomic frequency $\omega = 10^{15}\ \mathrm{s}^{-1}$, and the Rabi frequency of the pulse is calculated to be $\Omega_0 = 0.0038937\omega \sim 10^{12}\ \mathrm{s}^{-1}$. We take a parameter $a = 0.0005\omega^2$, which corresponds to FWHM $\approx$ 80fs. As we mentioned in a previous section, our Magnus expansion method converges well in the case of a weak pulse.

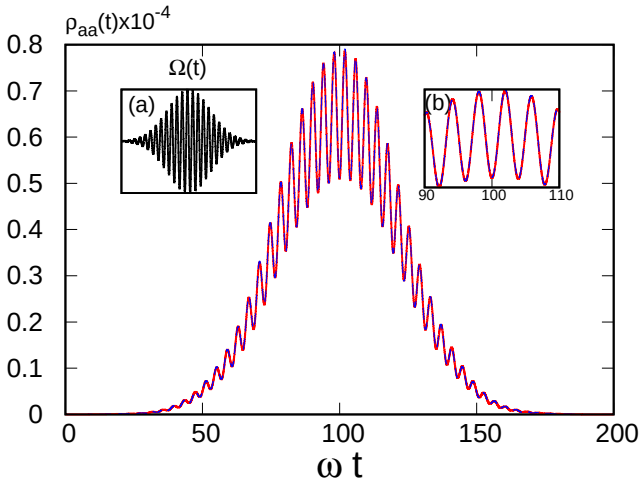

Figure G.1: The excited-state population is plotted as a function of time for a weak $\pi/20$ Gaussian envelope pulse of frequency $\nu = 0.8\omega$. The results of our numerical simulation are plotted as a solid red line, and the results of our 4th-order Magnus expansion result (Eq. (G.23)) are overlaid as dashed blue line. In inset (a), we show the pulse profile in the time domain, and in inset (b), we magnify the main plot (of the excited-state population) in the interval $90 \leq t \leq 110$. The parameters we use are $\Omega_0 = 0.0038937\omega$, $a = 0.0005\omega^2$, and $\tau = 100\omega^{-1}$. Reprinted with permission from [31].

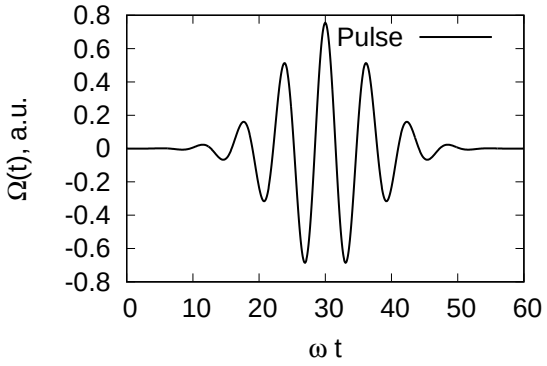

Figure G.2: Shape of the pulse used in the numerical calculation of Figures G.3 and G.4. Reprinted with permission from [31].

Strong short pulse

Next we study the possibility of applying the Magnus expansion method in the strong pulse regime. Using three different methods–our Magnus expansion methods of second and fourth

orders, the perturbation methods of fourth order and the fourth order Runge-Kutta numerical integration—we calculated the time evolution of the two-level atom driven by a few-cycle pulse of the form of Eq. (G.28) with $a = 0.01\omega^2$ ($FWHM \approx 16.6$fs for $\omega = 10^{15}s^{-1}$) and different detunings $\Delta = \omega - \nu$ for the pulse area $\pi/2$ and $\pi/\sqrt{2}$. It is worth mentioning that few (~ 6) cycles are contained in our laser pulse (see Figure G.2). The dynamics of the excited-state populations determined by these methods are plotted in the Figure G.3. As shown in Figure G.3, the

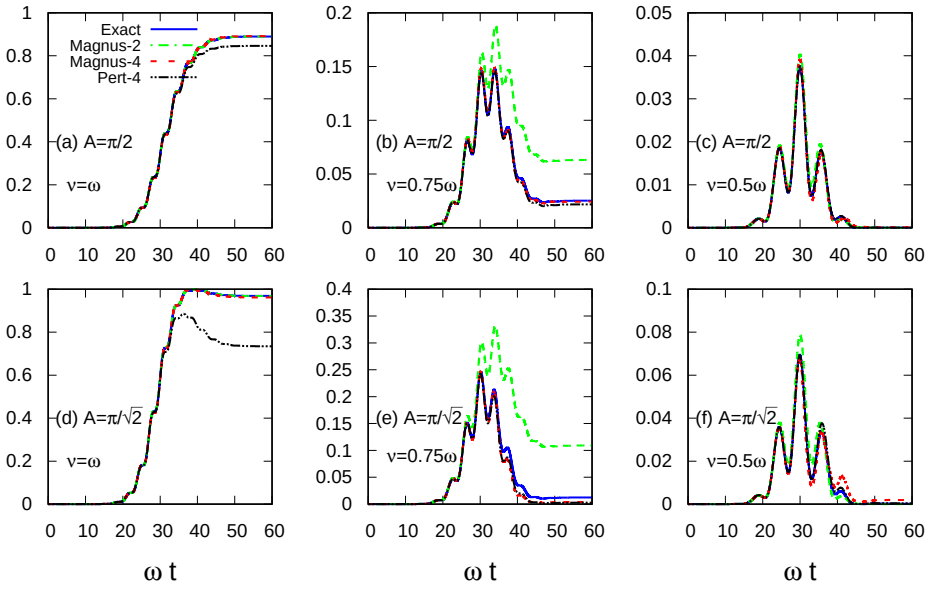

Figure G.3: Atomic excited state population as a function of ωt. The pulse area and detuning are indicated in each plot. Other parameters are $a = 0.01\omega^2$ and $\tau = 30\omega^{-1}$. The legend for the colors and line types, shown in plot (a), applies to all plots. Reprinted with permission from [31].

time evolution of the two-level system driven by the few-cycle pulse of area less than $\pi/\sqrt{2}$ is well described by the fourth order Magnus expansion method but not by the second order Magnus expansion. Because perturbation theory does not conserve the unitarity for low order, it cannot describe any strong atom–field interaction (see plots (a) and (d)). When the pulse area increases beyond $\pi/\sqrt{2}$ the validity of the Magnus fourth order method is not guaranteed.

To compare our method to the method developed in the paper [3], we have plotted the time

evolution of the excited-state population in Figure G.4 using the same areas and detunings as Figure G.3. Plots (b), (c), (e), and (f) demonstrate that method [3] works very well for large area or when the population in the excited state is smaller than that in the ground state. Meanwhile, 4th order Magnus expansion method works very well in the case of small area and when the atom-field interaction is strong, meaning that the excited state is highly populated during the interaction. The plots (a) and (f) in Figure G.4 indicate that these two methods, namely, 4th order Magnus expansion and the method in the paper [3], are complementary.

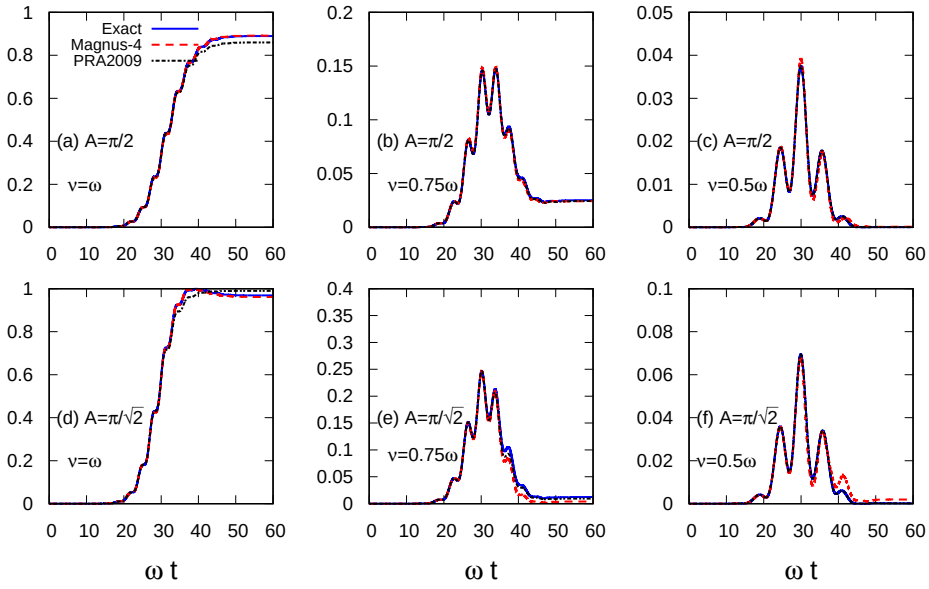

Figure G.4: Atomic excited state population as a function of ωt calculated using method in the paper [3] is compared to Magnus 4th order and 4th order Runge–Kutta method. The pulse area and detuning are shown in each plot. Other parameters are $a = 0.01\omega^2$ and $\tau = 30\omega^{-1}$. The legend for the colors and line types, shown in plot (a), applies to all plots. Reprinted with permission from [31].

Conclusions

We have derived analytical solutions based on the Magnus expansion for the time evolution of a two-level system excited by an external time-dependent electric field. Our method goes beyond

the rotating wave approximation and applies to a two-level atom interacting with an arbitrary-shaped laser pulse. We have also shown that our method performs better than other methods for an ultrashort pulse. Our approximate expressions work well for a pulse area below $\pi/\sqrt{2}$ for any detuning, but it is unclear whether this restriction, due to the finite convergence interval of the Magnus expansion, is strict, since more precise convergence criteria have not yet been found. We have also observed that the method developed in [3] works very well for large area pulse. In the sense of their applicable parameter range, we can consider that these two methods are complementary analytical techniques for describing the dynamics of the two-level system excited by a variable pulse.

REFERENCES

[1] E. T. Jaynes and F. W. Cummings, "Comparison of quantum and semiclassical radiation theories with application to the beam maser," *Proc. IEEE*, vol. 51, pp. 89–109, Jan 1963.

[2] M. A. Nielsen and I. L. Chuang, *Quantum Computation and Quantum Information: 10th Anniversary Edition*. Cambridge University Press, 2010.

[3] Y. V. Rostovtsev, H. Eleuch, A. Svidzinsky, H. Li, V. Sautenkov, and M. O. Scully, "Excitation of atomic coherence using off-resonant strong laser pulses," *Phys. Rev. A*, vol. 79, p. 063833, Jun 2009.

[4] P. K. Jha, H. Eleuch, and Y. V. Rostovtsev, "Coherent control of atomic excitation using off-resonant strong few-cycle pulses," *Phys. Rev. A*, vol. 82, p. 045805, Oct 2010.

[5] P. K. Jha, H. Eleuch, and F. Grazioso, "Ultra-short strong excitation of two-level systems," *Opt. Commun.*, vol. 331, pp. 198–203, Nov 2014.

[6] H. Eleuch, M. S. Abdalla, and Y. V. Rostovtsev, "Analytical solution for the one-dimensional scattering problem," *Opt. Commun.*, vol. 284, pp. 5457–5459, Nov. 2011.

[7] H. Jeffreys, "On certain approximate solutions of linear differential equations of second order," *Proc. London Math. Soc.*, vol. 23, pp. 428–436, 1923.

[8] G. Wentzel, "Eine verallgemeinerung der quantenbedingungen für die zwecke der wellenmechanik," *Zeitschrift für Physik*, vol. 38, no. 6, pp. 518–529, 1926.

[9] H. A. Kramers, "Wellenmechanik und halbzahlige quantisierung," *Z. Phys.*, vol. 39, pp. 828–840, 1926.

[10] L. Brillouin, "La mécanique ondulatoire de Schrödinger: une méthode générale de résolution par approximations successives," *C. R. Acad. Sci.*, vol. 183, p. 24, 1926.

[11] N. Fröman and P. O. Fröman, eds., *JWKB Approximation Contributions to the Theory*. North-Holland, Amsterdam: North Holland Publishing Company, 1965.

[12] H.-W. Lee and M. O. Scully, "The Wigner phase-space description of collision processes," *Found. Phys.*, vol. 13, pp. 61–72, Jan 1983.

[13] R. D. Levine, *Quantum Mechanics of Molecular Rate Processes*. New York: Dover Publications, 1999.

[14] W. P. Schleich, ed., *Quantum Optics in Phase Space*. Berlin: WILEY-VCH, 2001.

[15] O. Manasreh, *Semiconductor Heterojunctions and Nanostructures*. New York, NY, USA: McGraw-Hill, Inc., 1 ed., 2005.

[16] H. Eleuch, Y. V. Rostovtsev, and M. O. Scully, "New analytic solution of Schrödinger's equation," *Europhys. Lett.*, vol. 89, p. 50004, Mar 2010.

[17] W. Magnus, "On the exponential solution of differential equations for a linear operator," *Comm. Pure Appl. Math.*, vol. 7, no. 4, pp. 649–673, 1954.

[18] L. C. Biedenharn, "Angular correlations in nuclear spectroscopy," *Nuclear Spectroscopy*, vol. 9, Part B, p. 732, 1960.

[19] K. Keizo and T. Imamura, "A field theoretical investigation of multiple meson production. I: Pion-nucleon collisions," *Prog. Theor. Phys.*, vol. 23.1, p. 137, 1960.

[20] G. H. Weiss and A. A. Maradudin, "The Baker-Hausdorff formula and a problem in crystal physics," *J. Math. Phys.*, vol. 3, no. 4, pp. 771–777, 1962.

[21] U. Haeberlen and J. S. Waugh, "Coherent averaging effects in magnetic resonance," *Phys. Rev.*, vol. 175, pp. 453–467, Nov 1968.

[22] S. S. Mukamel, *Principles of nonlinear optical spectroscopy*. New York : Oxford University Press, 1995. Includes bibliographical references and index.

[23] S. Blanes, F. Casas, J. Oteo, and J. Ros, "The Magnus expansion and some of its applications," *Phys. Rep.*, vol. 470, no. 5–6, pp. 151–238, 2009.

[24] G. Shchedrin, C. O'Brien, Y. Rostovtsev, and M. O. Scully, "Analytic solution and pulse area theorem for three-level atoms," *Phys. Rev. A*, vol. 92, p. 063815, Dec 2015.

[25] F. J. Dyson, "The radiation theories of Tomonaga, Schwinger, and Feynman," *Phys. Rev.*, vol. 75, pp. 486–502, Feb 1949.

[26] D. Prato and P. W. Lamberti, "A note on Magnus formula," *J. Chem. Phys.*, vol. 106, no. 11, pp. 4640–4643, 1997.

[27] G. H. Golub and C. F. Van Loan, *Matrix Computations (3rd Ed.)*. Baltimore, MD, USA: Johns Hopkins University Press, 1996.

[28] P. Pechukas and J. C. Light, "On the exponential form of time-displacement operators in quantum mechanics," *J. Chem. Phys.*, vol. 44, no. 10, pp. 3897–3912, 1966.

[29] S. Blanes, F. Casas, J. A. Oteo, and J. Ros, "Magnus and Fer expansions for matrix differential equations: the convergence problem," *J. Phys. A: Math. Gen.*, vol. 31, no. 1, p. 259, 1998.

[30] P. C. Moan and J. Niesen, "Convergence of the Magnus series," *Found. Comput. Math.*, vol. 8, no. 3, pp. 291–301, 2008.

[31] T. Begzjav, J. S. Ben-Benjamin, H. Eleuch, R. Nessler, Y. Rostovtsev, and G. Shchedrin, "Magnus expansion method for two-level atom interacting with few-cycle pulse," *J. Mod. Opt.*, vol. 65, no. 11, pp. 1378–1384, 2018.